

**OPTOELECTRONIC PROPERTIES OF FLUORESCENT ORGANIC
LIGHT EMITTING DIODES: ROLE OF DEVICE ENGINEERING**

**Thesis Submitted to AcSIR for the Award of the Degree of
DOCTOR OF PHILOSOPHY
in Physical Sciences**



By

ANJALY SOMAN

Registration No: 10PP14J39013

Under the guidance of

Dr. K. N. NARAYANAN UNNI



**CSIR-NATIONAL INSTITUTE FOR INTERDISCIPLINARY
SCIENCE AND TECHNOLOGY (CSIR-NIIST)
THIRUVANANTHAPURAM-695 019, KERALA, INDIA**

June, 2019

Dedicated to my Amma and Achan

DECLARATION

I hereby declare that the matter embodied in the thesis entitled: “**Optoelectronic properties of fluorescent organic light emitting diodes: Role of device engineering**” is the result of the investigations carried out by me at the Photosciences and Photonics Group, Chemical Sciences and Technology Division, CSIR-National Institute for Interdisciplinary Science and Technology (CSIR-NIIST), Trivandrum, under the supervision of Dr. K. N. Narayanan Unni and the same has not been submitted elsewhere for any other degree.

In keeping with the general practice of reporting scientific observations, due acknowledgement has been made wherever the work described is based on the findings of other investigators.



Anjaly Soman



राष्ट्रीय अंतर्विषयी विज्ञान तथा प्रौद्योगिकी संस्थान
NATIONAL INSTITUTE FOR INTERDISCIPLINARY SCIENCE AND TECHNOLOGY

वैज्ञानिक तथा औद्योगिक अनुसंधान परिषद्

Council of Scientific and Industrial Research

इंडस्ट्रियल एस्टेट पी ओ, पाप्पनमकोड, तिरुवनंतपुरम, भारत – 695 019

Industrial Estate P O, Pappanamcode, Thiruvananthapuram, India – 695 019

डॉ. के एन नारायणन उष्णी

प्रिंसिपल वैज्ञानिक एवं प्रमुख
फोटो विज्ञान और फोटोनिक्स अनुभाग

Dr. K. N. Narayanan Unni

Principal Scientist and Head
Photosciences and Photonics Section

June 14, 2019

CERTIFICATE

*This is to certify that the work incorporated in this Ph.D. thesis entitled **Optoelectronic properties of fluorescent organic light emitting diodes: Role of device engineering** submitted by **Ms. Anjaly Soman** to Academy of Scientific and Innovative Research (AcSIR) in fulfilment of the requirements for the award of the **Degree of Doctor of Philosophy in Physical Sciences**, embodies original research work done under my supervision and guidance at the Photosciences and Photonics Section, Chemical Sciences and Technology Division of the CSIR-National Institute for Interdisciplinary Science and Technology (CSIR-NIIST), Trivandrum. I further certify that this work has not been submitted to any other University or Institution in part or full for the award of any degree or diploma. Research material obtained from other sources has been duly acknowledged in the thesis. Any text, illustration, table etc., used in the thesis from other sources, have been duly cited and acknowledged.*

It is also certified that this work done by the student, under my supervision, is plagiarism-free.

Anjaly Soman

K. N. Narayanan Unni

ACKNOWLEDGEMENTS

It is my great pleasure to express my deep sense of gratitude to Dr. K. N. Narayanan Unni, my thesis supervisor, for suggesting the research problem and for his invaluable guidance, support and encouragement that led to the successful completion of this work.

I thank Dr. Suresh Das and Dr. Gangan Pratap, former directors and Dr. A. Ajayaghosh, the present Director of the CSIR-National Institute for Interdisciplinary Science and Technology (CSIR-NIIST), Trivandrum, for providing the necessary facilities for carrying out this work.

I would like to express my sincere thanks to Professor M. V. George for his inspirational presence at CSIR-NIIST.

I would like to acknowledge all the help and support that I received from Dr. S. Mangalam Nair and Dr. R. Luxmi Varma, former AcSIR coordinators and Dr. C. H. Suresh, the present AcSIR coordinator at CSIR-NIIST.

My sincere thanks are due to Dr. Prabhakar Rao P, Dr. Yoosaf Karuvath and Dr. K. P. Surendran, my doctoral committee members for all the suggestions and encouragement.

I would like to thank Dr. K. R. Gopidas, Dr. Joshy Joseph, Dr. Karunakaran Venugopal, Dr. Vijayakuamar C. Nair, Dr. Biswapriya Deb, Dr. Suraj Soman, Dr. J. D. Sudha, Dr. Rakhi Raghavan Baby, Dr. V. K. Praveen, Dr. Ishita Neogi, Dr. Sreejith Shankar, Dr. Manas Panda, Dr. Animesh Samantha, present and former Scientists of the Photosciences and Photonics Section, Chemical Sciences and Technology Division, for the help and support.

I sincerely thank Samtel Centre for Display Technologies, IIT Kanpur & Physics Department, Cochin University for Science and Technology for the help in initial thin film thickness optimization studies.

I express my sincere thanks to Dr. Rahul, Dr. Aneesh, Dr. Viji, Dr. George, Dr. Shameel and Dr. Sreejith for their valuable help, and Ms. Chinju, Mr. Guruprasad, Ms. Sumitha, Ms. Afeefa for their help in the photoluminescence studies.

I am indebted to all my former and present group members, Mr. Rajeev, Ms. Hanna, Ms Anjali, Mr. Vibhu, Mr. Jayadev, Mr. Manuraj, Ms. Kavya, Mr. Vipin, Mr. Jayaram, Ms. Anjana, Dr. Nisha, Mr. Lingamoorthy, Mr. Sourav, Mr. Gokul, Ms. Anooja, Ms. Ansu, Ms. Liya, Mr. Vaishakh, Mr. Visakh, Ms. Surabhi, Mr. Akhil, Mr. Gopi and Ms.

Sradha for all their help, support and encouragement throughout my research career at NIIST.

I thank all the members of the Photosciences and Photonics Section and other Divisions of CSIR-NIIST for their help and cooperation. I would like to thank Mr. Robert Philip, Mr. J. S. Kiran, Mr. Kiran Mohan, Mr. Aswin for all their support throughout my stay at CSIR-NIIST.

Words are inadequate to express my gratitude to my family members who constantly stood as a source of encouragement and confidence. I take this opportunity to pay respect to all my teachers who guided and blessed me.

I thank UGC, DST, Government of India and CSIR for financial assistance.

Anjaly Soman

CONTENTS

| | Page |
|--|-------|
| Declaration | i |
| Certificate | ii |
| Acknowledgements | iii |
| Contents | v |
| Preface | ix |
| List of Figures | xiii |
| List of Tables | xvi |
| List of Abbreviations | xviii |
| | |
| Chapter 1 Organic light emitting diodes: The story so far and the remaining challenges | |
| | |
| 1.1 Introduction | 1 |
| 1.2 Organic semiconductors | 2 |
| 1.3 Organic electronic devices | 4 |
| 1.3.1 Organic field-effect transistors (OFETs) | 5 |
| 1.3.2 Organic photovoltaic cells | 6 |
| 1.3.3 Organic light emitting devices | 7 |
| 1.4 OLEDs: A brief history of the development | 8 |
| 1.4.1 Host-guest interactions | 9 |
| 1.4.2 Fluorescent and phosphorescent devices | 12 |
| 1.4.3 Tandem devices | 13 |
| 1.4.4 p-i-n devices | 14 |
| 1.4.5 Current status: White OLED (WOLED) | 15 |
| 1.5 OLED: Structure and operation | 18 |
| 1.6 Remaining challenges | 20 |

| | | |
|------------------|---|----|
| 1.7 | Theme of the thesis | 22 |
| 1.8 | Future directions | 23 |
| 1.9 | Summary | 24 |
| 1.10 | References | 24 |
| Chapter 2 | Device engineering in a fluorescent OLED by facile electron transport layer doping and carrier confinement | |
| 2.1 | Abstract | 48 |
| 2.2 | Introduction | 49 |
| 2.3. | Results and Discussion | 55 |
| 2.3.1 | Photoluminescence study | 55 |
| 2.3.2 | SCLC studies for determination of mobility | 56 |
| 2.3.3 | LiF bulk doping | 57 |
| 2.3.3.1 | Device structure | 57 |
| 2.3.3.2 | Device characteristics without blocking layer | 59 |
| 2.3.3.3 | Device characteristics with blocking layer | 61 |
| 2.3.4 | Studies on LiF doping concentration | 65 |
| 2.3.4.1 | Device structure | 65 |
| 2.3.4.2 | Device characteristics without blocking layers | 66 |
| 2.3.4.3 | Device characteristics with blocking layers | 67 |
| 2.4 | Conclusions | 71 |
| 2.5 | References | 72 |
| Chapter 3 | Tuning the optoelectronic properties of fluorescent OLEDs by deposition conditions and device engineering | |
| 3.1 | Abstract | 81 |
| 3.2 | Introduction | 82 |

| | | |
|-------------------|---|-----|
| 3.3 | Results and Discussion | 87 |
| 3.3.1 | Section A: C545T emitter and varying deposition conditions | 87 |
| 3.3.1.1 | Alq ₃ :C545T Emitter Unit | 88 |
| 3.3.1.2 | C545T Single Emitter Unit | 93 |
| 3.3.1.2.a | Effect of variation of the evaporation rate of C545T | 93 |
| 3.3.1.2.b | Effect of variation of the C545T thickness | 97 |
| 3.3.2 | Section B: Duel Emissive layer white OLED | 101 |
| 3.3.2.1 | Yellow: Blue Emitter Unit | 103 |
| 3.3.2.2 | Blue: Yellow Emitter Unit | 106 |
| 3.4 | Conclusions | 109 |
| 3.5 | References | 110 |
| Chapter 4 | Singlet and triplet exciton migration: Optimized emission zone in electron transporting host Alq₃ | |
| 4.1 | Abstract | 113 |
| 4.2 | Introduction | 114 |
| 4.3 | Results and Discussion | 121 |
| 4.3.1 | Singlet exciton sensing in Alq ₃ | 123 |
| 4.3.2 | Triplet exciton sensing in Alq ₃ | 128 |
| 4.3.3 | Combined fluorescent and phosphorescent emitters in host Alq ₃ | 133 |
| 4.4 | Conclusions | 135 |
| 4.5 | References | 136 |
| Annexure A | OLED performance metrics and fabrication details | |
| A.1 | OLED: Characterization details | 141 |
| A.2 | OLED: Fabrication details | 145 |

| | | |
|-----|---|-----|
| A.3 | Materials used in the thesis | 146 |
| | List of Publications | 149 |
| | Posters Presented at Conferences | 150 |

PREFACE

Impressive progress has been recorded in the development of science and technology of organic light emitting diodes (OLEDs) since its inception in 1987 by Tang and Vanslyke from Kodak. Over the past couple of decades, OLEDs came to the forefront of 'advanced technology' predominantly in the form of displays and lighting panels, which led to the commercialization of the technology. OLEDs are planar light sources which can be used to fabricate large area structures with high brightness and good chromaticity along with unique form factors, which address most of the challenges faced by inorganic LEDs, especially concerning the energy demand and the physical and psychological effects of blue LEDs. Even though this green technology can improve quality of life, the current high cost of the same makes it off limits to the common people. With better cost-effectiveness, they do have the potential to improve the quality of life in the form of affordable and comfortable lighting, displays, and wearable sensors. They can support healthy living by individualizing people's needs aesthetically.

The fluorescent OLEDs are of considerable interest despite the availability of highly efficient phosphorescent devices, due to longer material and device lifetime, low-efficiency roll-off and low-cost. Performance enhancements in fluorescent OLEDs by simpler techniques while simultaneously reducing process complexity were studied as part of the present thesis, which is divided into four chapters. Some of these aspects include luminance, power efficiency, and external quantum efficiency enhancement,

exciton confinement, and emission tuning. In addition, the exciton diffusion and emission zone in fluorescent OLEDs have also been studied.

Most of the n-dopants for the electron transport layer (ETL) doping of OLEDs are either very expensive or ineffective due to dopant material diffusion into the emission layer (EML) where it acts as non-radiative recombination centers. In the second chapter, with inexpensive lithium fluoride (LiF) as n-dopant, bulk doping in the ETL is optimized by varying the thickness of the undoped ETL buffer layer, located between the EML and doped ETL. An electron blocking layer (EBL) was introduced between the hole transport layer (HTL) and EML, and its effect on the efficiency of this n-doped device when compared to the undoped control device was studied. The doping concentration was also optimized to explore the exciton confinement effect of different EBLs on the n-doped device architecture. 27.8% improvement in external quantum efficiency was observed at 1000 cd/m² for a device with Tris(4-carbazoyl-9-ylphenyl)amine (TCTA) as EBL when compared with the device having only N,N'-Di(1-naphthyl)-N,N'-diphenyl-(1,1'-biphenyl)-4,4'-diamine (NPB) as both HTL and EBL. This work combining inexpensive n-dopant with the carrier confinement effect of the electron blocking layer in fluorescent OLED generated two publications. This work also confirmed the shift in the recombination zone due to the decreased carrier balance resulting from the difference in charge carrier mobilities.

In the third chapter, the impact of heavy luminescent doping on the electrical and optical properties and its dependence on deposition conditions were studied to explore the possibility of tuning the emission spectra of a single dopant with an aim to reduce the number of layers and process steps and to bring down the production cost

of device fabrication. The concentration of dopant in EML is varied from 3% to 50% and a device with only dopant molecule as EML as a limiting case of heavy doping was also employed, changing deposition rate and EML thickness. With the increase in doping, reduction in pure exciton emission and increased excimer emission was observed, resulting in electroluminescent spectral red shift and broadening. The CIE color coordinates shifted from green to yellow region.

We have further explored the potential for white emission from a simplified device architecture. With only an additional fluorescent blue emitter, inserted on either side of EML, the emission was recorded. The recorded CIE coordinates have shown a tunability ranging from (0.39, 0.45) to (0.33, 0.45), exhibiting flexibility in tuning and demonstrating the potential to emit white light of CIE coordinates (0.33, 0.33), probably with a more suitable dopant material. Thus the emission tuning could realize white OLED with less number of materials and less number of process steps, which indicates the possibility of less expensive devices.

The mapping of exciton diffusion and emission profile was done in the fourth chapter to optimize the EML thickness for maximum exciton harvesting without sacrificing carriers towards non-recombination current by the spatial deployment of luminescent probes and studying the EL spectra. Emission zone profile was mapped both in presence and absence of transport doping, and the profiles were compared, which confirmed the importance of transport doping in device performance. In the EML, the part of the dopant distribution outside the emission zone mostly acts as a resistor and can affect the current density and carrier balance, without any contribution towards emission, the device efficiency being influenced in turn. The

singlet, as well as triplet emission zone in Alq₃, was mapped by inserting a fluorescent probe layer of 4-(Dicyanomethylene)-2-tert-butyl-6-(1,1,7,7-tetramethyljulolidin-4-yl-vinyl)-4H-pyran (DCJTB) and a phosphorescent probe layer of Platinum octaethylporphyrin (PtOEP) of thickness 30Å, which was doped in Alq₃ host. By combining both of these probes, singlets and triplets could be harvested simultaneously in Alq₃ host, in a most efficient manner, simultaneously suppressing any host emission. This is an excellent indicator of how to optimize the EML thickness as well as composition, which again can reduce the fabrication cost of OLEDs.

Thus, an attempt has been made in this thesis to address some of the challenges in OLED technology by device engineering.

Anjaly Soman

List of Figures

| Sl. No | List of Figures | Page |
|--------|---|------|
| 1. | Figure 1.1 a) Benzene with six 2p orbitals, and b) parallel 2p orbitals overlap to form torus above and below the plane of the ring | 3 |
| 2. | Figure 1.2 a) A typical OLED structure, and b) OLED device operation diagram | 19 |
| 3. | Figure 2.1 Photoluminescence spectra of neat and LiF-doped Alq ₃ films. | 55 |
| 4. | Figure 2.2 log J vs. log V plot for neat and doped Alq ₃ films | 56 |
| 5. | Figure 2.3 a) Typical device structure of the OLED used in this study, b) Energy level diagrams for devices i) A, ii) B and C, iii) D and iv) E. The HOMO-LUMO values and work functions are given in eV | 58 |
| 6. | Figure 2.4 a) J-V-L characteristics of devices A, B and C, b) Current efficiency vs. Current density for devices A and C and c) Power efficiency vs. Luminescence for devices A and C | 60 |
| 7. | Figure 2.5 a) J-V-L characteristics of devices C, D and E, b) Current efficiency vs. Current density for devices C and D and E and c) Power efficiency vs. Luminance plot for devices C, D and E | 63 |
| 8. | Figure 2.6 Energy level diagram of the device. The HOMO-LUMO values are given in eV | 65 |
| 9. | Figure 2.7 a) Current Density-Voltage-Luminance Characteristics, b) Power Efficiency, and c) Current Efficiency characteristics of the OLEDs with different percentages of ETL doping | 66 |
| 10. | Figure 2.8 a) Current Density-Voltage-Luminance Characteristics, b) Power Efficiency, c) Current Efficiency, and d) EQE characteristics of the devices with different Electron Blocking Layers | 68 |
| 11. | Figure 2.9 Electroluminescence spectra | 70 |
| 12. | Figure 3.1 The molecular structure of a) C-6, b) C545, and c) C545T | 83 |

| | | |
|-----|--|-----|
| 13. | Figure 3.2 a) OLED device structure for the variation in C545T doping concentration study, b) Current density-Voltage characteristics, c) Current density-Luminance-Current efficiency characteristics, d) Photoluminescence spectrum of C545T doped Alq ₃ thin film with doping concentration of 5% and 50%, and e) Normalized electroluminescence spectrum of C545T: Alq ₃ device with different doping concentration ranging from 3% - 50% | 89 |
| 14. | Figure 3.3 a) CIE x and y coordinates with voltage for different doping concentration; CIE 1931 colour chart in the inset and b) Normalized EL spectra with a change in voltage for i) 3% and ii) 50% doping | 92 |
| 15. | Figure 3.4 a) Architecture of the OLED device with C545T single emitter, and b) energy level diagram of the device. The HOMO-LUMO values are given in eV | 94 |
| 16. | Figure 3.5 a) Photoluminescence spectrum of C545T in solution and neat C545T film, b) Normalized electroluminescence spectrum of C545T single emitter device with varying EML deposition rate, c) Variation of CIE x and y coordinates with voltage for different deposition rates, and d) Current Density-Voltage-Luminance Characteristics of the C545T single emitter devices with various EML deposition rate. | 95 |
| 17. | Figure 3.6 Normalized EL spectra for different biasing voltages for C545T single emitter devices with deposition rates of a) 0.1 Å/s, b) 2.0 Å/s, and c) 5.0 Å/s | 96 |
| 18. | Figure 3.7 a) Current Density-Voltage-Luminance Characteristics of the C545T single emitter OLED with varying EML thickness, b) Normalized electroluminescence spectrum for different EML thickness, and c) Variation of CIE x and y coordinates with voltage for different EML thickness | 98 |
| 19. | Figure 3.8 Normalized electroluminescence spectra of the OLEDs for different EML thickness and operating voltage: (a) 10 nm, (b) 20 nm, (c) 30 nm, (d) 60 nm, and (e) 70 nm | 100 |
| 20. | Figure 3.9 Energy level Diagram of devices a) A-D, b) | 102 |

E-F

21. **Figure 3.10** Electro-optical characteristics of Yellow: Blue emitter OLEDs a) Luminance-Current Density Characteristics, b) Current Efficiency- Current Density Characteristics, c) Electroluminescence spectrum d) CIE (x y) coordinates 104
22. **Figure 3.11** Electro-optical characteristics of Blue: Yellow emitter OLEDs a) Luminance-Current Density Characteristics, b) Current Efficiency- Current Density Characteristics, c) Electroluminescence spectrum d) CIE x and y coordinates, e) CIE 1931 Colour Chart 108
23. **Figure 4.1** a) Energy level diagram, b) Current density-Voltage-Luminance characteristics, and c) Normalized EL spectra for devices A1, A2, A3 and A4. The HOMO-LUMO values are given in eV 122
24. **Figure 4.2** a) Energy level diagram of the devices with the probe layer inserted in devices, undoped and doped, b1) J-V-L characteristics for the undoped device with DCJTB sensing layer, b2) J-V-L characteristics for the doped HTL and ETL device with DCJTB sensing layer, and EL spectra at 8V for the c1) undoped device, c2) doped device; legends show the distance of the probe location in nm from HTL-EML interface with respect to the control devices A1 or A4. The HOMO-LUMO values are given in eV. 124
25. **Figure 4.3** a) EL spectra for the undoped device having DCJTB sensing layer at different voltages, b) EL spectra for the doped device having DCJTB sensing layer at different voltages; legends show the distance of the probe location in nm from HTL-EML interface with respect to the control devices A1 or A4, and c) Ratio of EL intensity peak between red and green with respect to the sensor layer position for i) undoped device, and ii) doped device 127-128
26. **Figure 4.4** a) J-V-L characteristics for the undoped device with PtOEP sensing layer, b) J-V-L characteristics for the doped device with PtOEP sensing layer, c) EL spectra of the i) undoped device, ii) doped device; legends show the distance in nm 129

| | | |
|-----|--|---------|
| | from HTL-EML interface with respect to the control devices A1 or A4 | |
| 27. | Figure 4.5 a) EL spectra for the undoped device having PtOEP sensing layer at different voltages, b) EL spectra for the doped device having PtOEP sensing layer with different voltages; legends show the distance of the probe location in nm from HTL-EML interface with respect to the control devices A1 or A4, and c) percentage of red sensor contribution to the total emission with respect to the sensor layer position for i) undoped device and ii) doped device | 131-132 |
| 28. | Figure 4.6 a) J-V-L characteristics for the undoped and doped devices with both DCJTB and PtOEP, b) Normalized EL spectra of the i) undoped device, ii) doped device with change in voltage, and (c) Comparison of EL spectra of devices with either DCJTB or PtOEP alone and the combined device; open: undoped devices, closed: doped devices | 133-134 |
| 29. | Figure A.1 Glovebox integrated evaporation system; inset shows the internal view of the evaporation chamber | 145 |
| 30. | Figure A.2 a) A typical substrate design, b) OLED device, and c) PR655 Spectro-radiometer | 146 |

List of Tables

| | | |
|----|--|----|
| 1. | Table 2.1 Summary of the performance of devices A, B, C, D and E | 64 |
| 2. | Table 2.2 Summary of the performance of devices with different LiF doping percentage and blocking layer | 69 |
| 3. | Table 3.1 Electroluminescent intensity ratio between pure exciton and excimer emission for different doping percentages for C545T single emitter device | 90 |
| 4. | Table 3.2 Electroluminescent intensity ratio between pure exciton and excimer emission for | 99 |

different EML thicknesses for C545T single emitter device

5. **Table 3.3** Device structures for the blue and yellow emitter combinations to yield white emission 103

List of Abbreviations

| | |
|------------------|---|
| A | Ampere |
| Å | Angstrom |
| AC | Alternating current |
| Al | Aluminium |
| Alq ₃ | Tris-(8-hydroxyquinoline) aluminium |
| a-Si | Amorphous silicon |
| Au | Gold |
| Ba | Barium |
| BCP | Bathocuproine |
| BCzVBi | 4,4'-Bis(9-ethyl-3-carbazovinylene)-1,4,4'-Bis(9-ethyl-3-carbazovinylene)-1,1'-biphenyl |
| Bphen | Bathophenanthroline |
| C-545 | 10-[2-benzothiazolyl]-2,3,6,7-tetrahydro-1H,5H,11H-benzo-[l]pyrano[6,7,8-ij]quinolizin-11-one |
| C545T | 2,3,6,7-Tetrahydro-1,1,7,7,- tetramethyl-1H, 5H,11H-10-(2-benzothiazolyl) quinolizino-[9,9a, 1n gh]Coumarin |
| C-6 | 3-(2-benzothiazolyl)-7-(diethylamino)-2H-1-benzopyran-2- |
| Ca | Calcium |
| Cd | Cadmium |
| CGL | Charge generation layer |
| CIE | Commission Internationale de l'Éclairage (International Commission on Illumination) |
| cm | Centimetre |
| CRI | Color rendering index |
| Cs | Cesium |
| CsF | Cesium Fluoride |
| Cu | Copper |
| DC | Direct current |
| DCJT | 4-(Dicyanomethylene)-2-methyl-6-(1,1,7,7-tetramethyljulolidyl-9-enyl)-4H-pyran |

| | |
|---|--|
| DCJTb | 4-(Dicyanomethylene)-2-tert-butyl-6-(1,1,7,7-tetramethyljulolidin-4-yl-vinyl)-4H-pyran |
| DCM | 4-(Dicyanomethylene)-2-methyl-6-(4-dimethylaminostyryl)-4H-pyran |
| DCzIPN | 4,6-di(carbazol-9-yl)isophthalonitrile |
| DPVBi | 4,4'-bis(2,2'-diphenylvinyl)-1,1'-diphenyl |
| EBL | Electron blocking layer |
| EIL | Electron injection layer |
| EL | Electroluminescence |
| EML | Emission layer |
| EQE | External quantum efficiency |
| Et ₂ N- | Diethyl amide |
| ETL | Electron transport layer |
| EtOH | Ethanol |
| F ⁻ | Fluoride anion |
| F4-TCNQ | 2,3,5,6-Tetrafluoro-7,7,8,8-tetracyanoquinodimethane |
| FET | Field effect transistor |
| Flrpic | Bis[2-(4,6-difluorophenyl)pyridinato-C2,N](picolinato)iridium(III) |
| FOLED | Fluorescent organic light emitting diode |
| HAT-CN | Hexaazatriphenylenehexacarbonitrile |
| HBL | Hole blocking layer |
| High-K | High dielectric constant |
| HIL | Hole injection layer |
| HOMO | Highest occupied molecular orbital |
| HTL | Hole transport layer |
| IQE | Internal quantum efficiency |
| Ir | Iridium |
| ITO | Indium tin oxide |
| J | Current density |
| J _A , J _B , J _C , J _D | Current density (J) of devices A, B, C and D, respectively |
| J-V | Current density-Voltage |

| | |
|---|--|
| J-V-L | Current density-Voltage -Luminance |
| K | Dielectric constant |
| L _A , L _B , L _C , L _D | Luminance (L) of devices A, B, C and D, respectively |
| LED | Light emitting diode |
| Li | Lithium |
| LiF | Lithium fluoride |
| Lm | Lumen |
| LUMO | Lowest unoccupied molecular orbital |
| MEHPPV | Poly[2-methoxy-5-(2-ethylhexyloxy)-1,4-phenylenevinylene] |
| MIM | Metal-insulator-metal |
| m-MTDATA | 4,4',4''-Tris[phenyl(mtolyl) amino] triphenyl amine |
| MoO ₃ | Molybdenum trioxide |
| NI-1-PhTPA | Naphtho[1,2-d]imidazole derived compound |
| nm | Nanometre |
| NPB | N,N'-Bis(naphthalen-1-yl)-N,N'-bis(phenyl)-benzidine |
| OFET | Organic field-effect transistor |
| OLED | Organic light emitting diode |
| OLET | Organic light emitting transistor |
| Os | Osmium |
| OSC | Organic semiconductor |
| PEDOT:PSS | poly(3,4-ethylenedioxythiophene) polystyrene sulfonate |
| PFO | Poly(9,9-di-n-octylfluorenyl-2,7-diyl) |
| PhOLED | Phosphorescent organic light emitting diode |
| PIN | P doped semiconductor-insulator-n doped semiconductor |
| PL | Photoluminescence |
| PLQY | Photoluminescence quantum yield |
| PO-01 | Iridium(III) bis(4-phenylthieno[3,2-c]pyridinato-N,C2')acetylacetonate |
| PPV | Poly(p-phenylene vinylene) |
| PtOEP | Platinum octaethylporphyrin |
| PXZDSO ₂ | 2-(4-phenoxazinephenyl) thianthrene-9,9',10,10'-tetraoxide |

| | |
|---|---|
| Ru | Ruthenium |
| SCLC | Space charge limited current |
| Sm | Samarium |
| Sr | Strontium |
| Super-Yellow Poly | Poly[$\{2,5\text{-di}(3',7'\text{-dimethyloctyloxy})\text{-}1,4\text{-phenylene-vinylene}\}\text{-co-}\{3\text{-}(4'\text{-}(3'',7''\text{-dimethyloctyloxy})\text{phenyl})\text{-}1,4\text{-phenylenevinylene}\}\text{-co-}\{3\text{-}(3'\text{-}(3',7'\text{-dimethyloctyloxy})\text{phenyl})\text{-}1,4\text{-phenylenevinylene}\}$] |
| TADF | Thermally activated delayed fluorescence |
| TAPC | Di-[4-(N,N-di-p-tolyl-amino)-phenyl]cyclohexane |
| TCTA | Tris (4-carbazoyl-9-ylphenyl)amine |
| T _g | Glass transition temperature |
| TPBi | 1,3,5-Tris(1-phenyl-1Hbenzimidazol- 2-yl)benzene |
| TTA | Triplet-triplet annihilation |
| V | Volt |
| W | Watt |
| WO ₃ | Tungsten trioxide |
| WOLED | White organic light emitting diode |
| X _{CIE} | CIE x coordinate |
| XPS | X-ray photoelectron spectroscopy |
| Y _A , Y _B , Y _C , Y _D | Yellow emission intensity of devices A, B, C and D, respectively |
| Y _{CIE} | CIE y coordinate |
| ε | Relative permittivity of dielectric material |
| π | Pi, value equals ~3.14 |

Organic light emitting diodes: The story so far and the remaining challenges

1.1 Introduction

Organic light emitting diodes (OLED) are right now at the zenith of high-quality technology, by providing the best ever image quality. They represent the future of display technology because of their potential to be made into ultra-thin, transparent, flexible, rollable, stretchable and foldable forms. The high quality of OLED displays is featured by high brightness and contrast ratio, wide colour gamut and wider viewing angle and fastest refreshing rates. They can also produce true black just by turning the device off, as they are an emissive technology, unlike the backlight dependent displays. OLEDs are surface emitting light sources having very low power consumption. Their performance and unique form factors open up a new realm of technological advancement in the form of curved displays, wearable electronics, smart windows, etc. In 2018, more than 500 million OLED displays were produced worldwide. Foldable displays are already in the market, integrated to smart phones by Lenovo, Samsung, Huawei, etc. and there are LG's curved and roll-able TVs as well. Apart from display applications, OLED light sources are used in lighting and sensors. However, currently, OLED technology is far more expensive than the competing technologies available in the market, mostly due to the low production yield. Hopefully, the cost could come down with optimized production methods and an increase in production.

OLEDs are semiconductor-based devices with thickness in the nanometre range. They use different organic materials deposited in the form of thin films and sandwiched between two electrodes to generate distinct colours by electroluminescence. The basic building blocks used for OLED fabrication are divided into two classes- small molecule organic materials or polymers. These organic semiconducting materials act as either light emitting materials or charge carrier transporters, where the former is achieved by electroluminescence (EL) that is light emission on the application of electrical current. Organic semiconductors can also be used to fabricate several other optoelectronic devices like organic solar cells, field-effect transistors, memory devices, etc. This whole field of study including material design, synthesis, characterization of organic semiconductors and corresponding optoelectronic device fabrication is termed as organic electronics. Due to the low-temperature processing and potential for printing, organic electronics presents a promise for low-cost electronic devices.

1.2 Organic semiconductors

Organic semiconductors are molecular semiconductors made up of carbon-based π -conjugated molecules or polymers. The earlier works on organic semiconductors were on single-crystalline organics and were soon overtaken by the far more practical thin film organics. In reality, organic semiconductors are insulators but can be made conducting by charge carrier injection^{1,2}, doping³⁻⁵ or optical excitations. For their pioneering work in conductive polymers⁶, Alan J. Heeger, Alan G. MacDiarmid, and Hideki Shirakawa were awarded the Nobel Prize in Chemistry in 2000⁷. Organic chemistry offers flexibility for the synthesis of a wide range of materials, often tailor-made. When molecules are formed from atoms, the atomic orbitals combine to form molecular orbitals of the same valency. The carbon atoms in these molecules can re-arrange its valence orbitals to form hybrid orbitals,

which lead to the formation of molecular orbitals. For example, three such degenerate hybrid orbitals can form sp^2 hybridization, and the hybridized orbitals align in plane and perpendicular perpendicular to the remaining p orbital. Whereas the hybrid orbitals form a covalent bond with with the nearby atoms, the p orbitals form π bonds leading to the delocalization of π electrons. Fig 1.1 shows the π system of benzene where the overlap of the parallel 2p orbitals represent the lowest lying molecular orbital.

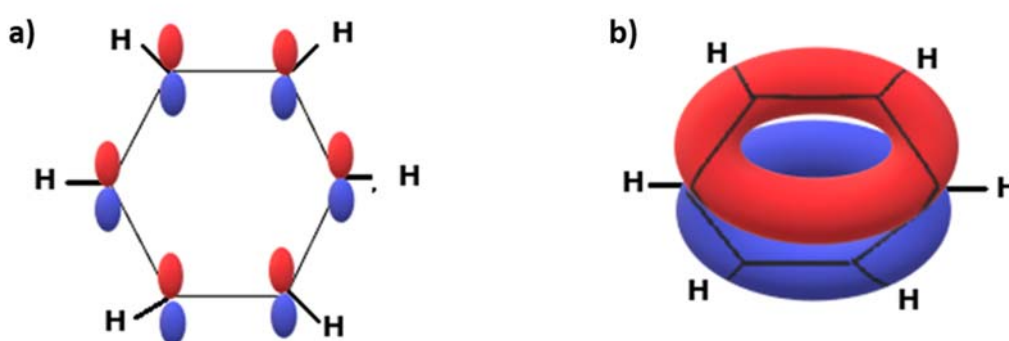


Figure 1.1 a) Benzene with six 2p orbitals, and b) parallel 2p orbitals overlap to form torus above and below the plane of the ring

These π electrons are not confined to a single atom and the adjacent delocalized electrons are transported through hopping mechanism. Compared to the hybrid orbitals, the π orbitals have the smaller differences between the highest occupied and the lowest unoccupied energy levels, which get further decreased when the delocalization is extended over atoms. When the difference between the highest occupied molecular orbital (HOMO) and the lowest unoccupied molecular orbital (LUMO) is small enough, the molecule can become semiconducting. Organic semiconductors have carrier mobilities comparable to amorphous silicon (a-Si $\sim 1 \text{ cm}^2\text{V}^{-1}\text{s}^{-1}$), which is good enough for many optoelectronic applications. Unlike inorganic semiconductors, organic semiconducting molecules interact through van der Waal's forces, resulting in a polycrystalline or most often amorphous structure. It also causes very low dielectric constants as well in the range of $\epsilon = 3.5\text{--}5.5$.^{5,8-11} Organic materials can offer high absorption coefficients,

low refractive indices, and large redshift from absorption to emission and lower defect densities. Most organics can be processed at low temperature, making the fabrication of on flexible substrates feasible. It was found that photo-excitation of a dye molecule adsorbed at the surface or incorporated in the bulk can create charge carriers, termed sensitized photoconductivity¹² which became the basis of today's organic solar cells.

1.3 Organic electronic devices

Organic electronic devices are high-tech products established using organic semiconductors. The processing techniques of small molecules and polymers for this purpose are quite different. While small molecular semiconductors are usually deposited by thermal evaporation in vacuum, as they are usually insoluble in most of the solvents, the heavier polymers are commonly solution processed. The small molecules undergo sublimation from a hot source and are then transported to the substrates in vacuum, in thermal evaporation. This leads to the formation of thin films of the organic material on the substrate surface. Polymers, on the other hand, are converted into solution and deposited using several different processes including spin-coating, drop-casting, printing, etc. in both these processing routes, the deposition conditions are the deciding factors in determining thin film morphology and the degree of disorder. Organic electronic devices also make use of dielectrics, transparent conductive oxides, conductors, etc. Investigations on different aspects of organic electronic devices are ongoing to further optimize the device structure and fabrication methodology to increase the efficiency and to explore the integration possibility of different devices. Three most important organic electronic devices are briefly discussed below.

1.3.1 Organic field-effect transistors (OFETs)

Organic field-effect transistors (OFETs) were first proposed in 1930 by J.E. Lilienfeld¹³ but were realized only in 1960 by Kahng and Atalla¹⁴, who reported first ever metal oxide semiconductor FET (MOSFET) at a conference. Later, Koezuka et al. reported the first ever OFET fabricated from polythiophene in 1987¹⁵. A typical OFET can be considered as a standard capacitor with its metal-insulator-semiconductor (MIS) structure, the gate electrode and semiconductor acting as capacitor plates separated by an insulator layer. Source and drain electrodes act as conduction probes across the semiconductor. OFETs are three terminal devices with source, drain and gate electrodes.

OFETs have organic semiconductors, either the small molecules or polymers, as the active material, in the channel. These devices can be developed to be integrated with large area electronics. There are several geometries for OFET fabrication available, e.g., bottom gate-top contact, top gate-bottom contact, etc. Here, high dielectric constant (high-K) polymeric materials can be used as the gate dielectric. Interest in OFETs has intensified in the past decade as they can be used as the backplane to fabricate fully flexible displays on plastic substrates. As transistors are the basic building blocks of all electronic circuits, FETs made with organic materials raise exciting possibilities. Even though the performance of OFETs does not match with that of conventional transistors, they do not necessarily have to replace silicon-based transistors to become relevant. OFETs have found its niche in fields like RF ID tags and sensors.

In reality, OFET acts as a variable resistance controlled by the gate voltage. On applying a voltage between source electrode and gate, equal numbers of positive and negative charges are induced on opposite sides of the dielectric layer. The voltage applied between source and drain can drive those induced at the insulator-semiconductor interface. Due to the lower mobilities

of organic semiconductors, OFETS have comparatively low ON/OFF ratio and cannot be used in fast switching applications. Mobility can also be affected by the molecular packing in the thin film, which makes the deposition conditions including the rate of deposition and substrate temperature more important. Using an ambipolar active layer, OFET structure can also be used for light emission, more commonly called light emitting transistor (OLET)¹⁶. In this case, both charge carriers are injected into the active layer by the source-drain electrodes, which recombine and emit light.

1.3.2 Organic photovoltaic cells

Photovoltaic effect, which is current generation on illumination was discovered by Becquerel in 1839¹⁷ and the first organic small molecule material to display this characteristic is anthracene in 1906¹⁸, and the first polymer is poly(N-vinyl-carbazole) in 1957¹⁹. Bell Laboratories were the first to make a solar cell based on crystalline silicon, which exhibited an efficiency of 6%²⁰. Now, the silicon-based solar cells without any concentrators have reached an efficiency of 26.6%²¹. Silicon solar cells account for 99% of the world solar cell production, but altogether they contribute only 0.1% to the total world energy production due to its high-cost. This is where the less expensive organic semiconductor based photovoltaics become relevant, even though they have been reported to have lower power conversion efficiencies. Since the 80s, intense work has been reported in the field of organic material based solar cells²²⁻²⁵.

Organic solar cells (OSCs) are photovoltaic devices fabricated using organic semiconductors, which generate charge carriers on light absorption. Similar to the other organic electronic devices, OSCs also have the potential to be fabricated at low-cost. A typical OSC structure consists of electron donor and acceptor sandwiched by electrodes. The excitons generated upon light absorption by donor molecules are separated at the donor-

acceptor interface by its built-in potential and are collected at the respective electrodes. As organic materials have high absorption coefficients, by tuning the bandgap, a wide range of spectrum can be absorbed. Along with high-cost efficiency, OSCs have the potential to be fabricated as flexible and transparent devices, which make them suitable for applications like smart windows. By optimizing the OSC fabrication on paper/ plastic substrates through printing, low-cost disposable devices can be fabricated. During the last decade, research on OSCs have gathered momentum, reaching good efficiencies of 17.3%²⁶. The main challenges to be faced in this field are on improving the efficiency, stability and optimizing the process for scaling up. Then a day might come when we get delivered disposable solar cells like newspapers every day.

1.3.3 Organic light emitting devices

Electroluminescence is an optoelectronic effect where materials, usually semiconductors emit light upon charge carrier recombination. Electroluminescent devices have been used in the automotive industry in instrument panels as backlight, from the 1960s onwards. They have also been used as backlight for liquid crystal displays. Bernanose and co-workers first observed electroluminescence in organic dye materials in the 1950s, which was AC driven²⁷⁻²⁹. In the 1960s, Pope et al. reported DC driven electroluminescence from anthracene crystals of varying sizes with electrodes for better carrier injection and explained the need to use electrodes with suitable work function as the reported devices required high electric field^{1,2,30,31}. First ever observed electroluminescence in polymers was in a poly(N-vinylcarbazole) (PVK) film sandwiched between two electrodes³²⁻³⁵. These works paved the way for the modern organic light emitting diodes, which are dominant among the organic light emitting devices. There is also organic light emitting transistors^{16,36-38} as mentioned in the previous section, light emitting capacitors³⁹⁻⁴¹ and electrochemical cells⁴²⁻⁴⁴.

1.4 OLEDs: A brief history of the development*

Ching W. Tang and Steven A. VanSlyke started their work on organic electroluminescent devices in 1980s^{45,46}. They reported the first practical OLED consisting of thin films of organic materials in 1987, which was also the first vacuum deposited device⁴⁷. They used a bilayer structure with Tris(8-hydroxyquinolino)aluminium (Alq₃) thin film as both the emission layer (EML) and electron transporting layer (ETL) and a diamine thin film as hole transport layer (HTL). Transparent indium tin oxide (ITO) was the anode and a Mg: Ag film was the cathode. The former improved light extraction and the latter improved the charge carrier injection. The device emission was entirely from Alq₃ as no electrons penetrated the diamine layer. The device achieved 1% quantum efficiency, 1.5 lm/W of power efficiency and luminance above 1000 cd/m² below an operating voltage of 10 V. The same device architecture and fabrication principles are used with the organic small molecules to date without much alteration.

Burroughes et al. used conjugated polymers, which are solution processed, instead of evaporated small molecules to establish a device design regime⁴⁸. They used a 100 nm thick poly(p-phenylene vinylene) (PPV) as the emitting layer and sandwiched it between ITO and Al electrodes. Solution-processed polymer-based OLEDs (POLEDs) are fascinating as they could potentially utilize the simple and high yield-infrastructure developed by the printing industry. This can realize the large area fabrication at low cost, with reduced material wastage and process complexity resulting in cost reduction. The high molecular weight of the polymer materials brings lots of flexibility to the material design as well. Braun et al., who confirmed the same and modified the device structure and the material for better performance, immediately followed this work⁴⁹⁻⁵¹. An avalanche of publications came on

* A detailed discussion on the various metrics used for the performance evaluation of the OLED is provided in annexure A

the heels of this, paving the way for the commercialization of wholly printed devices^{52,53}. Two of the most widely studied families of conjugated polymers are based on (i) PPV, e.g., the orange-red emitting poly(2-methoxy-5-(2-ethylhexyloxy)-1,4-phenylenevinylene) (MEHPPV)⁴⁹ and “Super-Yellow,” a PPV derivative developed by Covion Semiconductors Semiconductors GmbH⁵⁴, and (ii) poly(9,9-dialkylfluorene), e.g., the blue-emitting poly(9,9-di-n-octylfluorenyl-2,7-diyl) (PFO)^{55,56}.

1.4.1 Host-guest interactions

Electroluminescence (EL) in OLEDs originates from the radiative recombination of electrons and holes injected from the respective electrodes and subsequent formation of excitons. Electron-hole formation and exciton recombination do not necessarily have to happen in the emitting species only, as there is a possibility of exciton migration after recombination. The emission in an EL device can be influenced by the presence of dopant molecules in the luminescent layer or the presence of adjacent layers, which are charge carrier transporters or carrier blockers⁵⁷. The strategy to use sensitized luminescence⁵⁸ and its usage to shift emission spectra in an anthracene doped system⁵⁹ have been reported previously. The simplest mechanism of exciton trapping in the dye for a host-guest matrix in an OLED is that of the photon emitted by the host being reabsorbed by the guest molecule, which causes an emission by the dye. For OLEDs, though this is impractical as the devices have very thin layers (<500 Å) and low dopant concentration to effectively reabsorb and emit photons. Increasing the dopant concentration to a high level to make the energy transfer mechanism possible though, cause self-quenching and accelerate device degradation. Therefore, these simple processes are highly unlikely, and often not followed.

The dominant processes for energy transfer in OLEDs can involve charge carrier and/or exciton trapping by the dye molecule. The Coulombic interaction between the exciton and dye

molecule, leading to energy transfer is referred to as Förster energy transfer. The carrier exchange interaction between exciton and dye is called Dexter energy transfer. Another mechanism for emission is the carrier trapping by the dye molecule. When the dye has either HOMO energy level higher or LUMO energy level lower than that of the host matrix, the positive charge carrier or negative charge carrier can get trapped respectively in the dye on carrier injection. The trapped carrier can eventually recombine with its conjugate one to form dye bound excitons. This carrier trapping mechanism can occur any time parallel to the aforementioned Förster or Dexter energy transfer. The probability of transfer via this radiative transfer process is given approximately by:

$$P_{r,t} \propto [A]xJ \quad (1)$$

where J is the spectral overlap integral, $[A]$ is the concentration of the acceptor, and x is the specimen thickness^{60,61}.

In the case of Förster energy transfer⁶², transition dipole moments for excited donor and the dye in its ground state undergo dipole-dipole coupling. As the excited donor relaxes, the excitonic energy is transferred via a strong Coulombic interaction to the dye molecule. This dipole-dipole interaction can allow the transfer up to a distance of 100 Å. The transfer rate constant $k_D \rightarrow A$ is given by:

$$k_D \rightarrow A = \frac{K^2 J 8.8 \times 10^{-28} \text{ mol}}{n^4 \omega r^6} \quad (2)$$

where K is an orientation factor, n the refractive index of the medium, ω the radiative lifetime of the donor, r the distance (cm) between donor (D) and acceptor (A), and J the spectral overlap (in coherent units $\text{cm}^6 \text{ mol}^{-1}$) between the absorption spectrum of the acceptor and the fluorescence spectrum of the donor^{60,61}. In addition, an exciton can diffuse several times the dye molecule's Förster radius. Therefore, the exciton formed outside the Förster radius of the

nearest dye dopant can migrate to a position close enough to the dopant and make the energy transfer before it relaxes.

Energy transfer by carrier exchange mechanism is the Dexter transfer⁵⁸. Electron transfer between the donor and acceptor bring the donor to the ground state and acceptor to the electronic excited state. An overlap between donor and acceptor wave functions are required.

The transfer rate constant, k_{ET} , is given by:

$$k_{ET} \propto [h/(2\pi)] P^2 J \exp[-2r/L] \quad (3)$$

where r is the distance between the donor (D) and acceptor (A), L and P , and J is the spectral overlap integral⁶¹. The rate of energy transfer by Dexter mechanism drops significantly down beyond 15-20 Å. Unlike Förster, which requires both the donor and the acceptor states to be singlets, Dexter transfer can occur between triplet states as well as singlet states. In either of these cases, Dexter transfer is significantly faster than Förster. Nevertheless, at large distances, Förster transfer will be the only prevailing mechanism as the Dexter transfer will require carrier exchange.

The earliest demonstration of bi-layer⁴⁷ and tri-layer^{63,64} EL devices following the first report on OLED were single emitter devices. Undoped devices might seem to be preferable over doped as it can offer ease of fabrication due to its simplified processing as well as the performance reliability. But, most of the highest efficiency OLEDs reported were doped devices^{65,66}. Controlled doping can reduce self-quenching in the emitter and generate narrow emission spectrum. By doping, tuning the electrical properties of host materials and optical properties of dopants separately become possible, and the dopants also can prevent crystallization of the host. Thus, the quantum efficiency and the device lifetime can be improved.

1.4.2 Fluorescent and phosphorescent devices

Most of the luminescent materials are fluorescent as they have weak spin-orbit coupling and singlet ground states. Due to spin conservation and multiplicities, only 25% of the injected carriers are predicted to result in fluorescence. The remaining 75% can potentially give phosphorescence from its triplet states^{67,68}. Therefore, as decay of triplet excitons is forbidden in fluorescent OLED, theoretical maximum of internal quantum efficiency (IQE) is 25%, resulting in a maximum of 5% of external quantum efficiency due to the light extraction losses. On the other hand, phosphorescent OLEDs (PhOLEDs) in theory can reach 100% IQE, as both singlets as well as triplet can be used for emission⁶⁹. Baldo et al. was the first to report a PhOLED, doped a phosphorescent dye 2,3,7,8,12,13,17,18-octaethyl-21H,23H-porphine platinum(II) (PtOEP) achieving maximum internal and external quantum efficiencies of 4% and 23%, respectively⁷⁰. Due the large spin-orbit coupling of the heavy Pt, it can facilitate intersystem crossing to enable phosphorescence. This is why commonly used phosphorescent materials are organometallic complexes⁷¹, like iridium (Ir(III)),⁷² osmium (Os(II)),⁷³ gold (Au(III)),⁷⁴ ruthenium (Ru(II)),⁷⁵ and copper (Cu(I))⁷⁶ complexes, most of which suffer from concentration quenching⁷⁷.

However, PhOLED device structure is often complex with several layers tailored for carrier transport, carrier confinement, etc. as the triplet excitons have longer diffusion length and the materials have higher triplet energy, which makes the exciton confinement in emission layer difficult. But, its potential high efficiency makes it a commercial favourite. The main challenges faced by PhOLEDs are that i) they have very high efficiency roll-off, ii) the phosphorescent materials are highly expensive, and iii) phosphorescent blue OLED has very short lifetime. A viable alternative for PhOLED is thermally activated delayed fluorescence (TADF) based OLEDs, which was introduced by Adachi and his workers^{78,79}.

Using completely pure organic materials, they could achieve around 20% external quantum efficiency (EQE). When the energy gap between singlets and triplets is very low, it can facilitate reverse intersystem crossing (RISC), which is the non-radiative up conversion from from lowest triplet to lowest singlet state, resulting in a second fluorescence, which is delayed. Therefore, TADF materials can harvest both singlets as well as triplets. Now, TADF based OLEDs have reached high EQE values of 37.8% for a green device,⁸⁰ 29.2% for a red device,⁸¹ and 37% for a sky-blue device⁸².

1.4.3 Tandem devices

In 1997, Forrest et al.,⁸³ reported a device with vertically stacked 12 layers which are independently tunable, which initiated studies on similar structures where each unit was independently controlled.^{84,85} However, the first real tandem OLED was proposed by Kido et al. in 2003⁸⁶, who reported that when an OLED was fabricated by three EL stacks separated by two charge generation layers (CGL), the quantum efficiency was observed to have a three times enhancement. On applying an electric field, in addition to the injected pair of charge carriers, an extra pair per CGL was created, which were transferred to the nearby EL unit. Thus, CGL acts as virtual electrodes, resulting in the generation of multiple photons per injected electrons.^{86,87} Due to this, tandem devices can achieve efficiencies over 100% with a longer lifetime than conventional devices. The latter is due to the higher luminescence at comparatively lower current density. Materials like ITO,^{86,87} vanadium pentoxide (V_2O_5),^{86,88} molybdenum oxide (MoO_3),^{89,90} and 2,3,5,6-tetrafluoro-7,7,8,8-tetracyanoquinodimethane (F4-TCNQ),⁹¹ etc. were explored as potential CGL⁹² giving possible combinations of doped organic/metal oxide^{89,90,92-108}, doped organic/(doped) organic bilayer^{91,109-127}, un-doped¹²⁸⁻¹³⁸, organic semiconductor heterojunction¹³⁹⁻¹⁴⁹. Now tandem white OLEDs have recorded EQE

values as high as 74% and 170% for a device without and with outcoupling (averaging at 34.2% per stack), respectively¹⁵⁰.

1.4.4 p-i-n devices

Similar to the case with conventional semiconductors, doping of organic semiconductor to achieve efficient carrier injection and transport led to the breakthrough of organic semiconductor technology. Controlled doping can increase the conductivities of transport layers by many orders of magnitude. Conductivities achieved are high enough to avoid significant voltage drops even across thicker layers. Here, basic doping effects like Fermi level shifts can also be observed. Doping can generate Ohmic contacts at the interface by tunneling through a thin barrier formed by space charge layers. p-doping was first attempted in 1954 using halogen gases¹⁵¹, later followed by more of the same^{152,153} and oxygen^{154,155} as well. First reported organic p-dopant was ortho-chloranil in 1960¹⁵⁶. Instead of molecular p-dopant, which contains strong electronegative elements like fluorine, metal oxides like MoO₃, WO₃, etc. also were explored¹⁵⁷⁻¹⁵⁹. Successful n-doping for the first time, on the other hand, was reported long afterwards in 1990 using Cs¹⁶⁰ and other alkali metals¹⁶¹, which tend to diffuse into the emission layer⁵. This can be overcome by using heavy molecular dopants, the first of which was reported only in 2000¹⁶². This is because, to become an effective n-dopant, molecules have to have high HOMO level close to the LUMO of the host material, and as a consequence very high LUMO levels, which make the dopant unstable. This is why molecular n-dopants are rare and expensive. For n-doping, dopant donates an electron from its HOMO to the LUMO of the host, and in the case of p-doping, accepts an electron from the HOMO of the host to its LUMO. Thus, transport doping requires suitable alignment of the energy levels of the host and dopant.

In p-i-n type OLED, both hole and electron transport layers are doped which sandwich the emission layer along with respective blocking layer. Whereas the doped transport layer confirms efficient charge carrier injection and transport, the blocking layers support the proper confinement of carriers as well as generated excitons. Transport doping in OLED was first reported in 1998 by introducing p-doping the hole transport layer, phthalocyanine by F4-TCNQ by Karl Leo's group¹⁶³. Kido's group later reported OLEDs with lithium (Li), strontium (Sr), and samarium (Sm)-doped Alq₃ as electron transport layer¹⁶⁴. Karl Leo and co-workers reported the first p-i-n OLED^{165,166} in 2002 using, F4-TCNQ as p-dopant and Li as n-dopant. The tris(phenylpyridine)iridium(Ir(ppy)₃) based device structure could yield an efficiency of 27 lm/W at 1000 cd/m² luminescence and only 3 V. The work was followed by using F4-TCNQ and Cs as both p and n-dopant respectively and modifying the green device structure to achieve maximum efficiencies up to 53 lm/W¹⁶⁷ and 77 lm/W¹⁶⁸. Later on, most of the device structures reporting high efficiency red,¹⁶⁹⁻¹⁷¹ green^{172,173}, blue¹⁷⁴⁻¹⁷⁶, and white¹⁷⁷⁻¹⁷⁹ OLEDs have been p-i-n structures¹⁸⁰.

1.4.5 Current status: White OLED (WOLED)

Since the first reports of white-emitting devices by the Kido et al^{181,182}, many approaches to fabricate white light emitting OLEDs have been pursued. The initial devices exhibited efficiencies <1 lm/W which has grown to >50 lm/W over the last few years¹⁸³ and now white emission from OLEDs can be achieved in both small molecule and polymer systems. Wu et al. fabricated an eight-layer device stack containing two emissive blue layers and a complementary yellow emissive layer to give two-colour white, where the multiple charge-transport/blocking layers served to suppress the change in EL spectra with driving current density¹⁸⁴. The device achieved efficiencies of 3.9% EQE, 9.9 cd/A, 2.7 lm/W and CIE coordinates of (0.31, 0.41). The emissive materials in this device are the fluorescent molecules

2,8-Di-tert-butyl-5,11-bis(4-tert-butylphenyl)-6,12-diphenyltetracene (TBRb) (yellow) and 1-4-di-[4-(N,N-diphenyl)amino]styryl-benzene (DSA-Ph) (blue). Karl Leo and co-workers combined the fluorescent blue arylamine 4P-NPD¹⁸⁵ with green and orange iridium in a p-i-n structure to obtain outcoupled devices, which recorded a power efficiency of 32 lm/W and EQE 14% for CIE of (0.43, 0.43) and colour rendering index (CRI) of 82¹⁷⁹. Another modification placed a blue phosphor (Flrpic) with the emission layer placed further away from the reflective cathode and improved outcoupling. An impressive power efficiency of 90 lm/W was achieved with colour coordinates (0.44, 0.46) and CRI of 80 at 1000 cd/m². The short operating lifetimes were explained by the degradation of the Flrpic emission¹⁸⁶.

Tandem devices comprise two or more stacks layered on top of each other with CGLs between them. These stacked devices can achieve white emission either through multiple white layers to improve device lifetime, or by individual primary or complementary colour stacks which can be independently driven from different voltage sources¹⁴¹. Kido et al. demonstrated eight-stack devices that show long device lifetimes brought about by possessing multiple backup stacks in case a stack fails¹⁴². A 3-layer composition of 1,4,5,8,9,11-Hexaazatriphenylenehexacarbonitrile (HAT-CN)/ HAT-CN: 4,4'-Cyclohexylidenebis [N,N-bis(4-methylphenyl)benzenamine] (TAPC)/ TAPC was found to be an effective CGL where the middle layer is found to be enhancing charge generation and separation. At 1000 cd/m², the power efficiency of the three layers CGL based device was 113 lm/W, whereas that of the single unit device was 76 lm/W and an 86 lm/W for HAT-CN/ TAPC based tandem device. The former device exhibited a maximum current efficiency of 286 cd/A with 266 cd/A at 10000 cd/m² luminance^{149,187}.

Another approach to obtain broad emission from a single component is through excimers. While fluorescent excimers display much lower efficiency than that of the corresponding

monomer, phosphorescent excimers show good efficiencies. Devices with an emission layer of square planar platinum complexes can stack at high doping levels leading to emission from both the isolated complex molecules and red-shifted emission from the excimer. Jabbour et al. used a pyridine-analog as host, obtaining devices with 16% EQE (12 lm/W, 38cd/A) at a rather high drive voltage, i.e., 9.4 V for 500 cd/m².¹⁸⁸ The colour coordinates of (0.46, 0.47) demonstrated poor CRI of 69. The same group subsequently added another platinum complex in a vacuum-deposited device structure ITO/ Poly(3,4-ethylenedioxythiophene)-poly(styrenesulfonate) (PEDOT:PSS)/ TCTA/ complex1 (8%): complex2(2%)/ Bathocuproine (BCP)/ Cesium fluoride (CsF)/ Al, which showed an EQE of 14.5% (17 lm/W) at 500 cd/m² with CIE of (0.38, 0.40). CRI was improved to 81, which was almost independent of drive voltage in the range 2–7 V¹⁸⁹. Efficient white emission has been achieved from a single (vacuum deposited) emissive layer comprised of an electron donor and a phosphorescent electron acceptor, where it was possible to create exciplexes displaying a broad emission spectrum located between monomer and excimer spectra of the phosphor. Three different emissive states are produced efficiently at the same time: (i) molecular excitons (3A*) producing monomer phosphorescence, (ii) triplet excimers 3(AA)*, and (iii) an exciplex 3(DA)*. A maximum EQE of 6.5% was reported at very low luminance (0.1 cd/m²) changing to 3% at 500 cd/m². Devices displayed CIE coordinates (0.46, 0.46) and CRI of 88 at 16 V. At this high voltage, low device lifetimes would be expected. A new triaryl molecule based on benzene–benzothiadiazole–benzene core has been applied in a WOLED device. This very simple molecule emits from a combination of emissive states (exciton/electromer/exciplex/electroplex) to give white light with CIE coordinates of (0.38, 0.45) and a colour temperature of 4500 K¹⁹⁰.

In 2015, Cho et al. have also reported highly efficient WOLEDs based on the blue 4,6-di(9H-carbazol-9-yl)isophthalonitrile (DCzIPN) TADF dye acting both as a blue emitter and

a host for the yellow iridium phosphor PO-01¹⁹¹. In particular, the device architecture includes three stacked layers of DCzIPN, the central one embedded with the yellow emitting PO-01 complex. It has been reported that it is possible to manage electroluminescence from warm to cool white colour by properly changing the thickness of the central yellow emitting layer. High external quantum efficiencies (21.0 % and 22.9 %) have been observed for the cool and the warm white light emitting devices, respectively showing CIE coordinates (0.31, 0.33) and (0.39, 0.43). A rational device concept of organic WOLEDs based on conventional deep blue and red-fluorescent materials combined with a green TADF emitter to manipulate the excitons for blue, green, and red emission, respectively was reported utilizing a chromaticity adjustable TADF material PXZDSO2 (2-(4-phenoxazinephenyl) thianthrene-9,9',10,10'-tetraoxide)^{192,193}. A maximum EQE of 15.8% was achieved for two-colour pure organic WOLEDs consisting of yellow emission PXZDSO2 and a conventional deep-blue-fluorescence emitter NI-1-PhTPA.

1.5 OLED: Structure and operation

A typical OLED structure consists of organic layers between two electrodes, at least one of which being transparent. The devices are fabricated on glass or plastic substrates. The basic requirement only necessitates a single electroluminescent layer between the electrodes, but multilayer structures are essential for good device performance as well as emission tuning. In that convention, the organic layers should consist of materials, apart from emitting layer, for effortless charge carrier injection, carrier transport, and carrier blocking. In some of the modern architecture, sometimes a single material or a single layer consisting of a combination of different materials plays more than one of these functions and sometimes more than one material/layer plays a single function, depending on the material energy levels, carrier mobilities, etc. In that sense, we can assume the typical

structure to comprise of all these layers separately for posterity's sake as shown in Fig 1.2a, consisting of cathode, electron injection layer (EIL), electron transport layer (ETL), hole blocking layer (HBL), emission layer EML), electron blocking layer (EBL), hole transport layer (HTL), hole injection layer (HIL), and anode.

A simplified diagram depicting the operation of OLED is given in Fig 1.2b, which starts with charge carrier injection from the anode (hole) and the cathode (electron) to the HOMO of hole injection layer and LUMO of electron injection layer, respectively. The injected hole is transported through the hole transport layer and the injected electron through the electron transport layer to the EML, where the carriers recombine together to form excitons. Radiative relaxation of these excitons, through either fluorescence or phosphorescence, causes light emission. The blocking layer confines the carriers to the EML to confirm that the recombination is happening only there. The brightness of emission depends on the current, because of which OLEDs are usually driven under constant current source.

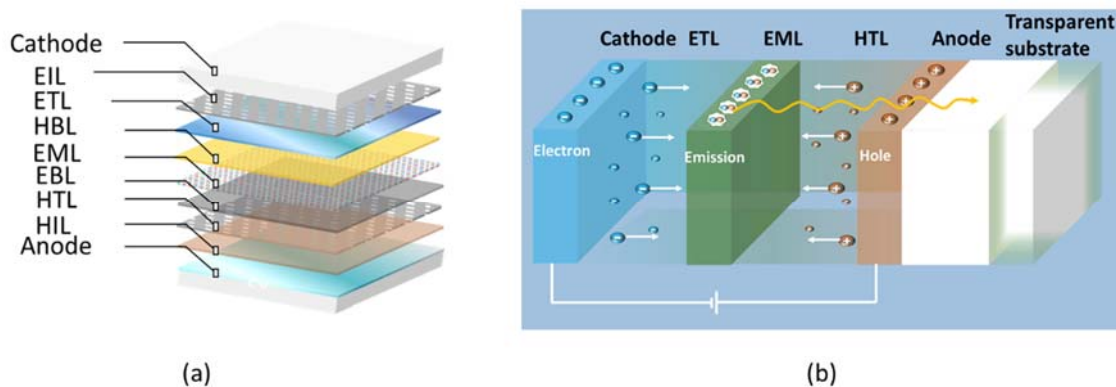


Figure 1.2 a) A typical OLED structure, and b) OLED device operation diagram

If the anode is transparent, the device structure is bottom emitting, and for a transparent cathode, the structure is called top emitting. Both of these electrodes can also be made transparent depending on the device application. The selection of these electrodes depends on the work function, transparency, film morphology and most importantly, conductivity. For a conventional bottom-emitting structure, ITO, which is transparent and having a high work

function, is usually used as anode and Al, calcium (Ca), barium (Ba), etc., which have low work function, are used as cathodes. This helps to match the work functions of the electrodes to the HOMO and LUMO of HIL and EIL, respectively, so that carrier injection will be most efficient. Here, utmost care has to be given in selecting the different organic layer, which can be tailored to the successive layers in energy levels as well as mobility values to make sure that an equal number of holes and electrons are reaching the EML in order to maintain the carrier balance in the device.

1.6 Remaining challenges

Despite its advantages, OLED technology still needs improvement on a lot of facets, including the cost-effectiveness. Most of the hurdles faced by this disruptive technology can be classified under its high cost compared to the alternatives. Material-wise, blue emitters are the weakest link, especially the phosphorescent blue, as they are the most unstable. A main contributor to the 'blue emitter problem' lies in finding a suitable host material having high triplet energy as well as deep HOMO-LUMO gap to efficiently confine the excitons generated in the dopant. This is why most of the commercially available RGB configuration use a hybrid structure with fluorescent blue emitters. However, as fluorescent emitters suffer from lower efficiencies, these hybrid devices waste at least half of the input power. Another material related challenge is to improve the solubility of these materials, which is required if the devices were to be printed. As most of the efficient small molecule materials have poor solubility in any solvent, there is still a long way to go.

The refractive index mismatch between different organic layers, electrodes, and substrates causes trapping of the emitted light due to different optical modes. By the basic device structure, only 20% of the light generated within can be extracted to outside. That is, even with the usage of most efficient materials and optimized device design, major

percentage of the generated light is getting lost. Therefore, poor extraction efficiency became another hurdle to further improvement and subsequent commercialization of OLED. Several internal and external extraction techniques like the usage of shaped substrates,¹⁹⁴ backside substrate modification,^{195,196} light scattering layers¹⁹⁷, internal extraction layers¹⁹⁸ ordered dielectric structure of silica microspheres,¹⁹⁹ attachment of microlens array to the glass substrate²⁰⁰, etc. were developed in order to increase the light extraction efficiencies of OLEDs. These structures either suppress or scatter the optical modes responsible for the loss in emission, essentially reducing the refractive index mismatch, recovering up to 70% of the extraction efficiency²⁰¹ in some rare cases. However, in most of the cases, extraction efficiency stays around 30%, especially for white OLED. By employing the currently available techniques, only some of the losses like substrate modes could be addressed. So, developing practical and inexpensive light extraction techniques for other loss modes, by developing the complete understanding of the physics behind them to optimize the device design needs to be performed. Also, more work is required to integrate the working outcoupling techniques in a practical and efficient manner, without affecting device performance.

As mentioned before, to make the OLED technology commercially viable, the production cost has to be brought down. One way to do it is to replace expensive materials and reducing the number of materials as well as fabrication steps. This has the potential to improve the production yield. Nowadays, majority of the efficient device structures demand transport doping. As the dopant materials, especially n-dopants are expensive, developing inexpensive alternatives are the need of the hour along with a deeper understanding of the efficiency roll-off. A detailed study of charge carrier recombination zone, as well as emission zone, can also help in reducing the material wastage by optimizing the device design. Only by overcoming these technical barriers can we bring this energy efficient and environment friendly technology to the main stream.

1.7 Theme of the thesis

The fluorescent OLEDs (FOLED) are still of considerable interest, despite the availability of highly efficient phosphorescent devices, due to longer material and device lifetime, low-efficiency roll-off and low-cost. In this thesis, different methods to improve the efficiency and stability of fluorescent OLEDs, simultaneously reducing the cost is explored.

Chapter 2 discusses facile and inexpensive doping procedures in FOLED. The potential of inexpensive lithium fluoride (LiF) to act as an n-dopant is explored by separating ETL into two parts and keeping the undoped buffer layer between doped ETL and EML. The device design is optimized for the thickness of the doping layer as well as the doping percentage. Various electron-blocking layers are employed, and suitable EBL is selected to improve the carrier balance in the device by efficient exciton confinement.

Chapter 3 discusses the influence of deposition parameters in the device performance as well as emission tuning and the inherent interplay of electrical and optical properties. Here, by varying the dopant concentration in the EML and EML thickness as well as the rate of deposition, we have tuned the FOLED emission from pure excitonic to excimeric one. Great flexibility is observed in the tuning, which helped to reduce the number of process steps as well as the material wastage. A potential for white emission with such a simplified architecture is established.

Chapter 4 explores exciton confinement, diffusion, and field induced effects in a FOLED by mapping its singlet and triplet emission zone. Such a study can be instrumental in optimizing the EML of devices as the emitters outside emission zone can affect emission as well as carrier transport. We have harvested both singlet and triplet excitons in the device

simultaneously and completely suppressed the host emission, by using these emission zone maps.

1.8 Future directions

Thermally activated delayed fluorescence (TADF) is an endothermal radiative exciton transition from the S1 state (delayed fluorescence) following non-radiative T1 to S1 transfer (reverse intersystem crossing-RISC), which was known from early 1960s itself²⁰². The actual concept of TADF for a working OLED was first realized by Adachi's group in 2009⁷⁸ which demonstrated that the delayed fluorescence can be used to effectively harvest both singlets as well as triplets. Therefore, TADF based OLEDs have the potential to reach 100% internal quantum efficiency like PhOLED, without the inherent problems like cost and efficiency roll-off as TADF materials are purely organic²⁰³. This also brings great flexibility in emission tuning as, unlike phosphorescent materials, these fully organic materials can be easily modified to suit the need. By integrating to an exciplex system, the devices can have external quantum efficiencies as high as 20-30%²⁰⁴⁻²⁰⁷ as opposed to the 5% for the conventional fluorescent devices. These impressive results have classified TADF materials as the third generation OLED materials²⁰⁸ making it the future of OLED materials.

The future of OLED device fabrication, on the other hand, lies with printing. Developing the field of organic printed electronics can find purpose in a long range of applications, especially in commercializing inexpensive displays, lights and wearable sensors. But the main challenge is that the majority of the available highly efficient materials are insoluble and cannot be used for solution processing. So, first step in the right direction will be to make these materials soluble or to develop new materials. Such solution-processed devices can potentially utilize the simple and high yield infrastructure developed by the printing industry to realize the

large area fabrication at low cost, with reduced material wastage and process complexity resulting in cost reduction.

1.9 Summary

Monumental progress has been recorded in the development of science and technology of OLEDs since its inception, especially in the last decade, to develop high-quality flat panel displays and innovative luminaire designs. This caused the current commercialization of OLED displays. OLEDs can be used to fabricate large area structures with high brightness and good chromaticity along with unique form factors, which address most of the challenges faced by inorganic LEDs, especially as recent reports show that the LED lights are photo-toxic and the continued exposure to the same poses a risk of eye damage. Even though this green technology can improve quality of life, the current high cost of the same makes it unattainable for the common people. So, challenges including cost-effectiveness need to be addressed to make it more accessible. This thesis is an attempt to do so by investigating different device engineering techniques.

1.10 References

- 1 Kallmann, H. & Pope, M. Bulk Conductivity in Organic Crystals. *Nature* **186**, 31-33, doi:10.1038/186031a0 (1960).
- 2 Kallmann, H. & Pope, M. Positive Hole Injection into Organic Crystals. *The Journal of Chemical Physics* **32**, 300-301, doi:10.1063/1.1700925 (1960).
- 3 Hideo, A., Hiroo, I. & Yoshio, M. Organic Semiconductors with High Conductivity. I. Complexes between Polycyclic Aromatic Hydrocarbons and Halogens. *Bulletin of the Chemical Society of Japan* **29**, 213-218, doi:10.1246/bcsj.29.213 (1956).

- 4 Heeger, A. J., Kivelson, S., Schrieffer, J. R. & Su, W. P. Solitons in conducting polymers. *Reviews of Modern Physics* **60**, 781-850, doi:10.1103/RevModPhys.60.781 (1988).
- 5 Walzer, K., Maennig, B., Pfeiffer, M. & Leo, K. Highly Efficient Organic Devices Based on Electrically Doped Transport Layers. *Chemical Reviews* **107**, 1233-1271, doi:10.1021/cr050156n (2007).
- 6 Shirakawa, H., Louis, E. J., MacDiarmid, A. G., Chiang, C. K. & Heeger, A. J. Synthesis of electrically conducting organic polymers: halogen derivatives of polyacetylene, (CH). *Journal of the Chemical Society, Chemical Communications*, 578-580, doi:10.1039/C39770000578 (1977).
- 7 Foundation, N. *The Nobel Prize in Chemistry*, <<https://www.nobelprize.org/prizes/chemistry/2000/8953-nobelprize-org-the-nobel-prize-in-chemistry-2000/>> (2000).
- 8 Forrest, S. R. The path to ubiquitous and low-cost organic electronic appliances on plastic. *Nature* **428**, 911-918, doi:10.1038/nature02498 (2004).
- 9 Rand, B. P., Genoe, J., Heremans, P. & Poortmans, J. Solar cells utilizing small molecular weight organic semiconductors. *Progress in Photovoltaics: Research and Applications* **15**, 659-676, doi:10.1002/pip.788 (2007).
- 10 Peumans, P., Yakimov, A. & Forrest, S. R. Small molecular weight organic thin-film photodetectors and solar cells. *Journal of Applied Physics* **93**, 3693-3723, doi:10.1063/1.1534621 (2003).
- 11 Gregg, B. A. Excitonic Solar Cells. *The Journal of Physical Chemistry B* **107**, 4688-4698, doi:10.1021/jp022507x (2003).
- 12 Kallmann, H. & Pope, M. Surface-controlled Bulk Conductivity in Organic Crystals. *Nature* **185**, 753-753, doi:10.1038/185753a0 (1960).
- 13 Edgar, L. J. Method and apparatus for controlling electric currents. (1930).

- 14 Kahng, D. & Atalla, M. in *Solid-state devices research conference* (Carnegie Institute of Technology, Pittsburgh, 1960).
- 15 Koezuka, H., Tsumura, A. & Ando, T. Field-effect transistor with polythiophene thin film. *Synthetic Metals* **18**, 699-704, doi:10.1016/0379-6779(87)90964-7 (1987).
- 16 Hepp, A. Heil H, Weise W, Ahles M, Schmechel R & von Seggern H. Light-Emitting Field-Effect Transistor Based on a Tetracene Thin Film. *Physical Review Letters* **91**, 157406, doi:10.1103/PhysRevLett.91.157406 (2003).
- 17 Becquerel, A. E. Memoire sur les Effects d'Electriques Produits Sous l'Influence des Rayons Solaires. *Comptes Rendus de l'Academie des Sciences* **9**, 561-567 (1839).
- 18 Pochettino, A. Atti reale Accad. **1**, 355 (1906).
- 19 Hoegl, H. On Photoelectric Effects in Polymers and Their Sensitization by Dopants I. *The Journal of Physical Chemistry* **69**, 755-766, doi:10.1021/j100887a008 (1965).
- 20 Chapin, D. M., Fuller, C. S. & Pearson, G. L. A New Silicon p-n Junction Photocell for Converting Solar Radiation into Electrical Power. *Journal of Applied Physics* **25**, 676-677, doi:10.1063/1.1721711 (1954).
- 21 Yoshikawa, K. *et al.* Silicon heterojunction solar cell with interdigitated back contacts for a photoconversion efficiency over 26%. *Nature Energy* **2**, 17032, doi:10.1038/nenergy.2017.32 (2017).
- 22 Minami, N., Sasaki, K. & Tsuda, K. Improvement of the performance of particulate phthalocyanine photovoltaic cells by the use of polar polymer binders. *Journal of Applied Physics* **54**, 6764-6766, doi:10.1063/1.331871 (1983).
- 23 Sasabe, H., Furuno, T. & Takimoto, K. Photovoltaics of photoactive protein/polypeptide LB films. *Synthetic Metals* **28**, 787-792, doi:10.1016/0379-6779(89)90605-X (1989).
- 24 Tang, C. W. Two-layer organic photovoltaic cell. *Applied Physics Letters* **48**, 183-185, doi:10.1063/1.96937 (1986).

- 25 Horowitz, G. Organic Semiconductors for new electronic devices. *Advanced Materials* **2**, 287-292, doi:10.1002/adma.19900020604 (1990).
- 26 Meng, L. *et al.* Organic and solution-processed tandem solar cells with 17.3% efficiency. *Science* **361**, 1094-1098, doi:10.1126/science.aat2612 (2018).
- 27 Bernanose, A., Comte, M. & Vouaux, P. Sur un nouveau mode d'émission lumineuse chez certains composés organiques. *Journal de Chimie Physique*. **50**, 64-68 (1953).
- 28 Bernanose, A. & Vouaux, P. Électroluminescence organique : étude du mode d'émission. *Journal de Chimie Physique*. **50**, 261-263 (1953).
- 29 Bernanose, A. Sur le mécanisme de l'électroluminescence organique. *Journal de Chimie Physique*. **52**, 396-400 (1955).
- 30 Mark, P. & Helfrich, W. Space-Charge-Limited Currents in Organic Crystals. *Journal of Applied Physics* **33**, 205-215, doi:10.1063/1.1728487 (1962).
- 31 Pope, M., Kallmann, H. P. & Magnante, P. Electroluminescence in Organic Crystals. *The Journal of Chemical Physics* **38**, 2042-2043, doi:10.1063/1.1733929 (1963).
- 32 Partridge, R. H. Electroluminescence from polyvinylcarbazole films: 1. Carbazole cations. *Polymer* **24**, 733-738, doi:10.1016/0032-3861(83)90012-5 (1983).
- 33 Partridge, R. H. Electroluminescence from polyvinylcarbazole films: 2. Polyvinylcarbazole films containing antimony pentachloride. *Polymer* **24**, 739-747, doi:10.1016/0032-3861(83)90013-7 (1983).
- 34 Partridge, R. H. Electroluminescence from polyvinylcarbazole films: 3. Electroluminescent devices. *Polymer* **24**, 748-754, doi: 10.1016/0032-3861(83)90014-9 (1983).
- 35 Partridge, R. H. Electroluminescence from polyvinylcarbazole films: 4. Electroluminescence using higher work function cathodes. *Polymer* **24**, 755-762, doi: 10.1016/0032-3861(83)90015-0 (1983).

- 36 Capelli, R. *et al.* Organic light-emitting transistors with an efficiency that outperforms the equivalent light-emitting diodes. *Nature materials* **9**, 496, doi:10.1038/nmat2751 (2010).
- 37 McCarthy, M. A. *et al.* Low-Voltage, Low-Power, Organic Light-Emitting Transistors for Active Matrix Displays. *Science* **332**, 570-573, doi:10.1126/science.1203052 (2011).
- 38 Dinelli, F. *et al.* High-Mobility Ambipolar Transport in Organic Light-Emitting Transistors. *Advanced Materials* **18**, 1416-1420, doi:10.1002/adma.200502164 (2006).
- 39 Xu, J. *et al.* Layered, Nanonetwork Composite Cathodes for Flexible, High-Efficiency, Organic Light Emitting Devices. *Advanced Functional Materials* **25**, 4397-4404, doi:10.1002/adfm.201501068 (2015).
- 40 Larson, C. *et al.* Highly stretchable electroluminescent skin for optical signaling and tactile sensing. *Science* **351**, 1071-1074, doi:10.1126/science.aac5082 (2016).
- 41 Alarcón-Salazar, J., Zaldívar-Huerta, I. E. & Aceves-Mijares, M. An optoelectronic circuit with a light source, an optical waveguide and a sensor all on silicon: Results and analysis of a novel system. *Optics & Laser Technology* **84**, 40-47, doi:https://doi.org/10.1016/j.optlastec.2016.04.013 (2016).
- 42 Tang, S. *et al.* Design rules for light-emitting electrochemical cells delivering bright luminance at 27.5 percent external quantum efficiency. *Nature communications* **8**, 1190, doi:10.1038/s41467-017-01339-0 (2017).
- 43 Liu, J. *et al.* Multi-Coloured Light-Emitting Electrochemical Cells Based on Thermal Activated Delayed Fluorescence Host. *Scientific reports* **7**, 1524, doi:10.1038/s41598-017-01812-2 (2017).
- 44 Shu, Z., Pabst, O., Beckert, E., Eberhardt, R. & Tünnermann, A. Inkjet Printed Organic Light-emitting Electrochemical Cells for Disposable Lab-on-chip Applications Manufactured at Ambient Atmosphere¹. *Materials Today: Proceedings* **3**, 733-738, doi:https://doi.org/10.1016/j.matpr.2016.02.004 (2016).

- 45 Tang, C. W. Organic electroluminescent cell (1980).
- 46 VanSlyke, S. A. & Tang, C. W. Organic electroluminescent devices having improved power conversion efficiencies (1983).
- 47 Tang, C. W. & VanSlyke, S. A. Organic electroluminescent diodes. *Applied Physics Letters* **51**, 913-915, doi:10.1063/1.98799 (1987).
- 48 Burroughes, J. H. *et al.* Light-emitting diodes based on conjugated polymers. *Nature* **347**, 539-541, doi:10.1038/347539a0 (1990).
- 49 Braun, D. & Heeger, A. J. Visible light emission from semiconducting polymer diodes. *Applied Physics Letters* **58**, 1982-1984, doi:10.1063/1.105039 (1991).
- 50 Braun, D., Moses, D., Zhang, C. & Heeger, A. J. Nanosecond transient electroluminescence from polymer light-emitting diodes. *Applied Physics Letters* **61**, 3092-3094, doi:10.1063/1.107971 (1992).
- 51 Sariciftci, N. S. *et al.* Semiconducting polymer-buckminsterfullerene heterojunctions: Diodes, photodiodes, and photovoltaic cells. *Applied Physics Letters* **62**, 585-587, doi:10.1063/1.108863 (1993).
- 52 Chen, S.-Z. *et al.* Organic light-emitting diodes with direct contact-printed red, green, blue, and white light-emitting layers. *Applied Physics Letters* **101**, 153304, doi:10.1063/1.4757279 (2012).
- 53 Budzelaar, F. P. M. *et al.* Video processing for active-matrix polymer OLED TV. *Journal of the Society for Information Display* **14**, 461-466, doi:10.1889/1.2206110 (2006).
- 54 Spreitzer, H. *et al.* Soluble Phenyl-Substituted PPVs—New Materials for Highly Efficient Polymer LEDs. *Advanced Materials* **10**, 1340-1343, doi:10.1002/(sici)1521-4095(199811)10:16<1340::aid-adma1340>3.0.co;2-g (1998).
- 55 Pei, Q. & Yang. Efficient Photoluminescence and Electroluminescence from a Soluble Polyfluorene. *Journal of the American Chemical Society* **118**, 7416-7417, doi:10.1021/ja9615233 (1996).

- 56 *Polyfluorenes*. (Springer, Heidelberg, 2009).
- 57 Nilar, S. H. & Dharma-wardana, M. W. C. Electronic structure calculations of doped organic materials for electroluminescent devices. *Journal of Applied Physics* **82**, 514-521, doi:10.1063/1.365609 (1997).
- 58 Dexter, D. L. A Theory of Sensitized Luminescence in Solids. *The Journal of Chemical Physics* **21**, 836-850, doi:10.1063/1.1699044 (1953).
- 59 Kawabe, M., Masuda, K. & Namba, S. Electroluminescence of Green Light Region in Doped Anthracene. *Japanese Journal of Applied Physics* **10**, 527-528, doi:10.1143/jjap.10.527 (1971).
- 60 *Exciton Diffusion - Mit Opencourseware*, <<https://ocw.mit.edu/courses/electrical-engineering-and-computer-science/6-973-or>>
- 61 McNaught, A. D. & Wilkinson, A. (Royal Society of Chemistry, Cambridge, UK, 1997).
- 62 Birks, J. B. *Photophysics of aromatic molecules*. (Wiley-Interscience, 1970).
- 63 Adachi, C., Tokito, S., Tsutsui, T. & Saito, S. Electroluminescence in Organic Films with Three-Layer Structure. *Japanese Journal of Applied Physics* **27**, L269-L271, doi:10.1143/jjap.27.l269 (1988).
- 64 Adachi, C., Tokito, S., Tsutsui, T. & Saito, S. Organic Electroluminescent Device with a Three-Layer Structure. *Japanese Journal of Applied Physics* **27**, L713-L715, doi:10.1143/jjap.27.l713 (1988).
- 65 Peng, T. *et al.* Highly efficient phosphorescent OLEDs with host-independent and concentration-insensitive properties based on a bipolar iridium complex. *Journal of Materials Chemistry C* **1**, 2920-2926, doi:10.1039/C3TC00500C (2013).
- 66 Adachi, C., Baldo, M. A. & Forrest, S. R. Electroluminescence mechanisms in organic light emitting devices employing a europium chelate doped in a wide energy gap bipolar conducting host. *Journal of Applied Physics* **87**, 8049-8055, doi:10.1063/1.373496 (2000).

- 67 Brown, A. R. *et al.* Optical spectroscopy of triplet excitons and charged excitations in poly(p-phenylenevinylene) light-emitting diodes. *Chemical Physics Letters* **210**, 61-66, doi:[https://doi.org/10.1016/0009-2614\(93\)89100-V](https://doi.org/10.1016/0009-2614(93)89100-V) (1993).
- 68 Baldo, M. A., O'Brien, D. F., Thompson, M. E. & Forrest, S. R. Excitonic singlet-triplet ratio in a semiconducting organic thin film. *Phys Rev B* **60**, 14422-14428, doi:[10.1103/PhysRevB.60.14422](https://doi.org/10.1103/PhysRevB.60.14422) (1999).
- 69 Adachi, C., Baldo, M. A., Thompson, M. E. & Forrest, S. R. Nearly 100% internal phosphorescence efficiency in an organic light-emitting device. *Journal of Applied Physics* **90**, 5048-5051, doi:[10.1063/1.1409582](https://doi.org/10.1063/1.1409582) (2001).
- 70 Baldo, M. A. *et al.* Highly efficient phosphorescent emission from organic electroluminescent devices. *Nature* **395**, 151-154, doi:[10.1038/25954](https://doi.org/10.1038/25954) (1998).
- 71 Yang, X., Zhou, G. & Wong, W.-Y. Functionalization of phosphorescent emitters and their host materials by main-group elements for phosphorescent organic light-emitting devices. *Chemical Society reviews* **44**, 8484-8575, doi:[10.1039/C5CS00424A](https://doi.org/10.1039/C5CS00424A) (2015).
- 72 You, Y. & Park, S. Y. Phosphorescent iridium(iii) complexes: toward high phosphorescence quantum efficiency through ligand control. *Dalton Transactions*, 1267-1282, doi:[10.1039/B812281D](https://doi.org/10.1039/B812281D) (2009).
- 73 Liao, J.-L. *et al.* Os(ii) metal phosphors bearing tridentate 2,6-di(pyrazol-3-yl)pyridine chelate: synthetic design, characterization and application in OLED fabrication. *Journal of Materials Chemistry C* **2**, 6269-6282, doi:[10.1039/C4TC00865K](https://doi.org/10.1039/C4TC00865K) (2014).
- 74 Cheng, G., Chan, K. T., To, W.-P. & Che, C.-M. Colour Tunable Organic Light-Emitting Devices with External Quantum Efficiency over 20% Based on Strongly Luminescent Gold(III) Complexes having Long-Lived Emissive Excited States. *Advanced Materials* **26**, 2540-2546, doi:[10.1002/adma.201304263](https://doi.org/10.1002/adma.201304263) (2014).
- 75 Shahroosvand, H., Najafi, L., Sousaraei, A., Mohajerani, E. & Janghour, M. Going from green to red electroluminescence through ancillary ligand substitution in ruthenium(ii) tetrazole benzoic acid emitters. *Journal of Materials Chemistry C* **1**, 6970-6980, doi:[10.1039/C3TC31350F](https://doi.org/10.1039/C3TC31350F) (2013).

- 76 Liu, Z. *et al.* Simple and High Efficiency Phosphorescence Organic Light-Emitting Diodes with Codeposited Copper(I) Emitter. *Chemistry of Materials* **26**, 2368-2373, doi:10.1021/cm5006086 (2014).
- 77 Wang, Y., Herron, N., Grushin, V. V., LeCloux, D. & Petrov, V. Highly efficient electroluminescent materials based on fluorinated organometallic iridium compounds. *Applied Physics Letters* **79**, 449-451, doi:10.1063/1.1384903 (2001).
- 78 Endo, A. *et al.* Thermally Activated Delayed Fluorescence from Sn⁴⁺-Porphyrin Complexes and Their Application to Organic Light Emitting Diodes — A Novel Mechanism for Electroluminescence. *Advanced Materials* **21**, 4802-4806, doi:10.1002/adma.200900983 (2009).
- 79 Uoyama, H., Goushi, K., Shizu, K., Nomura, H. & Adachi, C. Highly efficient organic light-emitting diodes from delayed fluorescence. *Nature* **492**, 234, doi:10.1038/nature11687 (2012).
- 80 Wu, T.-L. *et al.* Diboron compound-based organic light-emitting diodes with high efficiency and reduced efficiency roll-off. *Nature Photonics* **12**, 235-240, doi:10.1038/s41566-018-0112-9 (2018).
- 81 Zeng, W. *et al.* Achieving Nearly 30% External Quantum Efficiency for Orange-Red Organic Light Emitting Diodes by Employing Thermally Activated Delayed Fluorescence Emitters Composed of 1,8-Naphthalimide-Acridine Hybrids. *Advanced Materials* **30**, 1704961, doi:10.1002/adma.201704961 (2018).
- 82 Lin, T.-A. *et al.* Sky-Blue Organic Light Emitting Diode with 37% External Quantum Efficiency Using Thermally Activated Delayed Fluorescence from Spiroacridine-Triazine Hybrid. *Advanced Materials* **28**, 6976-6983, doi:10.1002/adma.201601675 (2016).
- 83 Shen, Z., Burrows, P. E., Bulović, V., Forrest, S. R. & Thompson, M. E. Three-Colour, Tunable, Organic Light-Emitting Devices. *Science* **276**, 2009-2011, doi:10.1126/science.276.5321.2009 (1997).

- 84 Gu, G. *et al.* Transparent stacked organic light emitting devices. I. Design principles and transparent compound electrodes. *Journal of Applied Physics* **86**, 4067, doi:10.1063/1.371331 (1999).
- 85 Gu, G., Parthasarathy, G., Tian, P., Burrows, P. E. & Forrest, S. R. Transparent stacked organic light emitting devices. II. Device performance and applications to displays. *Journal of Applied Physics* **86**, 4076, doi:10.1063/1.371428 (1999).
- 86 Kido, J. *et al.* 27.1: Invited Paper: High Efficiency Organic EL Devices having Charge Generation Layers. *SID Symposium Digest of Technical Papers* **34**, 964, doi:10.1889/1.1832444 (2003).
- 87 Matsumoto, T. *et al.* 27.5L: Late-News Paper: Multiphoton Organic EL device having Charge Generation Layer. *SID Symposium Digest of Technical Papers* **34**, 979, doi:10.1889/1.1832449 (2003).
- 88 Kondakov, D. Y., Sandifer, J. R., Tang, C. W. & Young, R. H. Nonradiative recombination centers and electrical aging of organic light-emitting diodes: Direct connection between accumulation of trapped charge and luminance loss. *Journal of Applied Physics* **93**, 1108, doi:10.1063/1.1531231 (2003).
- 89 Kanno, H., Holmes, R. J., Sun, Y., Kena-Cohen, S. & Forrest, S. R. White Stacked Electrophosphorescent Organic Light-Emitting Devices Employing MoO₃ as a Charge-Generation Layer. *Advanced materials* **18**, 339-342, doi:10.1002/adma.200501915 (2006).
- 90 Wang, Q. *et al.* A high-performance tandem white organic light-emitting diode combining highly effective white-units and their interconnection layer. *Journal of Applied Physics* **105**, 076101, doi:10.1063/1.3106051 (2009).
- 91 Liao, L. S. & Klubek, K. P. Power efficiency improvement in a tandem organic light-emitting diode. *Applied Physics Letters* **92**, 223311, doi:10.1063/1.2938269 (2008).
- 92 Chang, C.-C., Chen, J.-F., Hwang, S.-W. & Chen, C. H. Highly efficient white organic electroluminescent devices based on tandem architecture. *Applied Physics Letters* **87**, 253501, doi:10.1063/1.2147730 (2005).

- 93 Guo, F. & Ma, D. White organic light-emitting diodes based on tandem structures. *Applied Physics Letters* **87**, 173510, doi:10.1063/1.2120898 (2005).
- 94 Kanno, H., Giebink, N. C., Sun, Y. & Forrest, S. R. Stacked white organic light-emitting devices based on a combination of fluorescent and phosphorescent emitters. *Applied Physics Letters* **89**, 023503, doi:10.1063/1.2219725 (2006).
- 95 You, H., Fang, J., Xuan, Y. & Ma, D. Highly efficient red electroluminescence from stacked organic light-emitting devices based on a europium complex. *Materials Science and Engineering: B* **131**, 252-255, doi:10.1016/j.mseb.2006.04.025 (2006).
- 96 Lee, T.-W. *et al.* High-efficiency stacked white organic light-emitting diodes. *Applied Physics Letters* **92**, 043301, doi:10.1063/1.2837419 (2008).
- 97 Bao, Q. Y., Yang, J. P., Li, Y. Q. & Tang, J. X. Electronic structures of MoO₃ based charge generation layer for tandem organic light-emitting diodes. *Applied Physics Letters* **97**, 063303, doi:10.1063/1.3479477 (2010).
- 98 Qi, X., Li, N. & Forrest, S. R. Analysis of metal-oxide-based charge generation layers used in stacked organic light-emitting diodes. *Journal of Applied Physics* **107**, 014514, doi:10.1063/1.3275050 (2010).
- 99 Duan, L., Tsuboi, T., Qiu, Y., Li, Y. & Zhang, G. Tandem organic light-emitting diodes with KBH₄ doped 9,10-bis(3-(pyridin-3-yl)phenyl) anthracene connected to the charge generation layer. *Optics express* **20**, 14564-14572, doi:10.1364/OE.20.014564 (2012).
- 100 Hong, K. & Lee, J.-L. Charge Generation Mechanism of Metal Oxide Interconnection in Tandem Organic Light Emitting Diodes. *The Journal of Physical Chemistry C* **116**, 6427-6433, doi:10.1021/jp212090b (2012).
- 101 Xiao, J. *et al.* Efficiency enhancement utilizing hybrid charge generation layer in tandem organic light-emitting diodes. *Applied Physics Letters* **101**, 013301, doi:10.1063/1.4732505 (2012).

- 102 Yang, J.-P. *et al.* Hybrid intermediate connector for tandem OLEDs with the combination of MoO₃-based interlayer and p-type doping. *Organic Electronics* **13**, 2243-2249, doi:10.1016/j.orgel.2012.06.037 (2012).
- 103 Yang, J.-P. *et al.* Electric-Field-Assisted Charge Generation and Separation Process in Transition Metal Oxide-Based Interconnectors for Tandem Organic Light-Emitting Diodes. *Advanced Functional Materials* **22**, 600-608, doi:10.1002/adfm.201102136 (2012).
- 104 Xiao, J. Balancing the white emission of OLEDs by a tandem structure with an effective charge generation layer. *Synthetic Metals* **172**, 11-13, doi:10.1016/j.synthmet.2013.03.013 (2013).
- 105 Zhou, D.-Y., Siboni, H. Z., Wang, Q., Liao, L.-S. & Aziz, H. The influence of charge injection from intermediate connectors on the performance of tandem organic light-emitting devices. *Journal of Applied Physics* **116**, 223708, doi:10.1063/1.4904189 (2014).
- 106 Hofle, S. *et al.* Charge generation layers for solution processed tandem organic light emitting diodes with regular device architecture. *ACS applied materials & interfaces* **7**, 8132-8137, doi:10.1021/acsami.5b00883 (2015).
- 107 Zhao, B. *et al.* Highly efficient tandem full exciplex orange and warm white OLEDs based on thermally activated delayed fluorescence mechanism. *Organic Electronics* **17**, 15-21, doi:10.1016/j.orgel.2014.11.014 (2015).
- 108 Zhao, Y., Tan, S. T., Demir, H. V. & Sun, X. W. Highly stable and high power efficiency tandem organic light-emitting diodes with transition metal oxide-based charge generation layers. *Organic Electronics* **23**, 70-75, doi:10.1016/j.orgel.2015.04.010 (2015).
- 109 Liao, L. S., Klubek, K. P. & Tang, C. W. High-efficiency tandem organic light-emitting diodes. *Applied Physics Letters* **84**, 167, doi:10.1063/1.1638624 (2004).
- 110 Leem, D.-S., Lee, J.-H., Kim, J.-J. & Kang, J.-W. Highly efficient tandem p-i-n organic light-emitting diodes adopting a low temperature evaporated rhenium oxide

- interconnecting layer. *Applied Physics Letters* **93**, 103304, doi:10.1063/1.2979706 (2008).
- 111 Fung, M. K. *et al.* Charge generation layer in stacked organic light-emitting devices. *Journal of Applied Physics* **104**, 034509, doi:10.1063/1.2942408 (2008).
- 112 Chan, M. Y. *et al.* Influences of Connecting Unit Architecture on the Performance of Tandem Organic Light-Emitting Devices. *Advanced Functional Materials* **17**, 2509-2514, doi:10.1002/adfm.200600642 (2007).
- 113 Cheng, Y.-M., Lu, H.-H., Jen, T.-H. & Chen, S.-A. Role of the Charge Generation Layer in Tandem Organic Light-Emitting Diodes Investigated by Time-Resolved Electroluminescence Spectroscopy. *The Journal of Physical Chemistry C* **115**, 582-588, doi:10.1021/jp1095085 (2011).
- 114 Lee, S., Lee, J.-H., Lee, J.-H. & Kim, J.-J. The Mechanism of Charge Generation in Charge-Generation Units Composed of p-Doped Hole-Transporting Layer/HATCN/n-Doped Electron-Transporting Layers. *Advanced Functional Materials* **22**, 855-860, doi:10.1002/adfm.201102212 (2012).
- 115 Meyer, J. *et al.* Transition metal oxides for organic electronics: energetics, device physics and applications. *Advanced materials* **24**, 5408-5427, doi:10.1002/adma.201201630 (2012).
- 116 So, F. *et al.* The mechanism of charge generation in charge generation units containing HATCN for high-luminance tandem OLED display. *Proc. of SPIE* **8476**, 84761N, doi:10.1117/12.929559 (2012).
- 117 Chen, Y. *et al.* Colour-stable and efficient tandem white organic light-emitting devices using a LiF n-doping layer and a MoOx p-doping layer as charge generating unit. *Thin Solid Films* **545**, 419-423, doi:10.1016/j.tsf.2013.07.024 (2013).
- 118 Lee, Y.-H., Lin, M.-W., Wen, T.-C. & Guo, T.-F. The metal interlayer in the charge generation layer of tandem organic light-emitting diodes. *Journal of Applied Physics* **114**, 154512, doi:10.1063/1.4825326 (2013).

- 119 Liu, J. *et al.* Charge Separation Process in an Ultrathin Electron-Injecting Bilayer-Assisted Charge Generation Unit for Tandem Organic Light-Emitting Diodes. *The Journal of Physical Chemistry C* **117**, 13887-13893, doi:10.1021/jp4040584 (2013).
- 120 Liu, J. *et al.* Double Hybrid Tandem White OLED Employing a Novel Charge Generation Unit. *SID Symposium Digest of Technical Papers* **44**, 1403-1406, doi:10.1002/j.2168-0159.2013.tb06505.x (2013).
- 121 Liu, J. *et al.* A highly efficient, transparent and stable charge generation unit based on a p-doped monolayer. *Organic Electronics* **14**, 1337-1343, doi:10.1016/j.orgel.2013.02.035 (2013).
- 122 Yan, F. & Wei Sun, X. A plasmonically enhanced charge generation layer for tandem organic light emitting device. *Applied Physics Letters* **102**, 043303, doi:10.1063/1.4789979 (2013).
- 123 Deng, Y.-H. *et al.* The role of charge generation layers in the operational stability of tandem organic light-emitting diodes. *Journal of Materials Chemistry C* **2**, 1982, doi:10.1039/c3tc32023e (2014).
- 124 Talik, N. A., Yeoh, K. H., Ng, C. Y. B., Yap, B. K. & Woon, K. L. Efficient green phosphorescent tandem organic light emitting diodes with solution processable mixed hosts charge generating layer. *Journal of Luminescence* **154**, 345-349, doi:10.1016/j.jlumin.2014.04.027 (2014).
- 125 Xiao, Z.-H. *et al.* Effect of NaCl doped into Bphen layer on the performance of tandem organic light-emitting diodes. *Chinese Physics B* **23**, 087811, doi:10.1088/1674-1056/23/8/087811 (2014).
- 126 Dai, Y. *et al.* Highly efficient and stable tandem organic light-emitting devices based on HAT-CN/HAT-CN:TAPC/TAPC as a charge generation layer. *Journal of Materials Chemistry C* **3**, 6809-6814, doi:10.1039/c4tc02875a (2015).
- 127 Miao, Y. *et al.* Multiple emissive layers white organic light emitting device with nanoplatfoms patterning structure for improved current efficiency and colour balance. *Synthetic Metals* **203**, 59-67, doi:10.1016/j.synthmet.2015.02.017 (2015).

- 128 Kanno, H. *et al.* High Efficiency Stacked Organic Light-Emitting Diodes Employing Li₂O as a Connecting Layer. *Japanese Journal of Applied Physics* **45**, 9219-9223, doi:10.1143/jjap.45.9219 (2006).
- 129 Sun, J. X., Zhu, X. L., Peng, H. J., Wong, M. & Kwok, H. S. Bright and efficient white stacked organic light-emitting diodes. *Organic Electronics* **8**, 305-310, doi:10.1016/j.orgel.2006.11.006 (2007).
- 130 Zhang, H., Dai, Y., Ma, D. & Zhang, H. High efficiency tandem organic light-emitting devices with Al₂WO₃/Au interconnecting layer. *Applied Physics Letters* **91**, 123504, doi:10.1063/1.2787877 (2007).
- 131 Zhang, H., Dai, Y. & Ma, D. Al₂WO₃/Au as the interconnecting layer for efficient tandem white organic light-emitting diodes. *Journal of Physics D: Applied Physics* **41**, 102006, doi:10.1088/0022-3727/41/10/102006 (2008).
- 132 zung-Fang Guo, T.-C. W., Yi-Shun Huang, Ming-Wei Lin, Chuan-Cheng Tsou, and Chia-Tin Chung. White-emissive tandem-type hybrid organic/polymer diodes with (0.33,-0.33) chromaticity coordinates. *Optics Express* **17**, 21205-21215, doi:10.1364/OE.17.021205 (2009).
- 133 Sasabe, H., Minamoto, K., Pu, Y.-J., Hirasawa, M. & Kido, J. Ultra high-efficiency multi-photon emission blue phosphorescent OLEDs with external quantum efficiency exceeding 40%. *Organic Electronics* **13**, 2615-2619, doi:10.1016/j.orgel.2012.07.019 (2012).
- 134 Jiao, B., Wu, Z., Yang, Z. & Hou, X. Tandem organic light-emitting diodes with an effective nondoped charge-generation unit. *physica status solidi (a)* **210**, 2583-2587, doi:10.1002/pssa.201330119 (2013).
- 135 So, F. *et al.* Extremely high-efficiency multiphoton emission blue phosphorescent OLEDs with external quantum efficiency exceeding 40%. *Proceedings of SPIE* **8476**, 847604, doi:10.1117/12.927997 (2012).

- 136 Hofle, S. *et al.* Solution processed, white emitting tandem organic light-emitting diodes with inverted device architecture. *Advanced materials* **26**, 5155-5159, doi:10.1002/adma.201400332 (2014).
- 137 Lee, H. *et al.* Hole injection enhancement of a single-walled carbon nanotube anode using an organic charge-generation layer. *Carbon* **71**, 268-275, doi:10.1016/j.carbon.2014.01.039 (2014).
- 138 Jun Liu, X. S., Xinkai Wu, Jing Wang, and Gufeng He. Inverted Tandem Phosphorescence Organic Light-Emitting Diodes Based on MoO₃/Al/Cs₂CO₃ Charge Generation Unit. *Journal of Display Technology* **11**, 341-345, doi:10.1109/JDT.2015.2392118 (2015).
- 139 Chen, Y., Chen, J., Ma, D., Yan, D. & Wang, L. Tandem white phosphorescent organic light-emitting diodes based on interface-modified C₆₀/pentacene organic heterojunction as charge generation layer. *Applied Physics Letters* **99**, 103304, doi:10.1063/1.3628317 (2011).
- 140 Chen, Y., Chen, J., Ma, D., Yan, D. & Wang, L. Effect of organic bulk heterojunction as charge generation layer on the performance of tandem organic light-emitting diodes. *Journal of Applied Physics* **110**, 074504, doi:10.1063/1.3644970 (2011).
- 141 Chen, Y. *et al.* High power efficiency tandem organic light-emitting diodes based on bulk heterojunction organic bipolar charge generation layer. *Applied Physics Letters* **98**, 243309, doi:10.1063/1.3599557 (2011).
- 142 Chen, Y. *et al.* Organic heterojunctions as a charge generation layer in tandem organic light-emitting diodes: the effect of interfacial energy level and charge carrier mobility. *Journal of Materials Chemistry* **21**, 15332-15336, doi:10.1039/C1JM12499D (2011).
- 143 Yang, Y. *et al.* A novel coumarin-based fluorescent probe for selective detection of bisulfite anions in water and sugar samples. *Sensors and Actuators B: Chemical* **166-167**, 665-670, doi:10.1016/j.snb.2012.03.034 (2012).

- 144 Chen, Y. *et al.* Highly efficient tandem white organic light-emitting diodes based upon C60/NaT4 organic heterojunction as charge generation layer. *Journal of Materials Chemistry* **22**, 8492, doi:10.1039/c2jm30557g (2012).
- 145 Chen, Y. *et al.* Organic semiconductor heterojunction as charge generation layer in tandem organic light-emitting diodes for high power efficiency. *Organic Electronics* **13**, 1121-1128, doi:10.1016/j.orgel.2012.03.013 (2012).
- 146 Kleemann, H. *et al.* Reverse breakdown behavior in organic pin-diodes comprising C60 and pentacene: Experiment and theory. *Organic Electronics* **14**, 193-199, doi:10.1016/j.orgel.2012.11.001 (2013).
- 147 Bi, W.-T. *et al.* Tandem white organic light-emitting diodes adopting a C60:rubrene charge generation layer. *Chinese Physics B* **23**, 017803, doi:10.1088/1674-1056/23/1/017803 (2014).
- 148 Liu, X., Wang, C., Wang, C., Irfan, I. & Gao, Y. Interfacial electronic structures of buffer-modified pentacene/C60-based charge generation layer. *Organic Electronics* **17**, 325-333, doi:10.1016/j.orgel.2014.12.005 (2015).
- 149 Sun, H. *et al.* High Efficiency Tandem Organic Light Emitting Diode Using an Organic Heterojunction as the Charge Generation Layer: An Investigation into the Charge Generation Model and Device Performance. *ACS Photonics* **2**, 271-279, doi:10.1021/acsp Photonics.5b00010 (2015).
- 150 Coburn, C., Jeong, C. & Forrest, S. R. Reliable, All-Phosphorescent Stacked White Organic Light Emitting Devices with a High Colour Rendering Index. *ACS Photonics* **5**, 630-635, doi:10.1021/acsp Photonics.7b01213 (2018).
- 151 Akamatu, H., Inokuchi, H. & Matsunaga, Y. Electrical Conductivity of the Perylene–Bromine Complex. *Nature* **173**, 168-169, doi:10.1038/173168a0 (1954).
- 152 Curry, J. & Cassidy, E. P. Effect of Halogens on the Resistance of Single Crystals of Copper Phthalocyanine. *The Journal of Chemical Physics* **37**, 2154-2155, doi:10.1063/1.1733442 (1962).

- 153 Yamamoto, Y., Yoshino, K. & Inuishi, Y. Electrical Properties of Phthalocyanine-Halogen Complexes. *Journal of the Physical Society of Japan* **47**, 1887-1891, doi:10.1143/JPSJ.47.1887 (1979).
- 154 Väterlein, C. *et al.* Electrical conductivity and oxygen doping of vapour-deposited oligothiophene films. *Synthetic Metals* **76**, 133-136, doi:10.1016/0379-6779(95)03436-N (1996).
- 155 Hamed, A., Sun, Y. Y., Tao, Y. K., Meng, R. L. & Hor, P. H. Effects of oxygen and illumination on the in situ conductivity of C60 thin films. *Physical review. B* **47**, 10873-10880, doi:10.1103/PhysRevB.47.10873 (1993).
- 156 Kearns, D. R., Tollin, G. & Calvin, M. Electrical Properties of Organic Solids. II. Effects of Added Electron Acceptor on Metal-Free Phthalocyanine. *The Journal of Chemical Physics* **32**, 1020-1025, doi:10.1063/1.1730844 (1960).
- 157 Chang, C.-C., Hsieh, M.-T., Chen, J.-F., Hwang, S.-W. & Chen, C. H. Highly power efficient organic light-emitting diodes with a p-doping layer. *Applied Physics Letters* **89**, 253504, doi:10.1063/1.2405856 (2006).
- 158 Meyer, J. *et al.* A strategy towards p-type doping of organic materials with HOMO levels beyond 6 eV using tungsten oxide. *Journal of Materials Chemistry* **19**, 702-705, doi:10.1039/B819485H (2009).
- 159 Kröger, M. *et al.* P-type doping of organic wide band gap materials by transition metal oxides: A case-study on Molybdenum trioxide. *Organic Electronics* **10**, 932-938, doi:https://doi.org/10.1016/j.orgel.2009.05.007 (2009).
- 160 Ramsey, M. G., Steinmüller, D. & Netzer, F. P. Explicit evidence for bipolaron formation: Cs-doped biphenyl. *Physical review. B* **42**, 5902-5905, doi:10.1103/PhysRevB.42.5902 (1990).
- 161 Haddon, R. C. *et al.* Conducting films of C60 and C70 by alkali-metal doping. *Nature* **350**, 320-322, doi:10.1038/350320a0 (1991).

- 162 Nollau, A., Pfeiffer, M., Fritz, T. & Leo, K. Controlled n-type doping of a molecular organic semiconductor: Naphthalenetetracarboxylic dianhydride (NTCDA) doped with bis(ethylenedithio)-tetrathiafulvalene (BEDT-TTF). *Journal of Applied Physics* **87**, 4340-4343, doi:10.1063/1.373413 (2000).
- 163 Blochwitz, J., Pfeiffer, M., Fritz, T. & Leo, K. Low voltage organic light emitting diodes featuring doped phthalocyanine as hole transport material. *Applied Physics Letters* **73**, 729-731, doi:10.1063/1.121982 (1998).
- 164 Kido, J. & Matsumoto, T. Bright organic electroluminescent devices having a metal-doped electron-injecting layer. *Applied Physics Letters* **73**, 2866-2868, doi:10.1063/1.122612 (1998).
- 165 Huang, J. *et al.* Low-voltage organic electroluminescent devices using pin structures. *Applied Physics Letters* **80**, 139-141, doi:10.1063/1.1432110 (2002).
- 166 Pfeiffer, M., Forrest, S. R., Leo, K. & Thompson, M. E. Electrophosphorescent p-i-n Organic Light-Emitting Devices for Very-High-Efficiency Flat-Panel Displays. *Advanced Materials* **14**, 1633-1636, doi:10.1002/1521-4095(20021118)14:22<1633::aid-adma1633>3.0.co;2-# (2002).
- 167 He, G. *et al.* Very high-efficiency and low voltage phosphorescent organic light-emitting diodes based on a p-i-n junction. *Journal of Applied Physics* **95**, 5773-5777, doi:10.1063/1.1702143 (2004).
- 168 He, G. *et al.* High-efficiency and low-voltage p-i-n electrophosphorescent organic light-emitting diodes with double-emission layers. *Applied Physics Letters* **85**, 3911-3913, doi:10.1063/1.1812378 (2004).
- 169 Okada, S. *et al.* Substituent effects of iridium complexes for highly efficient red OLEDs. *Dalton Transactions*, 1583-1590, doi:10.1039/B417058J (2005).
- 170 Qin, D. & Tao, Y. Increased electrophosphorescent efficiency in organic light emitting diodes by using an exciton-collecting structure. *Journal of Applied Physics* **97**, 044505, doi:10.1063/1.1853500 (2005).

- 171 Meerheim, R. *et al.* Influence of charge balance and exciton distribution on efficiency and lifetime of phosphorescent organic light-emitting devices. *Journal of Applied Physics* **104**, 014510, doi:10.1063/1.2951960 (2008).
- 172 Becker, H., Vestweber, H., Gerhard, A., Stoessel, P. & Fortte, R. 17.5L: Late-News Paper: Novel Host Materials for Efficient and Stable Phosphorescent OLED Devices. *SID Symposium Digest of Technical Papers* **35**, 796-799, doi:10.1889/1.1833139 (2004).
- 173 Birnstock, J. *et al.* 64.4: Novel Materials and Structures for Highly-Efficient, Temperature-Stable, and Long-Living AM OLED Displays. *SID Symposium Digest of Technical Papers* **37**, 1866-1869, doi:10.1889/1.2433408 (2006).
- 174 Tokito, S. *et al.* Confinement of triplet energy on phosphorescent molecules for highly-efficient organic blue-light-emitting devices. *Applied Physics Letters* **83**, 569-571, doi:10.1063/1.1594834 (2003).
- 175 Shih, P.-I. *et al.* Novel Carbazole/Fluorene Hybrids: Host Materials for Blue Phosphorescent OLEDs. *Organic Letters* **8**, 2799-2802, doi:10.1021/ol060884c (2006).
- 176 Gebeyehu, D. *et al.* Highly efficient deep-blue organic light-emitting diodes with doped transport layers. *Synthetic Metals* **148**, 205-211, doi:<https://doi.org/10.1016/j.synthmet.2004.09.024> (2005).
- 177 Sun, Y. & Forrest, S. R. Organic light emitting devices with enhanced outcoupling via microlenses fabricated by imprint lithography. *Journal of Applied Physics* **100**, 073106, doi:10.1063/1.2356904 (2006).
- 178 D'Andrade, B. W. & Forrest, S. R. White Organic Light-Emitting Devices for Solid-State Lighting. *Advanced Materials* **16**, 1585-1595, doi:10.1002/adma.200400684 (2004).
- 179 Schwartz, G., Reineke, S., Walzer, K. & Leo, K. Reduced efficiency roll-off in high-efficiency hybrid white organic light-emitting diodes. *Applied Physics Letters* **92**, 053311, doi:10.1063/1.2836772 (2008).

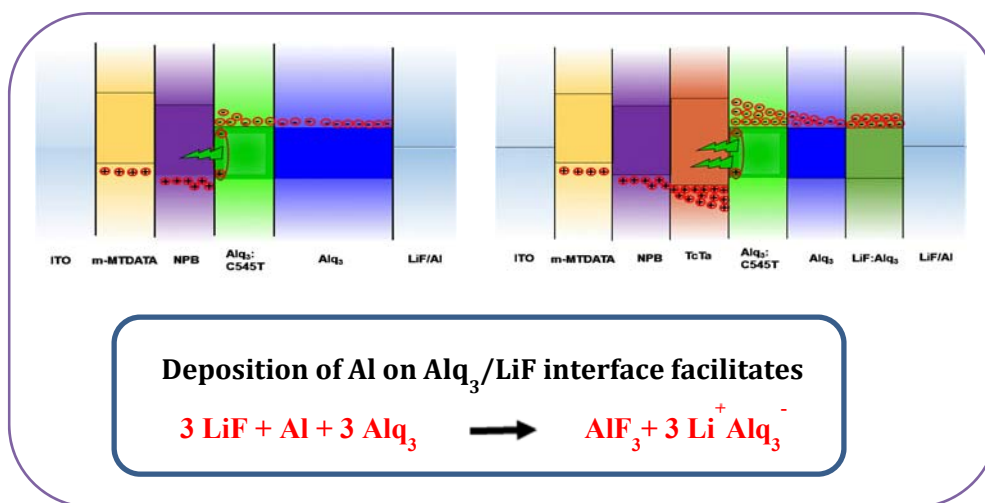
- 180 Meerheim, R., Lussem, B. & Leo, K. Efficiency and Stability of p-i-n Type Organic Light Emitting Diodes for Display and Lighting Applications. *Proceedings of the IEEE* **97**, 1606-1626, doi:10.1109/jproc.2009.2022418 (2009).
- 181 Kido, J., Hongawa, K., Okuyama, K. & Nagai, K. White light-emitting organic electroluminescent devices using the poly(N-vinylcarbazole) emitter layer doped with three fluorescent dyes. *Applied Physics Letters* **64**, 815-817, doi:10.1063/1.111023 (1994).
- 182 Kido, J., Kimura, M. & Nagai, K. Multilayer White Light-Emitting Organic Electroluminescent Device. *Science* **267**, 1332-1334, doi:10.1126/science.267.5202.1332 (1995).
- 183 Service, R. F. Organic LEDs Look Forward to a Bright, White Future. *Science* **310**, 1762-1763, doi:10.1126/science.310.5755.1762 (2005).
- 184 Wu, Y.-S. *et al.* Efficient white organic light emitting devices with dual emitting layers. *Thin Solid Films* **488**, 265-269, doi:https://doi.org/10.1016/j.tsf.2005.04.032 (2005).
- 185 Müller, C. D. *et al.* Multi-colour organic light-emitting displays by solution processing. *Nature* **421**, 829-833, doi:10.1038/nature01390 (2003).
- 186 Reineke, S. *et al.* White organic light-emitting diodes with fluorescent tube efficiency. *Nature* **459**, 234-238, doi:10.1038/nature08003 (2009).
- 187 Dai, Y. *et al.* Highly efficient and stable tandem organic light-emitting devices based on HAT-CN/HAT-CN:TAPC/TAPC as a charge generation layer. *Journal of Materials Chemistry C* **3**, 6809-6814, doi:10.1039/C4TC02875A (2015).
- 188 Williams, E. L., Haavisto, K., Li, J. & Jabbour, G. E. Excimer-Based White Phosphorescent Organic Light-Emitting Diodes with Nearly 100 % Internal Quantum Efficiency. *Advanced Materials* **19**, 197-202, doi:10.1002/adma.200602174 (2007).
- 189 Yang, X. *et al.* Efficient organic light-emitting devices with platinum-complex emissive layer. *Applied Physics Letters* **98**, 033302, doi:10.1063/1.3541447 (2011).

- 190 Angioni, E. *et al.* A single emitting layer white OLED based on exciplex interface emission. *Journal of Materials Chemistry C* **4**, 3851-3856, doi:10.1039/C6TC00750C (2016).
- 191 Cho, Y. J., Yook, K. S. & Lee, J. Y. Cool and warm hybrid white organic light-emitting diode with blue delayed fluorescent emitter both as blue emitter and triplet host. *Scientific reports* **5**, 7859, doi:10.1038/srep07859 (2015).
- 192 Xie, G. *et al.* Evaporation- and Solution-Process-Feasible Highly Efficient Thianthrene-9,9',10,10'-Tetraoxide-Based Thermally Activated Delayed Fluorescence Emitters with Reduced Efficiency Roll-Off. *Advanced Materials* **28**, 181-187, doi:10.1002/adma.201503225 (2016).
- 193 Li, X.-L. *et al.* High-Efficiency WOLEDs with High Colour-Rendering Index based on a Chromaticity-Adjustable Yellow Thermally Activated Delayed Fluorescence Emitter. *Advanced Materials* **28**, 4614-4619, doi:10.1002/adma.201505963 (2016).
- 194 Gu, G. *et al.* High-external-quantum-efficiency organic light-emitting devices. *Opt. Lett.* **22**, 396-398, doi:10.1364/OL.22.000396 (1997).
- 195 Madigan, C. F., Lu, M.-H. & Sturm, J. C. Improvement of output coupling efficiency of organic light-emitting diodes by backside substrate modification. *Applied Physics Letters* **76**, 1650-1652, doi:10.1063/1.126124 (2000).
- 196 Yambem, S. D., Ullah, M., Tandy, K., Burn, P. L. & Namdas, E. B. ITO-free top emitting organic light emitting diodes with enhanced light out-coupling. *Laser & Photonics Reviews* **8**, 165-171, doi:10.1002/lpor.201300148 (2014).
- 197 Koh, T.-W., Spechler, J. A., Lee, K. M., Arnold, C. B. & Rand, B. P. Enhanced Outcoupling in Organic Light-Emitting Diodes via a High-Index Contrast Scattering Layer. *ACS Photonics* **2**, 1366-1372, doi:10.1021/acsp Photonics.5b00346 (2015).
- 198 Preinfalk, J. B. *et al.* Large-Area Screen-Printed Internal Extraction Layers for Organic Light-Emitting Diodes. *ACS Photonics*, doi:10.1021/acsp Photonics.6b01027 (2017).

- 199 Yamasaki, T., Sumioka, K. & Tsutsui, T. Organic light-emitting device with an ordered monolayer of silica microspheres as a scattering medium. *Applied Physics Letters* **76**, 1243-1245, doi:10.1063/1.125997 (2000).
- 200 Möller, S. & Forrest, S. R. Improved light out-coupling in organic light emitting diodes employing ordered microlens arrays. *Journal of Applied Physics* **91**, 3324-3327, doi:10.1063/1.1435422 (2002).
- 201 Peng, H. J., Ho, Y. L., Qiu, C. F., Wong, M. & Kwok, H. S. 11.4: Coupling Efficiency Enhancement of Organic Light Emitting Devices with Refractive Microlens Array on High Index Glass Substrate. *SID Symposium Digest of Technical Papers* **35**, 158-161, doi:10.1889/1.1825995 (2004).
- 202 Parker, C. A. & Hatchard, C. G. Triplet-singlet emission in fluid solutions. Phosphorescence of eosin. *Transactions of the Faraday Society* **57**, 1894-1904, doi:10.1039/TF9615701894 (1961).
- 203 Endo, A. *et al.* Efficient up-conversion of triplet excitons into a singlet state and its application for organic light emitting diodes. *Applied Physics Letters* **98**, 083302, doi:10.1063/1.3558906 (2011).
- 204 Kim, S.-Y. *et al.* Organic Light-Emitting Diodes with 30% External Quantum Efficiency Based on a Horizontally Oriented Emitter. *Advanced Functional Materials* **23**, 3896-3900, doi:10.1002/adfm.201300104 (2013).
- 205 Sun, J. W. *et al.* A Fluorescent Organic Light-Emitting Diode with 30% External Quantum Efficiency. *Advanced Materials* **26**, 5684-5688, doi:10.1002/adma.201401407 (2014).
- 206 Lee, D. R., Hwang, S.-H., Jeon, S. K., Lee, C. W. & Lee, J. Y. Benzofurocarbazole and benzothienocarbazole as donors for improved quantum efficiency in blue thermally activated delayed fluorescent devices. *Chemical communications* **51**, 8105-8107, doi:10.1039/C5CC01940K (2015).
- 207 Kim, J. H., Lee, D. R., Han, S. H. & Lee, J. Y. Over 20% external quantum efficiency in red thermally activated delayed fluorescence organic light-emitting diodes using a

- reverse intersystem crossing activating host. *Journal of Materials Chemistry C* **6**, 5363-5368, doi:10.1039/C7TC05811J (2018).
- 208 Adachi, C. Third-generation organic electroluminescence materials. *Japanese Journal of Applied Physics* **53**, 060101, doi:10.7567/jjap.53.060101 (2014).

Device engineering in a fluorescent OLED by facile electron transport layer doping and carrier confinement



2.1. Abstract

Organic light emitting diodes (OLEDs) often face the issue of decreasing power efficiency with increasing brightness. Loss of charge carrier balance is one of the factors contributing to the efficiency roll-off. We demonstrate that by using a combination of doped electron transport layer (ETL) and a specially chosen electron blocking layer (EBL) having high hole mobility, this efficiency roll-off can be effectively suppressed. A tris-(8-hydroxyquinoline) aluminium(Alq₃) based OLED has been fabricated with 2,3,6,7-Tetrahydro-1,1,7,7,-tetramethyl-1H, 5H,11H-10-(2-benzothiazolyl) quinolizino-[9,9a, 1n gh]coumarin (C545T) as the emissive dopant. Bulk doping of the ETL with lithium fluoride (LiF) was optimized to

increase the luminous intensity as well as the current efficiency. An EBL with high hole mobility introduced between the EML and the hole transport layer (HTL) improved the performance drastically, and the device brightness at 9 V got improved by a factor of 2.5 compared to that of the control device. While increasing the brightness from 100 cd/m² to 1000 cd/m², the power efficiency drop was 47% for the control device whereas only a drop of 15% was observed for the modified device. The possible mechanisms for the enhanced performance are discussed.

We have also studied doping of the ETL Alq₃ with different percentages of LiF and the effect of different EBLs such as Tris (4-carbazoyl-9-ylphenyl)amine (TCTA), N,N'-Bis(naphthalen-1-yl)-N,N'-bis(phenyl)-benzidine (NPB), and Di-[4-(N,N-di-p-tolyl-amino)-phenyl]cyclohexane (TAPC) in an Alq₃: C545T based OLED with optimized ETL doping. TCTA was found to effectively block the electrons and influence the recombination region in the process. At a brightness of 1000 cd/m², an improvement of 27.8% was observed in external quantum efficiency (EQE) for the device with TCTA as the EBL and doped Alq₃ as the ETL, compared to the one with just NPB as both EBL and HTL.

2.2. Introduction

Since its inception¹, the research on the organic light emitting diode (OLED) gathered momentum due to the attractive properties such as surface emission, energy efficiency, lightweight, ease of processing, tunability of colour and brightness, and unique form factors leading to the current technology reign in display and lighting applications^{2,3}. Efficient electroluminescence from OLEDs is ensured by the assistance of separate electron transport layer (ETL) and hole transport layer (HTL) with electron and hole conduction being dominant respectively on each side of the emissive layer (EML). The energy barriers induced by this arrangement confine the exciton recombination to the EML, thereby increasing the probability

of radiative recombination. However, the energy barrier between the injecting electrode and the transport layer gives rise to high turn-on voltage and low power efficiency which necessitates the tailoring of “injection” layers as a buffer in between the electrode and transport layers⁴.

To attain good luminescence at a low driving voltage, the quantum efficiency of the device has to be improved. EQE depends on internal quantum efficiency (IQE) and outcoupling efficiency whereas the IQE, in turn, depends on the charge balance factor, the fraction of singlet exciton formation and radiative recombination efficiency. Transport doping with a suitable material combined with an efficient carrier blocking layer can realize an improved EQE as the charge imbalance in the device along with poor carrier mobility can affect exciton confinement in the EML⁵. Charge imbalance and poor carrier mobility can further cause both reduced radiative recombination efficiency and a shift in the recombination zone. Improving the efficiency and lifetime of OLED has always been a topic of great interest despite the great strides made in this area. Doping of the emissive layer has brought efficiency improvement as well as colour tuning of OLED⁶, and the introduction of a phosphorescent dye to the host material efficiently achieved triplet harvesting^{7,8} leading to a possible 100% internal quantum efficiency.

High fields are required for the field emission of carriers across the interfaces to commence light emission as the charge transport at low fields is space charge limited⁹. In inorganic semiconductor-based optoelectronic devices, controlled transport doping is a critical factor in achieving high efficiency with a low driving voltage. Doping of transport layers helps in increasing the conductivity and causes efficient charge injection by tunneling (from the electrodes). For example, in p-i-n devices, carriers are easily injected into the smaller bandgap active layer sandwiched between heavily doped transport layers. Here, the device shows flat band characteristics and the driving

voltage is reduced. The structure also brings about efficient carrier confinement in the emissive layer. Organic semiconductors on the other hand have low mobility values, therefore weak transport properties as well as weak injection properties and due to the offset of Fermi level from highest occupied molecular orbital (HOMO) and lowest unoccupied molecular orbital (LUMO).

Doping in conventional semiconductors is achieved by replacing host atoms by donor or acceptor guest impurities having one valence electron more or less than the host. Ionization of these dopants creates free charge carriers in the valence or conduction band when the electron (hole) transferred to the host overcomes the Coulombic attraction with the hole (electron) left at the dopant site. This holds true in the case of doping in organic materials as well. However, as the dielectric constant of organic materials is lower compared to the conventional semiconductors, the carrier dissociation requires longer distance to overcome the higher coulombic interaction. The dominant mechanism behind carrier transport enhancement in inorganic semiconductors is increased carrier density, whereas the increased carrier mobility plays the major role in the case of organic semiconductors. For organic light emitting diodes (OLEDs); several tailored layers, each having distinct properties to ensure efficient charge carrier injection, transport and confinement in the emissive layer are required in conjunction with each other to ensure good device performance. Even then, without transport doping, the ohmic losses at the interface can lead to increased driving voltage.

However, doping the transport layer can significantly reduce the barriers at the interface facilitating the carrier injection from electrodes and enhancing the carrier transport due to the increased carrier concentration and conductivity that further reduces the driving voltage and thereby power efficiency. Doping shifts the Fermi level

of the transport layer¹⁰ owing to the high charge carrier density and bring about charge carrier balance. Transport layer doping by either electron donors (n-type) or acceptors (p-type) for electron transport layer (ETL) and hole transport layer (HTL) respectively is found to increase the conductivity which in turn reduces the voltage drop across EML¹¹⁻¹⁴. Transport doping in OLEDs can shift Fermi levels improving carrier injection and reducing ohmic losses. It can also reduce the barriers at the interface and enhance the carrier transport due to the increased carrier concentration and conductivity, bringing about charge carrier balance. Transport doping leads to narrow space charge regions at contacts which can permits carrier tunneling, realizing ohmic contacts¹⁴. Similar to the doping of inorganic materials, added organic dopants act as either electron donors or acceptors. When the dopant donates electrons to the LUMO levels, n-doping is achieved and the p-dopants extract electrons from HOMO levels. p-doping in organic semiconductors is easier to attain for the common hole transporting materials with dopants like phthalocyanines¹⁵, F4-TCNQ(3,5,6-tetrafluoro-7,7,8,8-tetracyano-quinodi methane)¹⁶⁻¹⁸, DDQ(dicyano-dichloro-quinone)¹⁹, F6-TCNNQ(1,3,4,5,7,8-hexafluorotetracyanonaphthoquino dimethane)²⁰ etc. A P-I-N type OLED comprising of both the p-doped and n-doped transport layers can efficiently achieve the above condition¹⁴. Though p-type doping is quite prevalent, n-type doping has been difficult due to the stability of dopants and special requirements such as light activation²¹⁻²³.

n-doping is more difficult in OLEDs as organic materials have comparatively higher hole mobility than electron mobility and it is difficult to find dopants having a HOMO level above the LUMO levels of organic materials. Unlike p-doping, n-doping is restricted by the availability of suitable dopant material, ease of incorporation in the host matrix, etc.^{22,23}. Using alkali metals for n-type doping has been reported way back

in 1993²⁴. Different contact schemes of Al with electron injection layer lithium fluoride(LiF) have been reported²⁵ and XPS data give evidence for charge transfer between the electron transport layer Tris(8-hydroxyquinolato)aluminum (Alq_3) and LiF where Alq_3 gains electron charge from F^- anion acting as an n-type donor²⁶. It is also reported that the work function of Al gets modified to 3.4 eV in contact with LiF²⁷. But, due to the small size, metal n-dopants such as Li can readily diffuse into the EML forming non-radiative recombination centers^{10,28,29} whereas molecular dopants have the advantage of lower diffusion rate¹⁹. Both interface doping, as well as bulk doping, are possible. Cesium (Cs) has also been used as a dopant for ETL^{30,31} due to its larger atomic dimension, which retards the diffusion. However, Cs is a liquid at room temperature, and there are related difficulties in the evaporation process. Despite the issue of diffusion, Cs doping in BPhen has exhibited improved thermal stability of the device beyond the T_g of BPhen as Cs prevents recrystallization of BPhen³². Molecular dopants like NTCDA(naphthalenetetracarboxylic dianhydride)³⁴, TTN(tetrathianaphthacene)³⁵, CoCP_2 (cobaltocene)³⁶, and several molecular cationic dye precursors^{23,37,38} have also been studied as n-dopant. Recently, more detailed studies on n-dopants like lithium carbonate (Li_2CO_3)³⁹, cesium carbonate (Cs_2CO_3)⁴⁰ dimeric dopant like (pentamethylcyclopentadienyl)(1,3,5-trimethylbenzene) ruthenium dimer ($[\text{RuCp}^*\text{Mes}]_2$) have been reported⁴¹. Using LiF as n-dopant²⁵⁻²⁷ is favorable due to its cost-effectiveness and ease of application.

In the bulk doping by co-evaporation of LiF along with the ETL material Alq_3 , the problem with the diffusion is more severe. In fact due to the low electron mobility of Alq_3 , 1,3,5-Tri[(3-pyridyl)-phen-3-yl]benzene (TmPyPB), 1,3-Bis[3,5-di(pyridin-3-yl)phenyl]benzene (BmPyPhB) or 1,3,5-Tris(1-phenyl-1Hbenzimidazol-2-yl)benzene (TPBi) have become more popular choices for an electron transport material. However,

doping of Alq₃ with LiF is still interesting due to its low cost and facile processing. Hence, in section I, we have systematically studied the doping and efficiently separated ETL into two parts; LiF-doped Alq₃ and pristine Alq₃ in an Alq₃: C545T based OLED. We have also investigated the effect of different ratios between these two parts of the ETL on the performance of the device.

Another major challenge in the OLED technology is the efficiency roll-off, which means the efficiency of OLED decreases as the brightness increases. Singlet-Triplet annihilation, Singlet- Polaron annihilation, and loss of charge carrier balance are proposed to be the major reasons for the efficiency roll-off⁴². We have shown that while doped ETL indeed enhances the current density and brightness, it does not solve the problem of efficiency roll-off. Hence as a subsequent modification, we have employed an electron-blocking layer which improved the charge balance factor and thus improved the brightness by several times and also reduced the efficiency roll-off at higher voltages and brightness. To the best of our knowledge, the efficiency roll-off has not been studied in the context of ETL doping with alkali metals.

Although several EBLs have been used in OLED device structures, studies with different EBLs on the same emissive system are rare in literature, albeit blocking concepts are very important⁴³.⁴³. In fact, the selection of the suitable EBL would depend on many factors such as mobility of electrons and holes, the energy barrier for electron injection from the EML to the EBL, the energy barrier for the hole injection from the EBL to the EML and possibly the triplet energy. Blocking the electron or hole in the hole transporting and electron transporting side respectively can increase the local carrier density within the EML. This build-up will ensure the exciton confinement in the EML. Herein the section II, we have undertaken studies on a fluorescent OLED with an HTL acting as EBL and also with two additional EBLs. We have optimized OLEDs for different levels of doping concentration in the ETL and studied

the effect of various electron-blocking materials in the device performance such as N,N'-Bis(naphthalen-1-yl)-N,N'-bis(phenyl)-benzidine (NPB), TCTA, an TAPC.

2.3. Results and discussion

A detailed discussion on the device fabrication process and the materials used are given in annexure A.

2.3.1 Photoluminescence study

To verify the quenching effect, the Photoluminescence Quantum Yield (PLQY) of doped and undoped Alq₃ are compared and are shown in Fig 2.1. The PLQY of neat Alq₃ film is 13.42 ± 0.01%. A PLQY of 20% has been reported for Alq₃⁴⁴. It is also reported that when the Alq₃ film is not air sealed and exposed to ambient air, the PLQY may fall below 10%⁴⁵. Our slightly smaller value of PLQY may be due to this fact. More importantly, the PLQY of the LiF doped Alq₃ film drops to 2.87 ± 0.02%. This can be attributed to metal-induced quenching. An earlier report on conducting polymers suggests that EL efficiency suffers more compared to PL efficiency regarding metal induced quenching⁴⁶. Hence, the very low emission from the device B could be attributed to metal-induced quenching due to diffusion of Li from doped ETL to the EML through the undoped buffer.

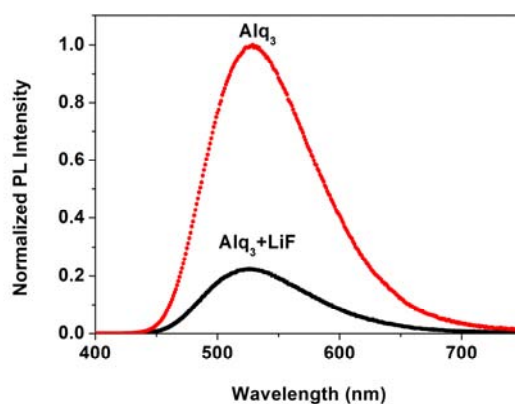


Figure 2.1 Photoluminescence spectra of neat and LiF-doped Alq₃ films.

2.3.2 SCLC studies for determination of mobility

The increased current density may be due to increase in carrier mobility or the carrier concentration or both due to ETL doping. The Space Charge Limited Conductivity (SCLC) ⁴⁷ is an efficient method to study the mobility of charge carriers in the organic devices. Its ease of use makes it reliable to get a first-order approximation of the carrier mobility. Mobility can be extracted for a single carrier diode in ambient condition, where the current density, which is limited by the space charge can be approximated as,

$$J = \frac{9}{8} \epsilon \mu \frac{V^2}{d^3} \quad (1)$$

where ϵ and d are the permittivity and thickness of the sample, respectively, and μ is the mobility of the semiconductor. In the present study, the electron mobility of the LiF-doped Alq₃ film is calculated by studying the SCLC characteristics in a MIM structure, sandwiching it between Aluminium electrodes. It is then compared with the undoped Alq₃ (electron-only) device. Fig 2.2 depicts the J-V characteristics of both the electron- only devices.

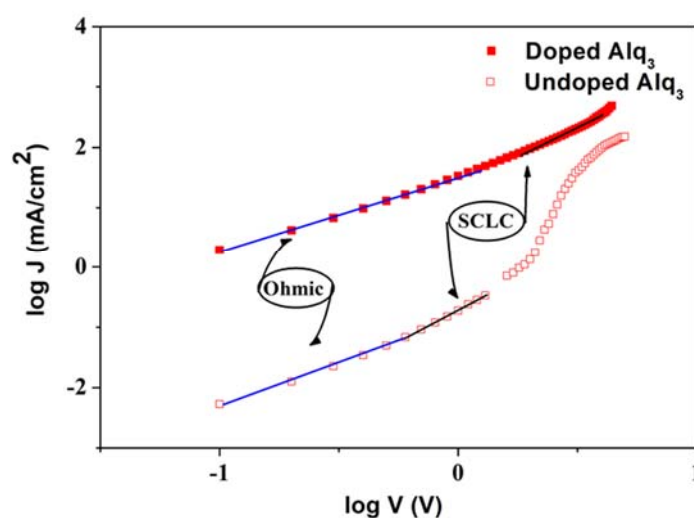


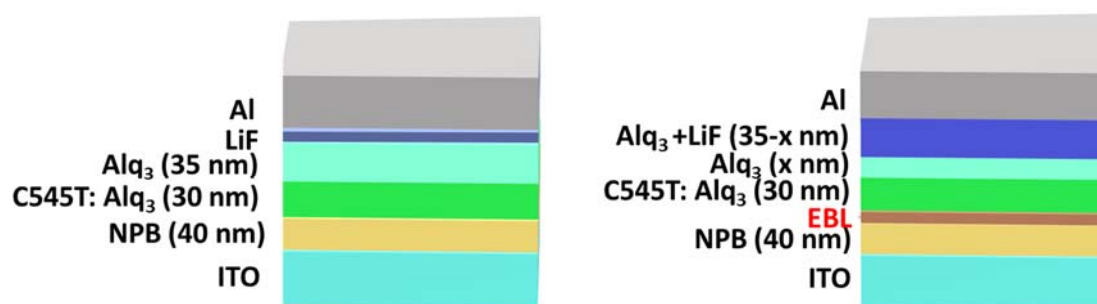
Figure 2.2 log J vs. log V plot for neat and doped Alq₃ films.

To study the effect of LiF-doping on the low field mobility of Alq₃, the SCLC studies were performed on electron-only devices of pristine and doped Alq₃ with the structure Al (60 nm)/ Alq₃ (60 nm) / Al (80 nm). The values of electron mobility of Alq₃ and doped Alq₃ in the SCLC region were estimated to be 1.29×10^{-7} cm²/V-s and 1.40×10^{-5} cm²/V-s respectively, the former being consistent with the reported value for undoped Alq₃⁴⁸. The recorded high mobility for the LiF-doped Alq₃ indicates that the charge carrier mobility is increased by the LiF doping. The increase in mobility could be due to the filling of shallow trap levels by the increased carrier concentration due to doping⁴⁹.

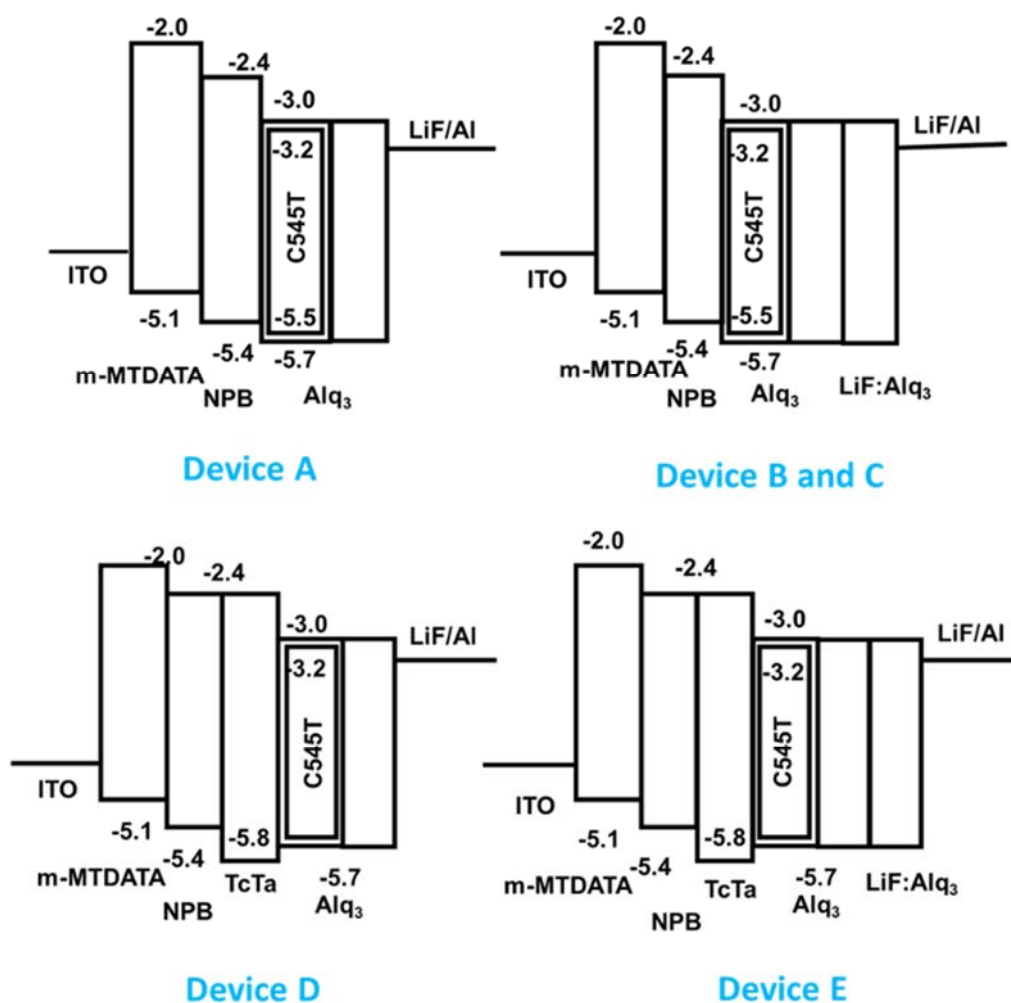
2.3.3 LiF bulk doping

2.3.3.1 Device structure

The structures of the OLED stacks that have been studied are given in Fig. 2.3. Typical control device structure (Device A) consisted of ITO/ 4,4',4''-Tris[phenyl(m-tolyl)amino] triphenyl amine (m-MTDATA)(100 nm)/ NPB (30 nm)/Alq₃:5 wt % of C545T (30 nm)/Alq₃ (35 nm)/LiF(1 nm)/ Al (100 nm). Device B has the structure ITO/ m-MTDATA (100 nm)/ NPB (30 nm)/ Alq₃: 5 wt % C545T(30 nm)/ Alq₃ (10 nm)/ Alq₃: 5 wt % LiF (25 nm)/ Al (100 nm). Device C has the structure ITO/ m-MTDATA (100nm)/ NPB (30 nm)/ Alq₃: C545T (30 nm)/ Alq₃ (20 nm)/ Alq₃: 5 wt % LiF (15 nm)/ Al (100 nm). Device D has the same structure as the control device except that there is a 3 nm TCTA layer between EML and HTL. Device E has the same structure as Device C except that there is a 3 nm thick TCTA layer between EML and NPB. LiF doping concentration was kept at 5% for all the devices.



(a)



(b)

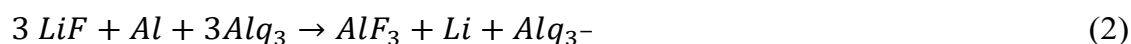
Figure 2.3 a) Typical device structure of the OLED used in this study, b) Energy level diagrams for devices i) A, ii) B and C, iii) D and iv) E. The HOMO-LUMO values and work functions are given in eV.

2.3.3.2 Device characteristics without blocking layer

The luminous efficiency or the current efficiency and the power efficiency are estimated from the J-V-L characteristics. External Quantum Efficiency (EQE) is the most appropriate parameter to compare the performance of different OLEDs. Current efficiency expressed in cd/A is considered to be equivalent to EQE except that the former weighs the photons as per the photopic response of the eye whereas the latter considers all photons with equal weightage⁵⁰. We have used current efficiency to compare the devices, since they are primarily intended for display applications, along with other performance parameters such as power efficiency, turn on voltage, peak luminance etc.

Fig. 2.4a shows the J-V-L characteristics of the devices with various pristine to doped ETL thickness ratios. For better presentation, the data is given in a logarithmic plot. The turn on voltages for 10 cd/m² is 3.27 V, 8.05 V and 3.27 V for devices A, B and C. As is evident, the device B, having heavily doped ETL with 10 nm pristine Alq₃ and 25 nm LiF-doped Alq₃ has a much higher current density compared to the control device. However, the light emission from device B was negligibly very poor. The turn on voltage for the device B is much higher.

At a biasing voltage of 9 V, the device exhibited a brightness of only 32 cd/m². Device C, with 20 nm undoped Alq₃ and 15 nm doped Alq₃ also exhibited higher current densities indicating a high electron injection and transport but retained the brightness. The current density of device B is much higher than that of device C, the latter being still higher than that of device A. LiF can dope Alq₃ n-type as given in equation (2),⁵¹



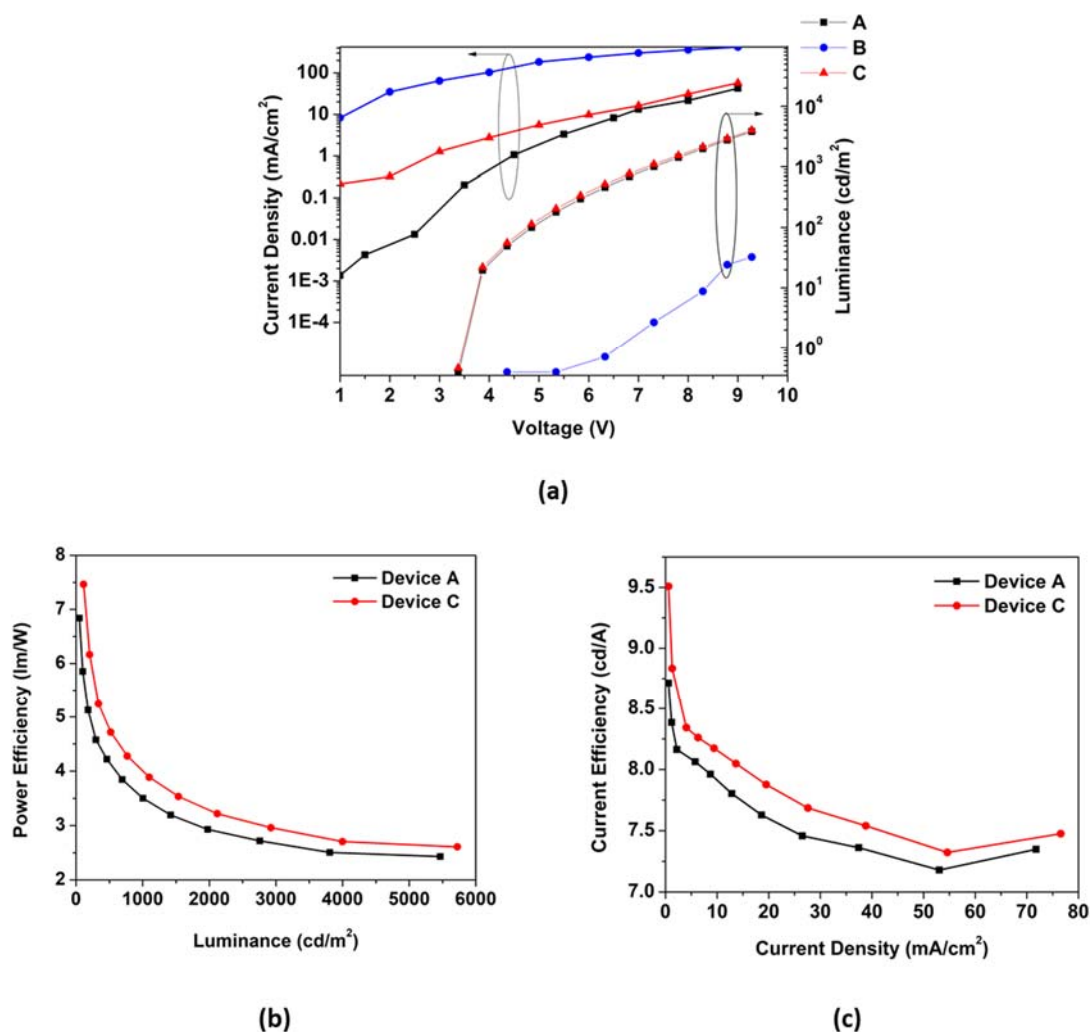


Figure 2.4 a) J-V-L characteristics of devices A, B and C, b) Current efficiency vs. Current density for devices A and C and c) Power efficiency vs. Luminescence for devices A and C.

Even though Al is deposited as a top cathode only, it has been shown with the help of secondary ion mass spectroscopic studies that the cathode can diffuse into the ETL and can create the desired bulk doping effect⁵¹. On the other hand, it is reported that Li can diffuse into the organic films and can act as a quenching site²⁵ which may cause the reduction in luminance. The light emission from the device B is indeed minimal. The high turn on voltage is also matching with this observation. The fact that there is no corresponding increase in luminance with the high current density indicates the

dominance of non-recombination current in the transport or non-radiative quenching of the excitons. The current balance factor, γ , in a device is given by,

$$\gamma = \frac{J_r}{J_r + J_{nr}} \quad (3)$$

where J_r is the recombination current density and J_{nr} is the non-recombination current density.

In the present case, the electron transport improves by doping as is evidenced by the J-V characteristics but, as the hole transport remains the same, the carrier imbalance in the device is increased, reducing radiative recombination efficiency. Fig 2.4b shows the current density vs. current efficiency characteristics of the devices. As the charge balance is better for device C, it exhibits higher current efficiency compared to control device. Data for device B is not shown in Fig.2.4b and c, as the efficiency value is very poor. Fig 2.4c gives the luminance vs. power efficiency data for device A and device C. It can be seen that the power efficiency is reduced to 60% when the brightness increases from 100 cd/m² to 1000 cd/m², for the control device A. Though the LiF doping results in increased brightness and power efficiency, the roll-off is only slightly improved for device C as the power efficiency drops to 53% when the brightness is increased from 100 cd/m² to 1000 cd/m². Though the current density of device C is higher than that of device A, brightness of device C is not having a corresponding increase, which indicates the possibility of quenching at higher fields.

2.3.3.3 Device characteristics with blocking layer

In the ETL, when the ratio of the pristine Alq₃ layer to LiF-doped layer increases, the current efficiency steadily increases. The device C showed increased carrier balance, and in an attempt to increase it further, we decided to incorporate an EBL. The selected EBL, TCTA having its lowest unoccupied molecular orbital (LUMO)

positioned at -2.3 eV and the HOMO at -5.7 eV, does pose a barrier for electron transport. Twofold improvement in maximum luminance has been observed for quantum dot LEDs with TCTA as an EBL⁵².

Fig 2.5a compares the J-V-L characteristics of devices D and E again with the control device C. Device D has lower current density than the control device, and this is expected as the EBL reduces the current. The turn on voltage for 10 cd/m² is also higher for device D (3.4 V). For device E where both ETL doping and EBL are present, the current density is low at high fields. The turn on voltage is also comparable (3.3 V). However, at higher voltages, this problem is overcome as the hole mobility of TCTA is greater than that of NPB⁵³. Additionally, it is reported that the hole mobility of TCTA increases with the applied field⁵⁴. Even though the use of EBL results in a reduction of current, by confining the electrons within the EML, use of one with HTL characteristics can actually increase the current as reported by Hagen et al^{55,56}. This seems to be the case in our study too, considering the higher hole mobility of TCTA.

As transport doping lowers the energy barriers across the interface, driving voltages of the doped devices are significantly reduced as is clearly seen from Fig 2.5a. Working voltage of the undoped device at a luminance of 100 cd/m² is 4.5 V whereas for device E, it is reduced close to 4 V. At 1000 cd/m², the driving voltage of device E becomes 6 V as compared to 7 V for the undoped device. The device E yields a brightness of 4460 cd/m² at 8 V, against 1978 cd/m² for the control device with undoped ETL. The luminance value reaches 9735 cd/m² against 3808 cd/m² with a 1 V increase in driving voltage. On inserting TCTA between HTL and emission layer, a distinct increase in the current efficiency is observed for both device D and E, as can be seen from Fig 2.5b. In device D, this is partly due to the reduced current density. However, device E presents an interesting picture where both current density and brightness are increased.

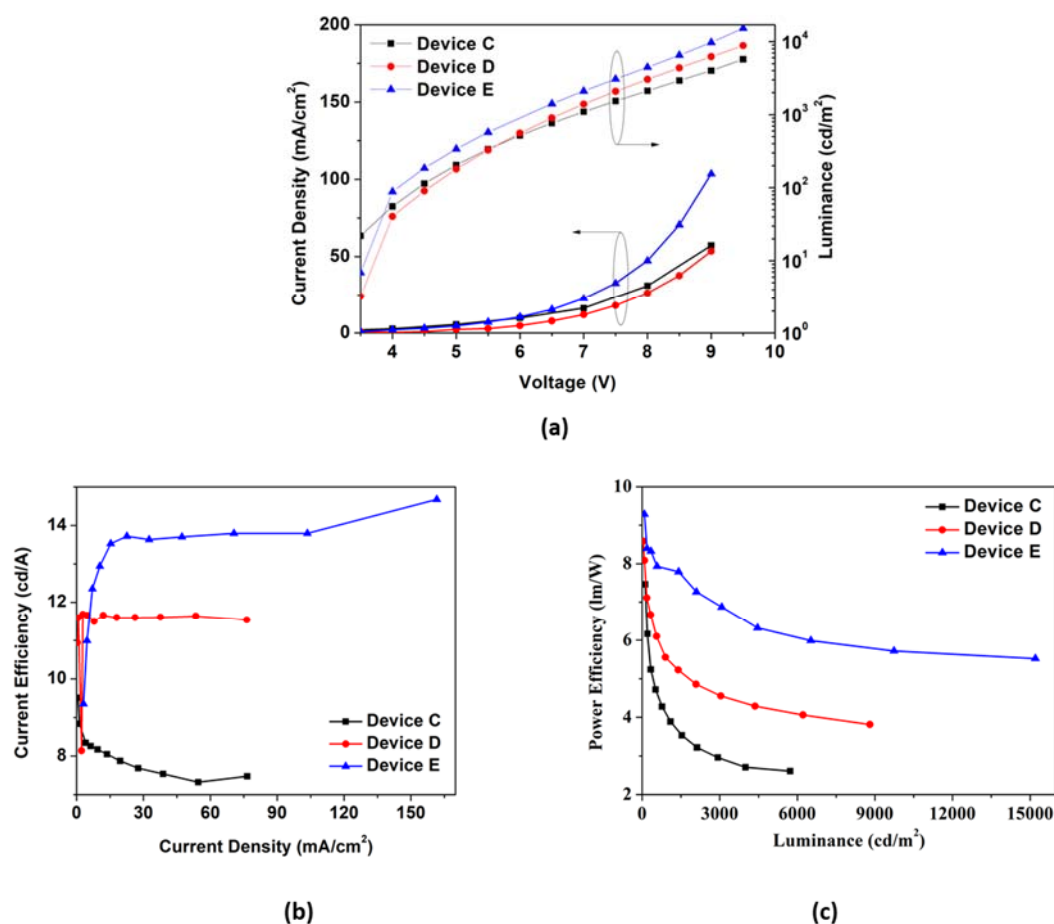


Figure 2.5 a) J-V-L characteristics of devices C, D and E, b) Current efficiency vs. Current density for devices C and D and E and c) Power efficiency vs. Luminance plot for devices C, D and E.

The plot of luminance vs. power efficiency is given in Fig 2.5c. It can be seen that the efficiency roll-off is considerably decreased for device E. While increasing the brightness from 100 cd/m² to 1000 cd/m², the efficiency drop was around 47% for the control device whereas only a drop of 15% was observed for device E. Increasing hole mobility of TCTA with increasing electric field could be the reason for this behavior. Important parameters of the devices A-E are summarized in Table 2.1. Being a fluorescent emitter, Alq₃:C545T system is inherently not very efficient. We have chosen this emitter system only as a model and the concept can be extended to other

emitters as well. It may be noted that the performance of the control device is comparable to earlier reports on Alq₃: C545T based OLEDs^{56,57}.

| <i>Device description</i> | <i>Turn on voltage for 10 cd/m²</i> | <i>Luminance @ 9 V (cd/m²)</i> | <i>Current Efficiency (cd/A) @ J=10 mA/cm²</i> | <i>Power Efficiency (lm/W) @ 1000 cd/m²</i> |
|---------------------------|--|---|---|--|
| device A | 3.27 | 3808 | 7.9 | 4.01 |
| device B | 8.05 | 32 | --- | --- |
| device C | 3.22 | 3999 | 8.11 | 2.65 |
| device D | 3.40 | 6222 | 11.56 | 5.50 |
| device E | 3.40 | 9735 | 12.87 | 7.85 |

Table 2.1 Summary of the performance of devices A, B, C, D and E.

Brightness linearly follows current density in a given device. As is evident, the current density increases as we dope the electron transport layer. However, the device with the highest current density has the lowest efficiency value pointing towards the need for a balanced injection and an optimized thickness of the undoped region to prevent any possible diffusion of Li into the EML. This enhancement in current density is not, in turn, linear with the increase in the thickness of the doped region, pointing towards a more balanced carrier injection at some point, for the reported device design. Similarly, the luminance values of the more balanced devices also are increasing with the current density. With the addition of TCTA layer, the device E exhibits an extremely high luminance value as well as efficiency along with high current density. As the luminance is increasing with current density, TCTA modified EML interface seems to favor increased radiative recombination. It is reported that the electron

confinement plays an important role in increasing the efficiency of OLEDs⁵⁸. Even though the current density of device E is less at lower voltages, after the onset of light emission, the device offers the highest current efficiency and power efficiency. Theoretical and experimental studies have shown that the hole mobility is at least 1-2 orders less than the electron mobility in Alq₃⁵⁹. Hence it is possible that the holes see a mobility barrier as suggested by de Mello et al. which also increases the chances of recombination at the interface⁶⁰.

2.3.4 Studies on LiF doping concentration

2.3.4.1 Device structure

The devices fabricated have the following structure: ITO/ NPB (30 nm)/ Alq₃: C545T (30 nm)/ Alq₃ (20 nm)/ Alq₃: x wt % of LiF (15 nm)/ Al; x = 2.7, 3.3, 4.6 and 10.2. A thin layer of EBL like NPB, TCTA and TAPC is inserted into the optimum performing device structure, and the performances are compared. See Fig 2.6 for the energy level diagram.

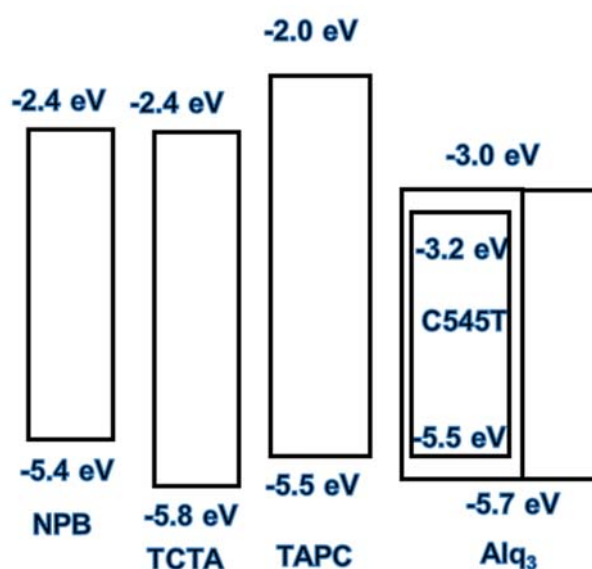


Figure 2.6 Device energy level diagram of the device. The HOMO-LUMO values are given in eV.

2.3.4.2 Device characteristics without blocking layers

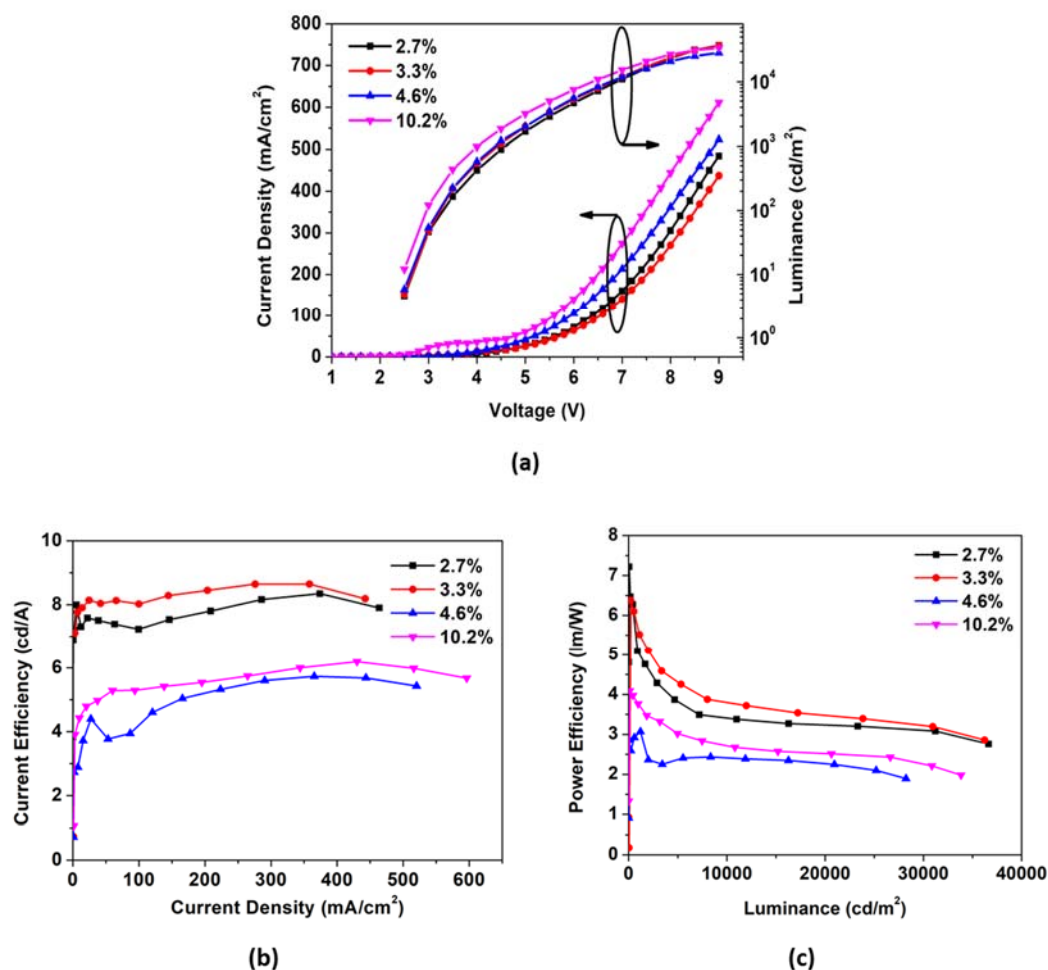


Figure 2.7 a) Current Density-Voltage-Luminance Characteristics, b) Power Efficiency, and c) Current Efficiency characteristics of the OLEDs with different percentages of ETL doping.

Fig 2.7 shows the device characteristics of the devices with only NPB on the hole injection side (i.e., without any additional blocking layer) and four different LiF: Alq₃ doping percentages. A device without the LiF bulk doping, but rather a LiF interlayer between Alq₃ and cathode is given as control device. Device with 10.2 % doping shows the highest current density and luminance for a given voltage, but a lower efficiency value. The 10.2% device has the highest current density at every voltage, which furthermore increases the luminescence, as is evident. Nevertheless, it is clear that the enhancement in luminescence is

not linear with the enhancement in current density. This point towards an increased non-recombination current along with the increased recombination current suggesting an increased charge imbalance in the device. This is further evidenced by the fact that when the device with 10.2 % doping recorded a maximum external quantum deficiency (EQE) of 1.6 %, the device with 3.3 % ETL doping exhibited a maximum EQE of 2.3 %. At 1000 cd/m² luminance, the devices with the doping concentration of 2.7, 3.3, 4.6 and 10.2 % show a stable current efficiency of 7.4, 8.0, 4.0 and 4.9 cd/A respectively. Device with 3.3 % ETL doping has the highest efficiencies at all values of current density as well as the luminescence.

2.3.4.3 Device characteristics with blocking layers

A comparison (of J-V-L characteristics) between the best combination of the LiF-doped device with NPB alone and with NPB and TCTA or TAPC blocking layers is given in Fig 2.8. Here, all the devices have Alq₃ doped with 3.3% LiF as the doped part of the ETL. There is a slight increase in the operating voltage and a decrease in electroluminescence at a given voltage for the devices with additional EBLs. Taking into account only Fig 2.8a, the device without an additional blocking layer has the highest luminescence and lower driving voltage. At 5 V, whereas the device without an EBL has recorded luminescence around 2000 cd/m², those with TCTA exhibited only 1000 cd/m² and the device with TAPC yielded even less than that. However, by 9 V, all the devices reach the brightness of 30,000 cd/m² with current densities 430, 350 and 330 mA/cm² for NPB, TCTA and TAPC respectively. Therefore, driving current is the defining factor of the performance of these devices. At a current density of 100 mA/cm², the recorded luminescence values are 8000, 10500 and 9100 cd/m² respectively. At a luminance of 1000 cd/m², the device with just NPB as HTL and without additional EBL has a current density around 16 mA/cm² but for the devices with additional EBL, it was only 10 mA/cm². Driving OLEDs with low current for high luminescence is very

important because, in this way, device degradation can be prevented due to the reduction in Joules heating.

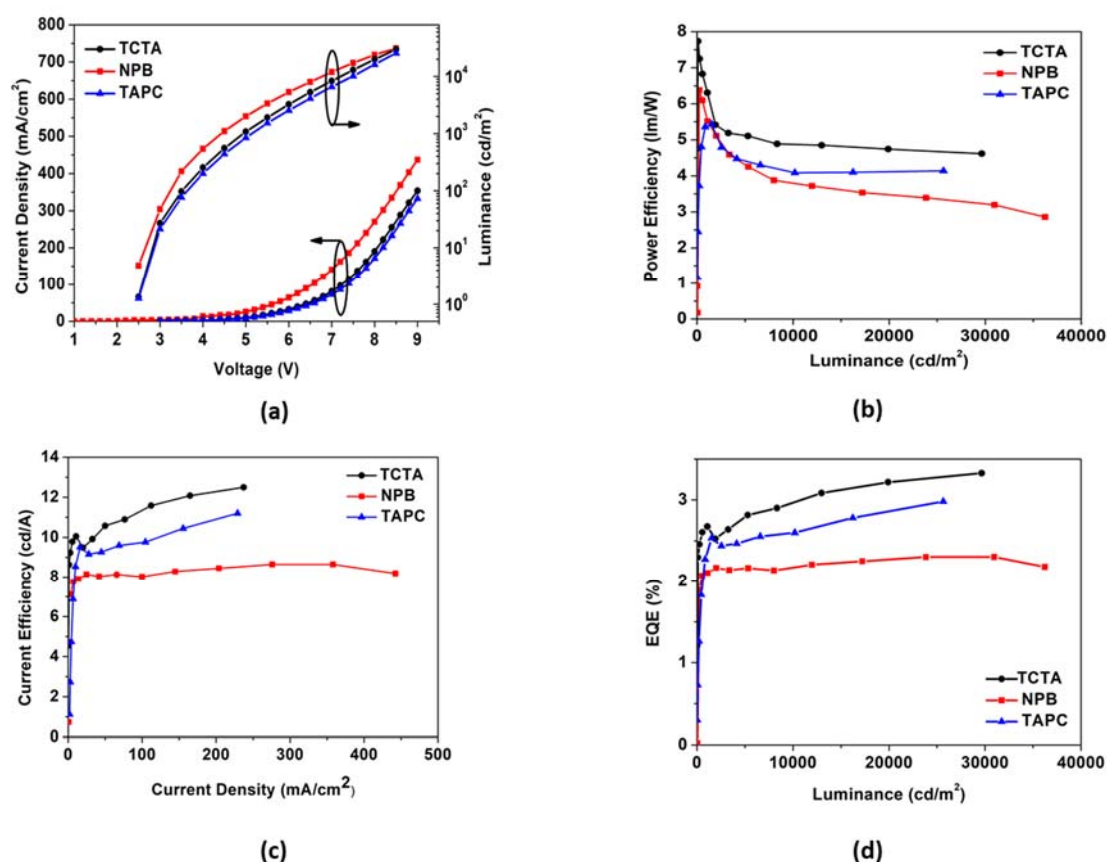


Figure 2.8 a) Current Density-Voltage-Luminance Characteristics b) Power Efficiency, c) Current Efficiency, and d) EQE characteristics of the devices with different Electron Blocking Layers.

Considering Figs 2.8b and 2.8c, the current and power efficiencies of the devices with EBL have a marked improvement. Power efficiency plot has a more stable output trend for the whole range of luminance. The power efficiencies for devices with TCTA and TAPC layers have a stable value of around 5.0, and 4.5 lm/W and current efficiency values reach 12 cd/A. The EQE values of the TCTA and TAPC devices reach close to 3.4% and 3.0% respectively from 2.3% for the device with only NPB as shown in Fig 2.8d. EQE for the device with TCTA is always above that of the device with only NPB. For the TAPC device, EQE is gradually

increasing up to 1500 cd/m² of luminance, below that of NPB device. Above 1500 cd/m², the EQE again increases and stabilizes around 2.5%. At a brightness of 1000 cd/m², there is an improvement of 27.8% for the device with TCTA, compared to that of the device with NPB only on the hole transport side. A summary of the device performance is given in Table 2.2.

| Device description | Turn on voltage for @ 10 cd/m ² | Luminance (cd/m ²) @ 8.5 V | Current Efficiency (cd/A) @ J=10 mA/cm ² | Power Efficiency (lm/W) @ 1000 cd/m ² | EQE Max % |
|--------------------|--|--|---|--|-----------|
| Control | 3.62 | 3696 | 5.34 | 2.89 | 2.01 |
| 2.7% | 2.56 | 31210 | 7.3 | 5.06 | 2.15 |
| 3.3%/ NPB | 2.55 | 30960 | 7.84 | 5.62 | 2.30 |
| 4.6% | 2.54 | 25200 | 3.5 | 3.01 | 1.55 |
| 10.2% | 2.50 | 30870 | 4.42 | 3.74 | 1.65 |
| TCTA | 2.66 | 29650 | 10.01 | 6.4 | 3.39 |
| TAPC | 2.71 | 25650 | 8.53 | 5.36 | 2.98 |

Table 2.2 Summary of the performance of devices with different LiF doping percentage and blocking layer.

As there is no direct contact between the highly doped transport layers and emission layers, we need not consider the quenching effect of the ETL dopant⁶¹. The combination of NPB and undoped Alq₃ can block electrons and holes respectively, thereby confining carriers within the emission zone. This can cause the excess carrier to accumulate at the interface. The space charge region can alter the field distribution to balance the charge carriers injected¹³. Reasons of efficiency roll-off in OLEDs include concentration quenching, triplet-triplet annihilation, singlet fission, exciton- polaron interactions; field induced quenching, change in charge carrier balance, Joules heating, etc. In fact roll-off is related to radiative life time in phosphorescent devices and charge imbalance in fluorescent devices⁶². Attaining better exciton/charge carrier confinement will improve the charge balance and hence will address the roll-off at least partially. To get maximum efficiency out of a typical device structure, an

equal number of holes and electrons should meet at the EML to form excitons, which has enough thickness to contain the exciton diffusion. This can potentially make sure that the excitons are recombining in the EML. Therefore, the LUMO or HOMO levels and carrier mobility of the blocking layers are the significant factors in improving device performance. The electron barrier exists due to the difference in LUMO levels between EBL and EML. With the ETL doping, the electron transport is significantly increased over the cathode side, which will need to be confined to the EML by using EBL as shown in Fig 2.6a.

TCTA and NPB have comparable hole mobility $\sim 10^{-4} \text{ cm}^2/\text{Vs}^{63}$. But, TCTA has a very low electron mobility of $\sim 10^{-8} \text{ cm}^2/\text{Vs}^{64}$ when compared with $\sim 10^{-4} \text{ cm}^2/\text{Vs}$ of NPB⁶³, even though both have similar LUMO levels. This also contributes towards exciton confinement towards EML in the presence of TCTA. Hole mobility of TAPC is even higher at $\sim 10^{-2} \text{ cm}^2/\text{Vs}^{65}$. With the high LUMO and low HOMO levels, TAPC should be the ideal choice. But, the holes experience a barrier, though small, for injection from the HOMO of TAPC to the HOMO of Alq₃. But, TCTA offers no barrier for holes flowing to the EML and the possibility of exciton formation at the interface is increased⁶⁶. These excitons then diffuse within the EML.

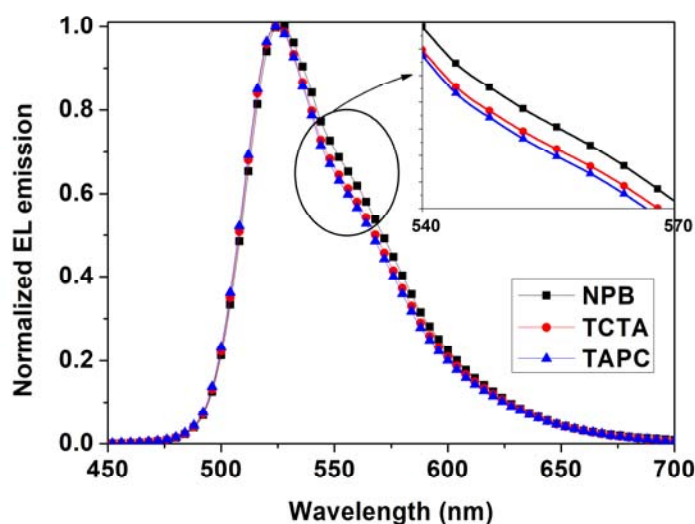


Figure 2.9 Electroluminescence spectra.

Thus, the LUMO-HOMO levels of TCTA can block the excitons from diffusing to the HTL. With TAPC, as there is a small barrier for holes, it seems a fraction of the carriers are not contributing towards exciton formation and recombination. The device with only NPB layer as the EBL also suffers by similar inefficient confinement. In the case of device with NPB only, there is a slight redshift for the emission peak (from 524 nm to 528 nm) and the shoulder at 564 nm becomes more pronounced, as can be seen from Fig 2.9. The red-shifted emission may be due to direct charge trapping by the luminescent dopant, C545T. There is a recent report about a similar redshift happening when the percentage of C545T doping increases in an Alq₃ based OLED⁶⁷. This has been explained as due to a change from Förster energy transfer to direct charge trapping by the dopant, C545T. It is likely that in the present case, a similar charge trapping and subsequent emission by the dopant is encouraged when no EBL is present. Electrons may be trapped in the dopant in both cases but in the case with EBL, holes injected to the EML interact with the blocked electrons form excitons and do Förster energy transfer to the dopant near the EBL/EML interface. Without the blocking layer, the holes diffuse deeper into the EML and may form excitons with the trapped electrons in the dopant, which may give rise to the red shifted emission. This is studied in more detail in chapter 3. Also, the recombination zone becomes wider when no EBL is used and as a result, the emission becomes broader.

2.4. Conclusions

Doping of thin films of Alq₃ with LiF increases the current density by several factors. Doping results in higher carrier mobility compared to undoped samples as confirmed by SCLC studies. Due to the greatly reduced resistivity, doping leads to enhanced transport and a significant decrease in the driving voltage in OLEDs. However, this need not necessarily translate into high luminescence efficiency because

of the luminescence quenching by diffused Li metal. Careful design by having an undoped buffer ETL between EML and doped ETL can obviate this problem. To reduce the contribution of the increased electron concentration to the non-recombination current, we have employed an EBL, which in fact led to higher recombination resulting in excellent device performance. This also addresses the power efficiency roll-off at high brightness effectively, probably due to the choice of the EBL material for which the hole mobility increases with electric field.

With an n-doped ETL and a suitable EBL it is possible to achieve a 27.8% improvement in the EQE at 1000 cd/m². The reduced injection current will be helpful in preventing the device degradation to some extent even at very high luminance. It is shown that with increased transport doping, luminescence can be increased as well. As this increase is not directly proportional to the increase in current density, there is no similar increase in current efficiency. In the presence of a suitable EBL, even though there is a slight decrease in the luminescence, device efficiency values are greatly improved. In the cases presently studied, TCTA having hole mobility in between that of NPB and TAPC, with LUMO similar to NPB and effectively no hole injection barrier is found to be the ideal electron blocking material. Thus it is established that along with the energy level offsets, the electron and hole mobility values of the EBL material are also critically important. It is also shown that the presence of EBL makes the emission slightly sharper indicating a narrower recombination zone.

2.5 References

- 1 Tang, C. W. & VanSlyke, S. A. Organic electroluminescent diodes. *Applied Physics Letters* **51**, 913-915, doi:10.1063/1.98799 (1987).

- 2 D'Andrade, B. W., Forrest, S. R. White Organic Light-Emitting Devices for Solid-State Lighting. *Advanced Materials* **16**, 1585-1595, doi:10.1002/adma.200400684 (2004).
- 3 Kido, J., Hongawa, K., Okuyama, K. & Nagai, K. White light-emitting organic electroluminescent devices using the poly(N-vinylcarbazole) emitter layer doped with three fluorescent dyes. *Applied Physics Letters* **64**, 815-817, doi: 10.1063/1.111023 (1994).
- 4 Van Slyke, S. A., Chen, C. H. & Tang, C. W. Organic electroluminescent devices with improved stability. *Applied Physics Letters* **69**, 2160-2162, doi:10.1063/1.117151 (1996).
- 5 Blades, C. D. J. & Walker, A. B. Simulation of organic light-emitting diodes. *Synthetic Metals* **111-112**, 335-340, doi:10.1016/s0379-6779(99)00359-8 (2000).
- 6 Tang, C. W., VanSlyke, S. A. & Chen, C. H. Electroluminescence of doped organic thin films. *Journal of Applied Physics* **65**, 3610-3616, doi: 10.1063/1.343409 (1989).
- 7 Baldo, M. A. *et al.* Highly efficient phosphorescent emission from organic electroluminescent devices. *Nature* **395**, 151-154, doi:10.1038/25954 (1998).
- 8 Adachi, C., Baldo, M. A., Thompson, M. E. & Forrest, S. R. Nearly 100% internal phosphorescence efficiency in an organic light-emitting device. *Journal of Applied Physics* **90**, 5048-5051, doi: 10.1063/1.1409582 (2001).
- 9 Marks, R. N., Bradley, D. D. C., Jackson, R. W., Burn, P. L. & Holmes, A. B. Charge injection and transport in poly(p-phenylene vinylene) light emitting diodes. *Synthetic Metals* **57**, 4128-4133, doi:10.1016/0379-6779(93)90569-i (1993).
- 10 Parthasarathy, G., Shen, C., Kahn, A. & Forrest, S. R. Lithium doping of semiconducting organic charge transport materials. *Journal of Applied Physics* **89**, 4986-4992, doi:10.1063/1.1359161 (2001).

- 11 Yamamori, A. *et al.* Doped organic light emitting diodes having a 650-nm-thick hole transport layer. *Applied Physics Letters* **72**, 2147-2149, doi:10.1063/1.121304 (1998).
- 12 Blochwitz, J., Pfeiffer, M., Fritz, T. & Leo, K. Low voltage organic light emitting diodes featuring doped phthalocyanine as hole transport material. *Applied Physics Letters* **73**, 729-731, doi:10.1063/1.121982 (1998).
- 13 Huang, J. *et al.* Low-voltage organic electroluminescent devices using pin structures. *Applied Physics Letters* **80**, 139-141, doi:10.1063/1.1432110 (2002).
- 14 Walzer, K., Maennig, B., Pfeiffer, M. & Leo, K. Highly efficient organic devices based on electrically doped transport layers. *Chemical Reviews* **107**, 1233-1271, doi:10.1021/cr050156n (2007).
- 15 Yakimov, A. & Forrest, S. R. High photovoltage multiple-heterojunction organic solar cells incorporating interfacial metallic nanoclusters. *Applied Physics Letters* **80**, 1667-1669, doi:10.1063/1.1457531 (2002).
- 16 Aziz, E. F. *et al.* Localized Charge Transfer in a Molecularly Doped Conducting Polymer. *Advanced Materials* **19**, 3257-3260, doi:doi:10.1002/adma.200700926 (2007).
- 17 Salzmann, I. *et al.* Intermolecular Hybridization Governs Molecular Electrical Doping. *Physical Review Letters* **108**, 035502, doi:10.1103/PhysRevLett.108.035502 (2012).
- 18 Mityashin, A. *et al.* Unraveling the Mechanism of Molecular Doping in Organic Semiconductors. *Advanced Materials* **24**, 1535-1539, doi:doi:10.1002/adma.201104269 (2012).
- 19 Maitrot, M., Guillaud, G., Boudjema, B., André, J. J. & Simon, J. Molecular material-based junctions: Formation of a Schottky contact with metallophthalocyanine thin films doped by the cosublimation method. *Journal of Applied Physics* **60**, 2396-2400, doi: 10.1063/1.337151 (1986).

- 20 Tietze, M. L. *et al.* Elementary steps in electrical doping of organic semiconductors. *Nature communications* **9**, 1182, doi:10.1038/s41467-018-03302-z (2018).
- 21 Gao, W. & Kahn, A. Controlled p-doping of zinc phthalocyanine by coevaporation with tetrafluorotetracyanoquinodimethane: A direct and inverse photoemission study. *Applied Physics Letters* **79**, 4040-4042, doi:10.1063/1.1424067 (2001).
- 22 Lüssem, B., Riede, M. & Leo, K. Doping of organic semiconductors. *physica status solidi (a)* **210**, 9, doi:10.1002/pssa.201228310 (2013).
- 23 Li, F., Werner, A., Pfeiffer, M., Leo, K. & Liu, X. Leuco Crystal Violet as a Dopant for n-Doping of Organic Thin Films of Fullerene C60. *The Journal of Physical Chemistry B* **108**, 17076-17082, doi:10.1021/jp0478615 (2004).
- 24 Kido, J., Nagai, K. & Okamoto, Y. Bright organic electroluminescent devices with double-layer cathode. *IEEE Transactions on Electron Devices* **40**, 1342-1344, doi:10.1109/16.216443 (1993).
- 25 Choong, V.-E., Shi, S., Curless, J. & So, F. Bipolar transport organic light emitting diodes with enhanced reliability by LiF doping. *Applied Physics Letters* **76**, 958-960, doi:10.1063/1.125904 (2000).
- 26 Yuan, Y., Grozea, D., Han, S. & Lu, Z. H. Interaction between organic semiconductors and LiF dopant. *Applied Physics Letters* **85**, 4959-4961, doi:10.1063/1.1821653 (2004).
- 27 Schlaf, R. *et al.* Photoemission spectroscopy of LiF coated Al and Pt electrodes. *Journal of Applied Physics* **84**, 6729-6736, doi:10.1063/1.369000 (1998).
- 28 D'Andrade, B. W., Forrest, S. R. & Chwang, A. B. Operational stability of electrophosphorescent devices containing p and n doped transport layers. *Applied Physics Letters* **83**, 3858-3860, doi:10.1063/1.1624473 (2003).

- 29 Choong, V. *et al.* Dramatic photoluminescence quenching of phenylene vinylene oligomer thin films upon submonolayer Ca deposition. *Applied Physics Letters* **69**, 1492-1494, doi:10.1063/1.116918 (1996).
- 30 Rosenow, T. C. *et al.* Highly efficient white organic light-emitting diodes based on fluorescent blue emitters. *Journal of Applied Physics* **108**, 113113, doi:10.1063/1.3516481 (2010).
- 31 Meerheim, R. *et al.* Influence of charge balance and exciton distribution on efficiency and lifetime of phosphorescent organic light-emitting devices. *Journal of Applied Physics* **104**, 014510, doi:10.1063/1.2951960 (2008).
- 32 Keum, C.-M. *et al.* The Role of Metallic Dopants in Improving the Thermal Stability of the Electron Transport Layer in Organic Light-Emitting Diodes. *Advanced Optical Materials* **6**, 1800496, doi:doi:10.1002/adom.201800496 (2018).
- 33 Kido, J. & Matsumoto, T. Bright organic electroluminescent devices having a metal-doped electron-injecting layer. *Applied Physics Letters* **73**, 2866-2868, doi:10.1063/1.122612 (1998).
- 34 Nollau, A., Pfeiffer, M., Fritz, T. & Leo, K. Controlled n-type doping of a molecular organic semiconductor: Naphthalenetetracarboxylic dianhydride (NTCDA) doped with bis(ethylenedithio)-tetrathiafulvalene (BEDT-TTF). *Journal of Applied Physics* **87**, 4340-4343, doi:10.1063/1.373413 (2000).
- 35 Tanaka, S. *et al.* Doping Effect of Tetrathianaphthacene Molecule in Organic Semiconductors on Their Interfacial Electronic Structures Studied by UV Photoemission Spectroscopy. *Japanese Journal of Applied Physics* **44**, 3760-3763, doi:10.1143/jjap.44.3760 (2005).
- 36 Chan, C. K. *et al.* N-type doping of an electron-transport material by controlled gas-phase incorporation of cobaltocene. *Chemical Physics Letters* **431**, 67-71, doi:https://doi.org/10.1016/j.cplett.2006.09.034 (2006).

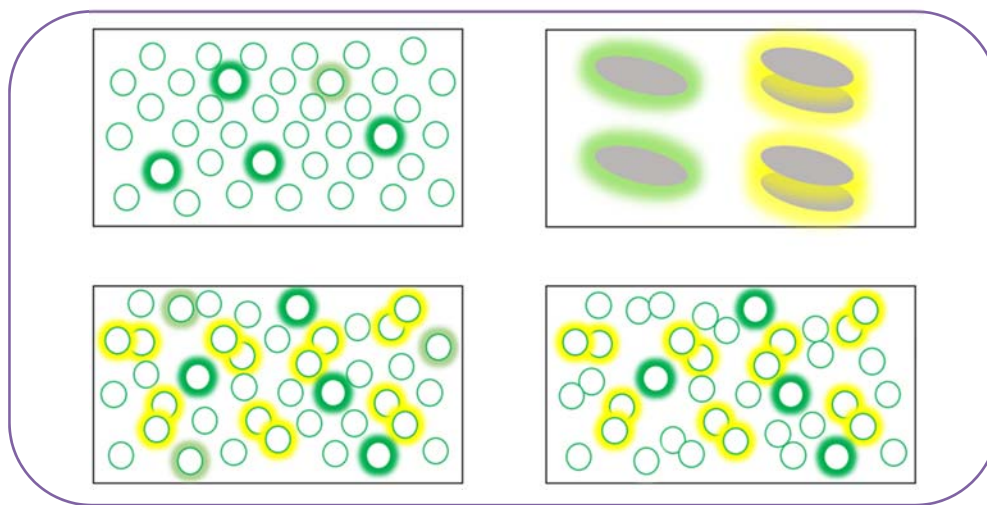
- 37 Werner, A. *et al.* n-Type Doping of Organic Thin Films Using Cationic Dyes. *Advanced Functional Materials* **14**, 255-260, doi:doi:10.1002/adfm.200305053 (2004).
- 38 Werner, A. G. *et al.* Pyronin B as a donor for n-type doping of organic thin films. *Applied Physics Letters* **82**, 4495-4497, doi:10.1063/1.1583872 (2003).
- 39 Wang, Y. *et al.* A comparative investigation of electron transport properties in Li₂CO₃ doped and undoped organic semiconductors by admittance spectroscopy. *Organic Electronics* **66**, 58-62, doi:https://doi.org/10.1016/j.orgel.2018.12.019 (2019).
- 40 Chen, N.-N. *et al.* Triarylphosphine oxide–phenanthroline molecular conjugate as a promising doped electron-transport layer for organic light-emitting diodes. *Organic Electronics* **48**, 271-275, doi:https://doi.org/10.1016/j.orgel.2017.06.021 (2017).
- 41 Lin, X. *et al.* Beating the thermodynamic limit with photo-activation of n-doping in organic semiconductors. *Nature materials* **16**, 1209, doi:10.1038/nmat5027
- 42 <https://www.nature.com/articles/nmat5027#supplementary-information> (2017).
- 43 Murawski, C., Leo, K. & Gather, M. C. Efficiency Roll-Off in Organic Light-Emitting Diodes. *Advanced Materials* **25**, 6801-6827, doi:10.1002/adma.201301603 (2013).
- 44 Weichsel, C., Reineke, S., Lüssem, B., & Leo, K. in *MRS Proceedings*.
- 45 Yuichiro, K., Hiroyuki, S. & Chihaya, A. Simple Accurate System for Measuring Absolute Photoluminescence Quantum Efficiency in Organic Solid-State Thin Films. *Japanese Journal of Applied Physics* **43**, 7729 (2004).
- 46 Tam, M. C., Su, H., Wong, K. S., Zhu, X. & Kwok, H. S. Surface-plasmon-enhanced photoluminescence from metal-capped Alq₃ thin Films. *Applied Physics Letters* **95**, 051503, doi:10.1063/1.3190501 (2009).

- 47 Cao, Y., Parker, I. D., Yu, G., Zhang, C. & Heeger, A. J. Improved quantum efficiency for electroluminescence in semiconducting polymers. *Nature* **397**, 414-417 (1999).
- 48 Lampert, M. A. & Mark, P. *Current injection in solids*. (Academic Press, 1970).
- 49 48 Kepler, R. G. *et al.* Electron and hole mobility in tris(8-hydroxyquinolinolato-N1,O8) aluminum. *Applied Physics Letters* **66**, 3618-3620, doi:10.1063/1.113806 (1995).
- 50 Olthof, S. *et al.* Ultralow Doping in Organic Semiconductors: Evidence of Trap Filling. *Physical Review Letters* **109**, 176601 (2012).
- 51 Forrest, S. R., Bradley, D. D. C. & Thompson, M. E. Measuring the Efficiency of Organic Light-Emitting Devices. *Advanced Materials* **15**, 1043-1048, doi:10.1002/adma.200302151 (2003).
- 52 Choudhury, K. R., Yoon, J.-h. & So, F. LiF as an n-Dopant in Tris(8-hydroxyquinoline) Aluminum Thin Films. *Advanced Materials* **20**, 1456-1461, doi:10.1002/adma.200701657 (2008).
- 53 Peng, H., Wang, W. & Chen, S. Efficient Quantum-Dot Light-Emitting Diodes With 4,4,4-Tris(N-Carbazolyl)-Triphenylamine (TCTA) Electron-Blocking Layer. *IEEE Electron Device Letters* **36**, 369-371, doi:10.1109/LED.2015.2398850 (2015).
- 54 Xian-Feng, Q., Jiang-Shan, C. & Dong-Ge, M. Comparative Study on Hole Transport in N, N'-bis(naphthalen-1-yl)-N,N'-bis(phenyl) Benzidine and 4, 4', 4"-tri(N-carbazolyl)triphenylamine. *Chinese Physics Letters* **27**, 088504, doi:10.1088/0256-307x/27/8/088504 (2010).
- 55 Noh, S., Suman, C. K., Hong, Y. & Lee, C. Carrier conduction mechanism for phosphorescent material doped organic semiconductor. *Journal of Applied Physics* **105**, 033709, doi:10.1063/1.3072693 (2009).
- 56 Hagen, J. A., Li, W., Steckl, A. J. & Grote, J. G. Enhanced emission efficiency in organic light-emitting diodes using deoxyribonucleic acid complex as an electron

- blocking layer. *Applied Physics Letters* **88**, 171109, doi:10.1063/1.2197973 (2006).
- 57 Chwang, A. B., Kwong, R. C. & Brown, J. J. Graded mixed-layer organic light-emitting devices. *Applied Physics Letters* **80**, 725-727, doi:10.1063/1.1446992 (2002).
- 58 Aziz, H., Liew, Y.-F., Grandin, H. M. & Popovic, Z. D. Reduced reflectance cathode for organic light-emitting devices using metalorganic mixtures. *Applied Physics Letters* **83**, 186-188, doi:10.1063/1.1591067 (2003).
- 59 Ji, C.-Y., Gu, Z.-T. & Kou, Z.-Q. Influence of confinement layers in the emitting layer of the blue phosphorescent organic light-emitting diodes. *Optical Materials* **60**, 541-545, doi:https://doi.org/10.1016/j.optmat.2016.09.023 (2016).
- 60 Fuchs, A. *et al.* Molecular origin of differences in hole and electron mobility in amorphous Alq3-a multiscale simulation study. *Physical Chemistry Chemical Physics* **14**, 4259-4270, doi:10.1039/C2CP23489K (2012).
- 61 Jin, R. *et al.* On the use and influence of electron-blocking interlayers in polymer light-emitting diodes. *Physical Chemistry Chemical Physics* **11**, 3455-3462, doi:10.1039/B819200F (2009).
- 62 Liu, F. & Nunzi, J.-M. *Noble metal nanoparticle enhanced organic light emitting diodes*. Vol. 8424 EPE (SPIE, 2012).
- 63 Giebink, N. C. & Forrest, S. R. Quantum efficiency roll-off at high brightness in fluorescent and phosphorescent organic light emitting diodes. *Physical Review. B* **77**, 235215, doi:10.1103/PhysRevB.77.235215 (2008).
- 64 Forsythe, E. W., Abkowitz, M. A. & Gao, Y. Tuning the Carrier Injection Efficiency for Organic Light-Emitting Diodes†. *The Journal of Physical Chemistry B* **104**, 3948-3952, doi:10.1021/jp993793o (2000).
- 65 Kang, J.-W. *et al.* Low roll-off of efficiency at high current density in phosphorescent organic light emitting diodes. *Applied Physics Letters* **90**, 223508, doi:10.1063/1.2745224 (2007).

-
- 66 Borsenberger, P. M., Pautmeier, L., Richert, R. & Bässler, H. Hole transport in 1,1-bis(di-4-tolylaminophenyl)cyclohexane. *The Journal of Chemical Physics* **94**, 8276-8281, doi:10.1063/1.460112 (1991).
- 67 Samal, G. S., Narayanan Unni, K. N., Bharat, S., Gupta, S. & Deepak. Improved efficiency in fluorescent blue organic light emitting diode with a carrier confining structure. *Organic Electronics* **10**, 1201-1208, doi:https://doi.org/10.1016/j.orgel.2009.06.009 (2009).
- 68 Rhee, S. H. *et al.* Heavily Doped, Charge-Balanced Fluorescent Organic Light-Emitting Diodes from Direct Charge Trapping of Dopants in Emission Layer. *ACS applied materials & interfaces* **7**, 16750-16759, doi:10.1021/acsami.5b04519 (2015).

Tuning the optoelectronic properties of fluorescent OLEDs by deposition conditions and device engineering



3.1. Abstract

Efficient organic light emitting diodes (OLEDs) require multilayer structure. Higher the complexity in design, the better the tuning of emission, which makes the production cost high as well. In this study, we are trying to tune the OLED emission by varying the deposition conditions, simultaneously while reducing the process complexity. The concentration of dopant in EML was varied from 3% to 50% and the single dopant emitter as a limiting case was also employed and the deposition rate and emission layer (EML) thickness were also varied. The impact of heavy luminescence doping on the electrical and optical properties and its dependence on deposition conditions were studied and a 10-(2-Benzothiazolyl)-2,3,6,7-

tetrahydro-1,1,7,7-tetramethyl-1H,5H,11H-(1)benzopyrroprano(6,7-8-I,j)quinolizin-11-one (C545T) emitter based OLED emission was observed to change from excitonic green to excimeric yellow. With the increase in doping, reduction in pure exciton emission and increase in excimer emission was observed, resulting in electroluminescent spectral red shift and broadening. Potential for white emission with this simple stack design was explored by inserting a fluorescent blue emitter. The recorded CIE coordinates have shown a tunability ranging from (0.39, 0.45) to (0.33, 0.43).

3.2 Introduction

An emitting layer consisting of Tris(8-hydroxyquinolato)aluminium (Alq_3) as host doped with a coumarin derivative and DCM (4-(Dicyanomethylene)-2-methyl-6-(4-dimethylaminostyryl)-4H-pyran) as the hole transport layer (HTL) was the first reported OLED with doped emitter¹. Doping the Alq_3 host with a suitable dopant is found to cause considerable gain in electroluminescence (EL) efficiencies as well as in device lifetime. The optimal dopant concentration in OLEDs is found to be typically below 5%. At low dopant level, an excited state complex can form between dopant dye and the host material in the host-guest matrix, which is called an exciplex. This can occur due to the charge carrier transfer from either host to guest or vice versa. This complex is only bound to the excited state. With increased dopant concentration in the host-guest matrix, a decrease in emission intensity and red shift to the emission peak was observed which was attributed to a possible excimer emission¹. As the dopant concentration increases, doped dye molecules begin to form aggregates leading to self-quenching and thereby emission loss. This can often comprise of the non-emissive excimer formation. In an excimer, the exciton is delocalized over two molecules, $A^* + A \rightarrow A_2^*$, the excimer². The dimer formed in the excited state is not bound to the ground state and dissociates upon relaxation. The emission from the excimer, if any, often would have low quantum

efficiency. In addition, it can broaden the emission spectrum. In a host-dopant matrix, carrier transport properties can also be tuned separately. When a fluorescent dye is used as the dopant, the light generation is due to singlet excitons only and the energy transfer between host and guest is Förster transfer.

Coumarin dye and its several derivatives have been in use for a long time in the case of flash lamp pumped organic lasers^{3,4}. After the introduction of guest-host emitter system in OLEDs¹, a few coumarin derivatives started appearing as dopants in the Alq₃ based host system⁵ which made it one of the earliest group of dopants used in OLEDs for efficient emission, eg. 3-(2-benzothiazolyl)-7-(diethylamino)-2H-1-benzopyran-2-one, known as C-6⁶ (Fig 3.1a) which fluoresces at a peak wavelength of 505 nm in EtOH with 78% photoluminescence quantum yield⁴. The quantum efficiency can be enhanced up to 90 % by rigidizing the donor moiety [Et₂N-] as in 10-[2-benzothiazolyl]-2,3,6,7-tetrahydro-1H,5H,11H-benzo-[l]pyrano[6,7,8-ij]quinolizin-11-one or C-545, Fig 3.1b. The enhancement is due to its structural coplanarity which aligns the p-orbital of nitrogen to overlap with the π -orbitals of the phenyl ring for more effective conjugation⁶.

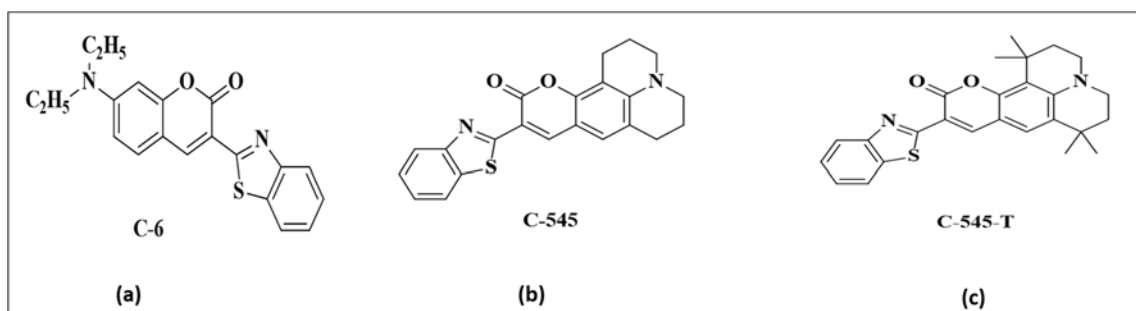


Figure 3.1 The molecular structure of a) C-6, b) C545, and c) C545T

With rigidization, the internal mobility of the [Et₂N-] moiety of C-6 is reduced which reduces the non-radiative relaxation of the excited state. The emission of C545 also is red-shifted to 519 nm from 506 nm of C-6. However, its planar structure may cause more

aggregation in the solid state. It has been shown that with increased concentration for photoluminescence and electroluminescence emission, a long wavelength shoulder starts to appear⁷. Introducing four methyl groups as steric spacers in C545 to reduce the dye-dye interaction at high concentration led to 10-(2-benzothiazolyl)-1,1,7,7-tetramethyl-2,3,6,7-tetrahydro-1H,5H,11H-benzo[*l*] pyrano[6,7,8-*ij*]quinolizin-11-one called C545T^{5,8-10}, Fig 3.1c.

10-(2-Benzothiazolyl)-2,3,6,7-tetrahydro-1,1,7,7-tetramethyl-1H,5H,11H-(1)benzo-pyropyrano (6,7-8-*I,j*)quinolizin-11-one (C545T) became the most commonly used dopant for Alq₃ due to its high luminance efficiency, unique hue and less concentration quenching compared to other derivatives. 1 % C545T: Alq₃ device is reported to have a current efficiency of 10 cd/A⁵. 2% concentration of C545T in Alq₃ have very fast energy transfer and maximum photoluminescence (PL) efficiency when the doping is varied from 1-5 %¹¹. C545T doped with Alq₃ is also reported to gain only marginally in trap state energy, from 0.25 eV of undoped Alq₃ to 0.32 eV on doping¹². This, in addition to the small energy level difference between the host and dopant, can facilitate a triplet-triplet annihilation (TTA) effect in the Alq₃: C545T system.

When a substantial number of triplet excited molecules are generated, they can interact with others to undergo annihilation forming singlet excited molecules¹³. Kido et al. identified the existence of TTA as the reason for the increased external quantum efficiency value above the theoretical limit (5%) at high bias voltage in a fluorescent device¹⁴. Wherein the TTA is responsible for efficiency roll-off at higher bias voltage in the case of phosphorescent devices, it can increase the efficiency values for the fluorescent devices. Efficiency enhancement through TTA for an Alq₃ based OLED which is charge balanced also has been reported¹⁵. The host-guest system with the dopant having limited charge trapping properties generally displays the strongest TTA¹⁶. This can be associated with the fact that reduced trapping causes a reduced quenching which helps in improving the efficiency beyond the theoretical limit. Carrier

trapping can be significantly reduced by decreasing the difference between host and guest energy levels. So selecting a suitable host-guest system can enhance TTA. As the triplet state density does not change significantly with a bias voltage, the electroluminescence spectra can be found to be more or less same with an increased electric field where TTA is most efficient. However, with a heavy doping concentration in the host-guest emitter system, a large number of carriers can be trapped, reducing TTA process assuming direct capture of the holes and the trapping of electrons by the dopant¹⁷. There are several other effects of heavy dye doping in the host-guest matrix of an OLED, which need further study.

Polarization effect in small molecule thin films was studied by varying the dopant concentration of DCM2 (4-(Dicyanomethylene)-2-methyl-6-julolidyl-9-enyl-4H -pyran) in Alq₃ from 1% to 10%¹⁸. The red shift of the emission spectra is pronounced with an increase in DCM2 concentration. As the shift is continuous, it is proposed that the DCM2 suspended in non-polar Alq₃ matrix undergoes self-polarization. With increased concentration, the distance between DCM2 molecules decreases thereby enhancing the local polarization field that causes the redshift. Over the whole range, the net dipole moment may be zero, but near any radiating molecule, there is a possible net local dipole moment from the nearby dipole, which can affect the emission spectrum. This solid-state solvation effect¹⁹ was accompanied by a decrease in luminescence due to quenching.

The energy transfer process in Alq₃: C545T system was studied by PL and time-resolved photoluminescence measurements¹¹. As the dopant concentration increased from 1% through 2% to 5%, the energy transfer time also changed as 1.4 ns, 400 ps, and 300 ps respectively. Carrier lifetime was decreasing proportionally with an increase in dopant concentration due to the increase of non-radiative recombination rate. The effect of the heavy dopant concentration of up to 7% on carrier transport properties and recombination dynamics of the Alq₃: C545T device was studied²⁰. With the increase in concentration, the dopants form aggregates, and the

resultant EL spectra are redshifted. Also, the radiative decay rate lowering while the non-radiative decay rate increasing suggests strong non-radiative recombination. On increasing the dopant concentration further up to 23%, yellow emission with Commission Internationale de l'Eclairage (CIE) coordinate of (0.45, 0.53) was obtained compared to the (0.29, 0.66) for a dopant concentration of 1%²¹. The redshift in the emission spectrum is attributed to the C545T excimer formation and emission at high dopant concentration.

Rhee et al¹⁷ studied a relatively increased doping concentration of Alq₃: C545T system which considered C545T molecules as charge carrier traps. As the doping concentration increases (1% to 6%), this limits the current density. As the host has high electron mobility, electrons can either be transported by the host or get trapped by the dopant. The holes would rather have to hop to the dopant molecules. As the energy barrier on the hole-side also favors direct hole injection to the dopant, heavy doping (6%) have the lowest current density and highest excimer emission, along with heavy exciton quenching. The EL spectra here generate a strong shoulder corresponding to excimer emission at ~550 nm. To correlate the excimer emission to C545T, two device schemes having C545T only as emitter with thickness 30 nm and 120 nm were studied which also gave rise to heavy self-quenching. The device with 120 nm thick C545T layer gave a broad spectrum with a peak at ~573 nm. For 30 nm thick EML device, along with strong excimer emission, weak C545T exciton emission with a peak at 530 nm was also present²¹.

The dopant emission in a host-dopant emissive system is explained as the host to guest energy transfer or the direct dopant recombination due to carrier trapping²². The highest device performance was obtained by doping of Alq₃ with C545T at low concentration^{1,21}. However, once the dopant concentration increases, the dopant monomers may aggregate to form dimers, and the excited state energy transfer due to dipole-dipole interaction between the dopants may increase. This may cause excitons to be trapped in the aggregates without any reverse transfer

to the monomer molecules. This may lead to a radiationless relaxation or a different radiative relaxation path causing fluorescence quenching²².

Still, there is a void in the study of devices with high dopant concentration and its effect regarding aggregation induced emission, self-quenching, charge balance, etc. Herein the section A; we study the effect that the doping concentration variation is having in the C545T:Alq₃ matrix up to a maximum of 50%. C545T as a single emitter deposited with a varying deposition rate as well as varied thickness and its effect on the resultant excimer emission are also studied. In section B, a fluorescent blue emitter is stacked with the emitter system in order to study the charge transfer mechanism with this scheme for exploring possible white emission.

3.3 Results and Discussions*

3.3.1 Section A: C545T emitter and varying deposition conditions

There are numerous studies focusing on finding the optimized doping concentration in different EML host-guest units to ensure efficient energy transfer between the host and the guest. As mentioned in the introduction, efficient transfer requires very low dopant concentration: usually less than 5% for most fluorescent devices. Nevertheless, there are not many works concentrating on increased dopant concentration, and the majority of them study up to 10-20 % dopant concentration range. These were aiming at studying TTA effects, or confirming excimer emission, etc. without any other detailed study. Even the study by Rhee et al.¹⁷ reporting a thick C545T single emitter, did not venture out of the excimer emission confirmation. In this work, we are systematically studying the effect of increased doping concentration on Alq₃:C545T system starting from 3% up to 50%. As a limiting case of this high doping concentration, we have also studied the C545T single emitter system, but under

* A detailed discussion on the device fabrication process and the materials used are given in annexure A

different deposition conditions. Keeping the EML thickness constant, we have changed the C545T evaporation rate from 0.1 to 5 Å/s. After optimizing the device for the rate of deposition to extract maximum emission, the EML thickness is varied in the subsequent part of the study.

3.3.1.1 Alq₃:C545T Emitter Unit

Fig 2a shows the OLED device structure prepared in order to study the effect of dopant concentration. Here, OLEDs are fabricated with Alq₃ doped with C545T as the emitter. The device structure is as follows (Fig 3.2a). ITO/ N,N'-Bis(naphthalen-1-yl)-N,N'-bis(phenyl)-benzidine (NPB) (40 nm)/ Alq₃: x wt % of C545T (30 nm)/ Alq₃ (35 nm)/ LiF (1 nm)/ Al, where x = 3, 10, 20 and 50 %. As the level of doping increases, a proportional increase in the current density can be expected. However, interestingly this is not the case as shown in Fig 3.2b. Current density reduces when the doping is increased from 3% to 10%. This is recovered when the doping is at 20% and then increases further by 50%. This is also not the trend followed by the luminance, which steadily decreases with increase in doping, as shown in Fig 3.2c. The same trend is followed by the current efficiency as shown in Fig 3.2c. Going up to 10%, current efficiency is reduced by half and is further reduced with an increase in doping.

The variation of current efficiency with current density is also worth studying. The current efficiency increases with current density for 3% doping, which indicates the enhancement in emission due to TTA effect. So, other effects due whatsoever may be blocking TTA effect upon heavy doping. Above 10% doping, no effect of TTA is previously reported. So, the effect of TTA can be expected not to influence the emission of OLED with heavy doping of C545T. The change from the expected trend in current density can be attributed to the change in carrier injection capabilities with variation in doping level. When doping increases, along with aggregation, there may a change in dipole-dipole interaction locally. This change in

polarization can reduce bandgap, which makes the excimer emission at long wavelength unpredictable, due to of several mechanisms.

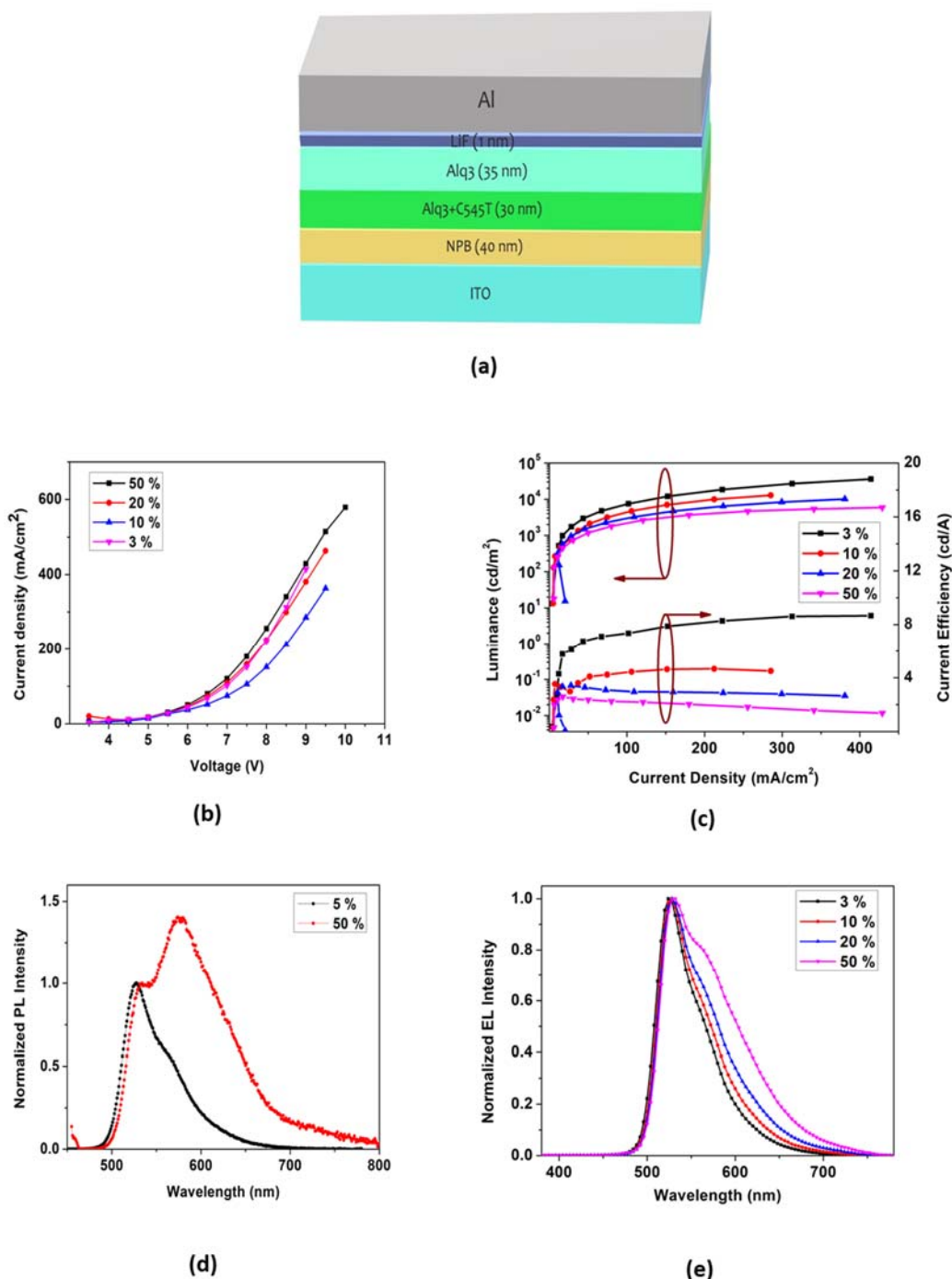


Figure 3.2. a) OLED device structure for the variation in C545T doping concentration study, b) Current density-Voltage characteristics, c) Current density-Luminance-Current efficiency characteristics, d) Photoluminescence spectrum of C545T doped Alq₃ thin film with doping concentration of 5% and 50%, and e) Normalized electroluminescence spectrum of C545T:Alq₃ device with different doping concentration ranging from 3% - 50%.

Fig 3.2d shows the PL spectrum of 5% and 50% C545T doped Alq₃ thin films. When the doping concentration increases, the 574 nm shoulder, which may be due to excimer emission, in the 5% doped film becomes dominant concerning the 528 nm peak, which is the excitonic emission. This relative intensity difference between the two peaks of emission spectra for the two differently doped films can be attributed to the aggregation-induced effect of C545T molecule in the film. This difference in relative intensity with increased doping is not pronounced in the EL spectra as much as in PL. In the electroluminescence spectrum in Fig 3.2e, when the dopant concentration is varied from 3% to 10% and then to 20%, there is a slight widening of the spectra and it is redshifted as well. The 574 nm shoulder in the spectra is not as distinct in this case as with the PL. 10% and 20% doped devices show a similar trend in their EL spectrum as opposed to the luminance as shown in Fig 3.2e. The relative intensity between the peak and the shoulder is decreasing with doping as shown in table 3.1. When doping goes from 3% to 50%, the relative intensity is almost halved. Up to 10% doping, quenching increases. However, above 10%, even though direct capture of charge carriers increases, the increase in local current density only contributes towards the non-radiative recombination current, J_{nr} . Therefore, the charge balance also deteriorates for heavily doped devices. Here, the charge imbalance and the non-radiative pathway compete with the excimer.

| Doping percentage | EL Intensity ratio between the 525 nm peak and 574 nm shoulder |
|-------------------|--|
| 3 | 2.50 |
| 10 | 2.11 |
| 20 | 1.76 |
| 50 | 1.31 |

Table 3.1 Electroluminescent intensity ratio between pure exciton and excimer emission for different doping percentages for C545T single emitter device

With the increase in doping percentage, luminance is decreasing as expected. This is attributed to the concentration quenching due to dye molecule aggregation. As can be seen from the CIE chart given in the inset to Fig 3.3a, CIE (x y) coordinates are shifting towards the yellow region from green with an increase in doping concentration. When the external bias is increased, the CIE coordinates tend to move towards the green region as indicated in the CIE chart. This indicates the decreased emission from the aggregate with an increased applied electric field. It may also be due to the field induced dissociation of the aggregate²³. As the charge carriers can easily overcome the energy barrier, at the higher applied electric field, the probability of charge transfer may increase leading to fast exciton dissociation. The C545T dopant concentration in Alq₃ host, thus, has a keen effect on the OLED EL spectrum as well as the device efficiency. With the increase in doping concentration, the spectrum is red shifted along with a distinct decrease in device efficiency. This is also evident from the normalized thin film PL spectra. It has also been suggested that the red shift due to the increased dopant concentration can be attributed to the excimer emission of the dopant¹. Here, the difference in intensity of red shifted excimer emission between PL and EL spectrum may be because, i) in the case of PL measurement, molecules can be excited throughout the film, whereas in the case of EL, the recombination region is situated close to the NPB-Alq₃ interface as the host is an electron transport material, ii) effects of carrier traps and iii) optical cavity effects.

Field dependence of colour coordinates increases with doping concentration. At heavy doping, the emission mechanism follows a different pathway. However, even this change in favored pathway changes with bias voltage at high doping as shown in Fig 3.3b. Apparently, for the heavily doped device, with increased bias the emission tries to shift back to the 3% emission range. That is the new predominant emission mechanism is weakened. However, direct capture may prevail. The polarization effects are diminished at high bias along with the

reduced excimer emission. Excimer dissociation, as well as reduced charge balance, may be a reason. The reduction in 574 nm shoulder is prominent as shown in Fig 3.3b.

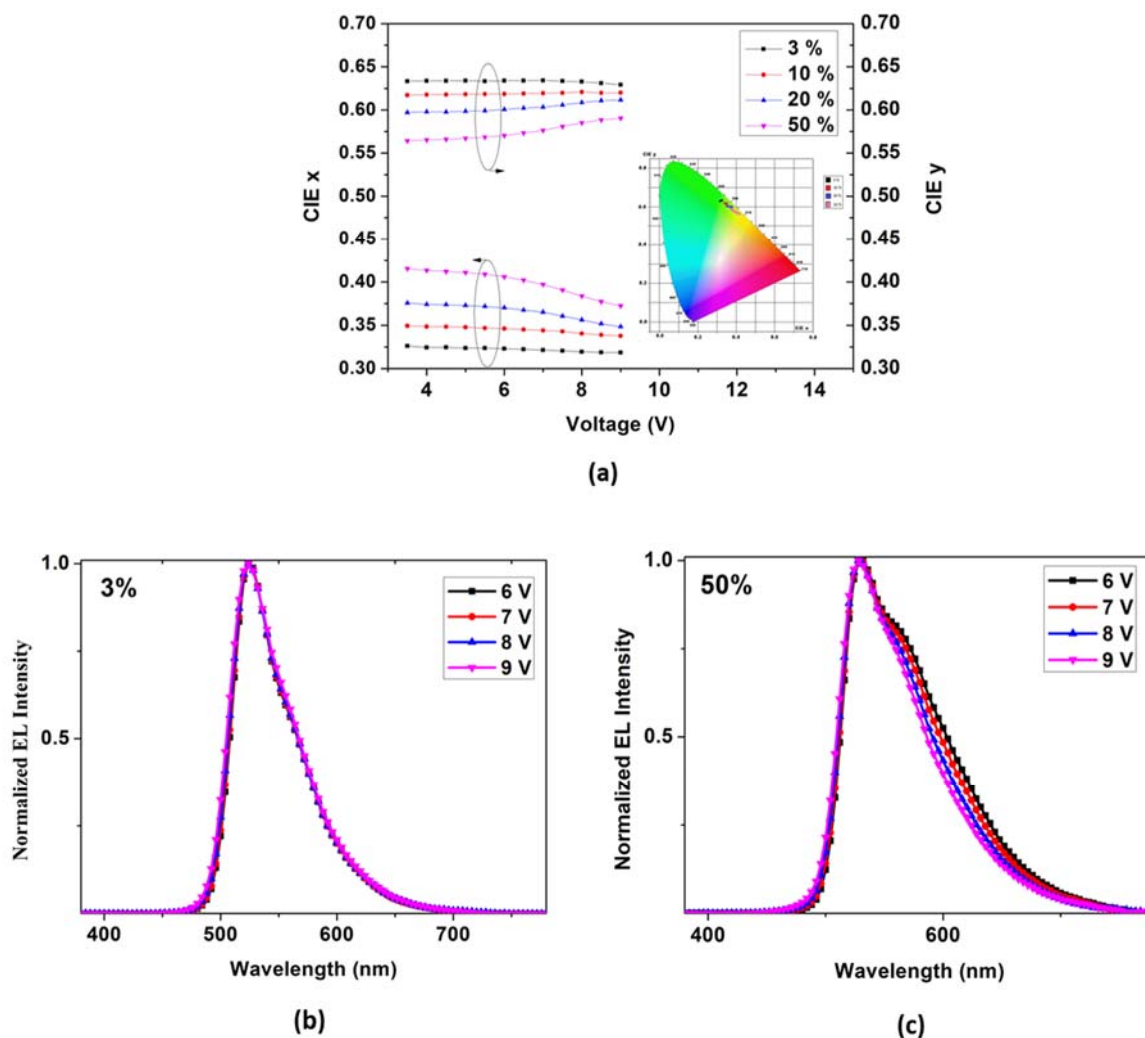


Figure 3.3 a) CIE x and y coordinates with voltage for different doping concentration; CIE 1931 colour chart in the inset and b) Normalized EL spectra with a change in voltage for i) 3% and ii) 50% doping

Increasing dopant concentration and decreasing the bandgap may decrease electric field induced fluorescence quenching²⁴. When the current increases, charge carrier induced quenching is also possible. With the decrease in the bandgap, field-induced quenching decreases. Narrower the energy gap, the excited states are less prone to dissociation. Aggregation may reduce the bandgap as previously reported. Hence, quenching decreases

initially. However, with an increase in concentration, trapping increases which support non-radiative pathways. Therefore, current may increase without a corresponding increase in luminance beyond 10% doping. Above a certain percentage of doping, concentration quenching and luminescence due to direct charge trapping compete with each other. The 3% doped device exhibits an excellent charge balance using the direct excitation and energy transfer mechanisms. In the case of 10% doping, current density decreases because of the enhancement in charge trapping. For 20% doping, aggregation changes the bandgap and assists in carrier transport. The same phenomenon continues with 50% and current increase due to direct injection into C545T, which does not contribute towards luminescence due to concentration quenching. Since aggregation plays a role in defining the optoelectronic properties of these devices, we decided to further study this with a variation of the rate of evaporation of C545T in a single emitter device.

3.3.1.2 C545T Single Emitter Unit

3.3.1.2.a Effect of variation of the evaporation rate of C545T

There has not been any comprehensive study on the effect of C545T single emitter devices. The available works were only aiming towards confirming that excimer emission at higher doping¹⁷. Effect of aggregation is expected to be aggravated at a higher evaporation rate. As the rate increases, the shoulders in the doped devices may broaden. The polarization effects also become maximized. Here, we are studying the C545T single emitter as a limiting case of high doping. A single layer of C545T of thickness 30 nm is deposited as emission layer (EML) of OLED (Fig 3.4a) at rates of 0.1 Å/s, 2 Å/s, and 5 Å/s. The energy level diagram for the HTL-EML-ETL part of the device is given in Fig 3.4b.

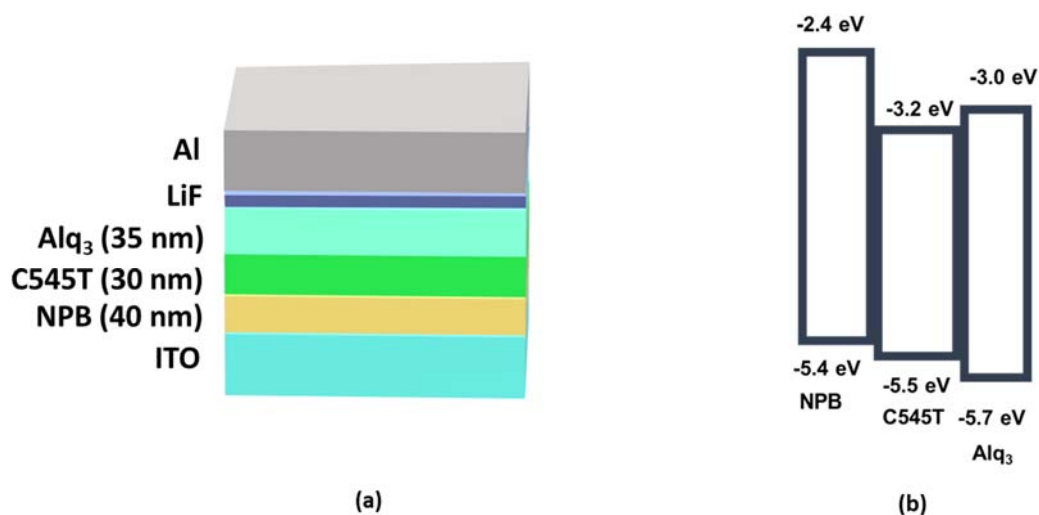


Figure 3.4 a) Architecture of the OLED device with C545T single emitter, and b) energy level diagram of the device. The HOMO-LUMO values are given in eV

Fig 3.5a shows the PL spectrum of C545T in solution (chloroform) and for a neat film of 30 nm thickness. The 503 nm peak wavelength for the C545T emission in solution is shifted towards ~586 nm for the neat film deposited at a rate of 2 Å/s. Both the solution and film has a shoulder at 532 nm. As mentioned in the previous section, this red shift of the major peak may be attributed to the excimer formation of the C545T dye and the emission from the corresponding aggregate. There is also a possibility of solid-state solvation effect^{18,19}. Due to the close packing, C545T molecule can self-polarize thereby increasing the local polarization field. This polarization also can contribute towards the red shifted spectrum. Unlike in the case of Alq₃: C545T emitter, all the molecules are surrounded by the neighbouring C545T molecules. This made the spectrum slightly more red shifted than that of the Alq₃: C545T 50% doped layer.

From the electroluminescence spectra in Fig 3.5b, EL spectrum of each of the C545T single emitter OLED peaks at a wavelength 532 nm, the shoulder peak in the PL spectra. Nevertheless, on increasing the deposition rate, the spectrum widens towards longer wavelength. This can only come from the difference in the molecular packing due to the change in deposition rate. Slow deposition can lead to non-structured defects and trapping. Therefore, the effect of self-

polarization might be less at low deposition rate. Therefore, the red shift can be comparatively less in this case. However, the device having EML deposited at 2 Å/s rate shows the maximum emission intensity.

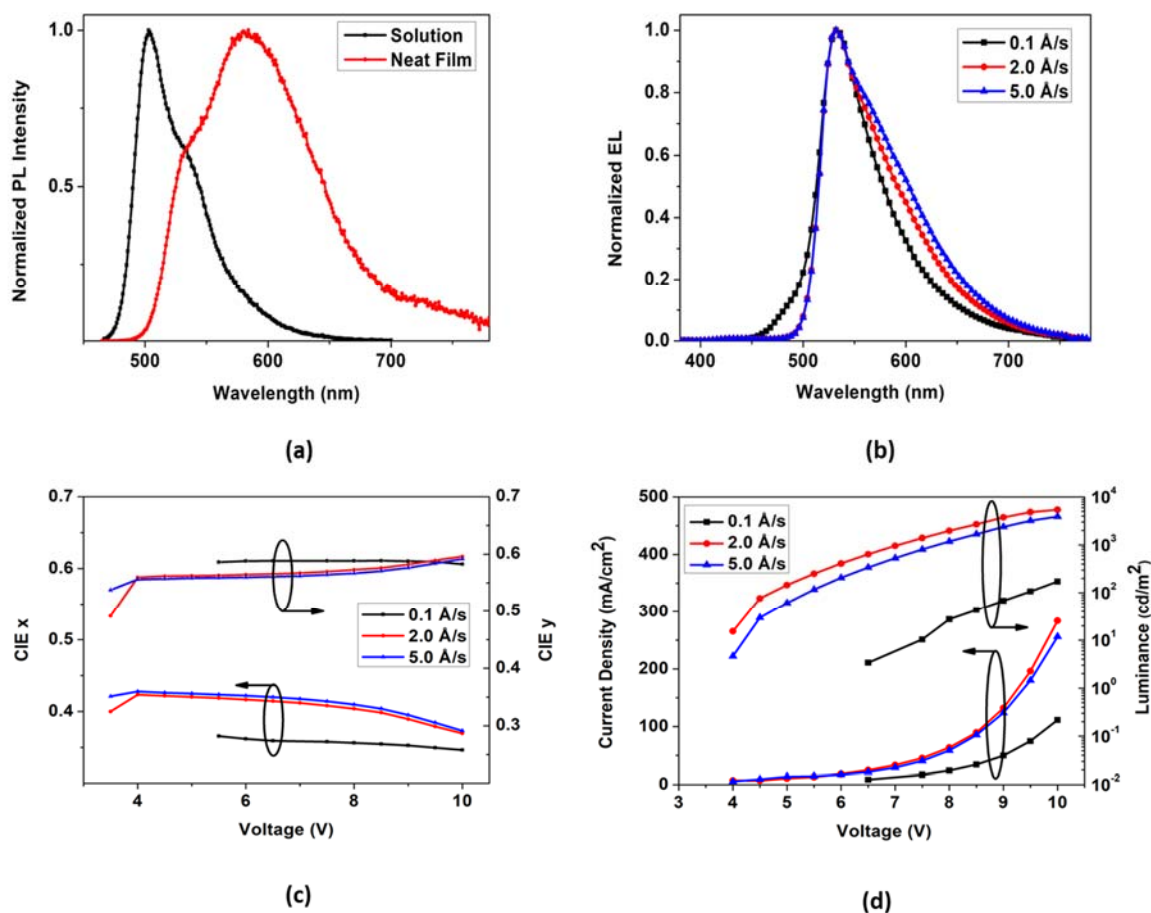


Figure 3.5 a) Photoluminescence spectrum of C545T in solution and neat C545T film, b) Normalized electroluminescence spectrum of C545T single emitter device with varying EML deposition rate, c) Variation of CIE x and y coordinates with voltage for different deposition rates, and d) Current Density-Voltage-Luminance Characteristics of the C545T single emitter devices with various EML deposition rate.

On further increasing the rate, the luminescence is reduced. Both of the devices with EML deposited at 2 Å/s and 5 Å/s show similar current density while the device of 0.1 Å/s deposited EML exhibiting poorer performance. The latter can be attributed to poor morphology of the EML. CIE colour chart in Fig 3.5c also shows a similar trend with EML of 0.1 Å/s leaning towards hue that is more greenish. Both the other devices show closer CIE coordinates

following the trend in EL spectra and J-V-L characteristics with a more yellowish emission resulting from the broadening of the spectrum.

Whereas the emission of 0.1 Å/s device is located more or less in yellow-green edge in the CIE chart with a dominant contribution from green, 2 Å/s and 5 Å/s devices are giving yellow emission as evidenced by the CIE coordinates in Fig 3.5c. These CIE coordinates of the 0.1 Å/s device remain almost same in the whole range of biasing voltage. However, for the higher rates, they tend to move towards the green region in the colour chart. This is also evidenced by the normalized EL spectra at different bias voltages in Fig 3.6. The EL spectrum for 0.1 Å/s remains the same for all voltages, but for the other two the same is narrowing with an increase in voltage at the longer wavelength region. Even with this kind of stability, the 0.1 Å/s is showing very poor device performance, as shown in Fig 3.5d. It has recorded a very low current density as well as luminance. This may be due to the poor film connectivity.

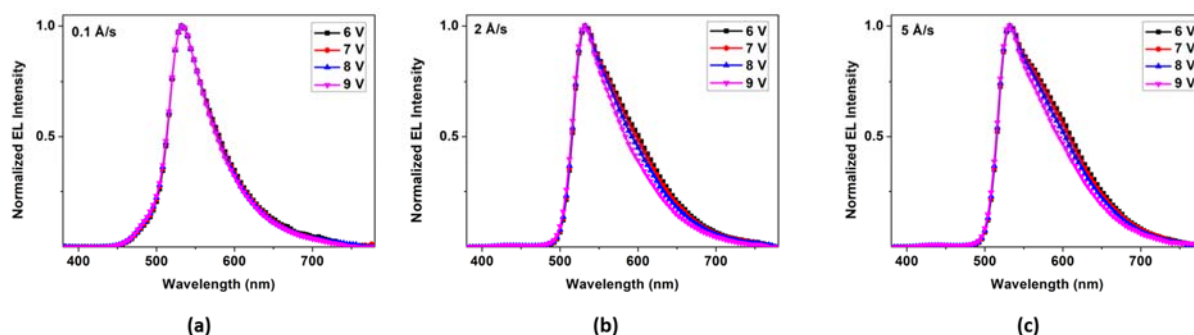


Figure 3.6 Normalized EL spectra for different biasing voltages for C545T single emitter devices with deposition rates of a) 0.1 Å/s, b) 2.0 Å/s, and c) 5.0 Å/s.

As the polarization effects are minimum, colour coordinates remain unchanged with voltage indicating the absence of any reversible conformation changes. The poor morphology of 0.1 Å/s also brings about a large number of traps in the layer. The presence of traps without the smooth connectivity between the molecules is substantiated by the slight increase in current density with a negligible enhancement in luminance when the driving voltage is increased. Due

to its conformational weakness, charge carrier mobility in the layer does suffer. This badly affects the charge balance in the structure. The connectivity issues and absence of any local polarization effects cause a virtual depletion effect, and the possibility of an electron-hole pair is reduced. The fraction of dimers formed on deposition of the layer may emit relatively weakly, but the excitons emission is the only pathway that gets benefitted by the increase in carrier injection due to increase in voltage, which is again negligible. All other aggregates follow a non-radiative pathway with an increase in the electric field. Only a minimal number of excitons and excimers are formed, and the dominant fraction of them relaxes non-radiatively.

On the other hand, 2 Å/s and 5 Å/s devices show comparable current density and luminance with 2 Å/s having the relatively high luminance. Both of them should have shown similar luminance as well. However, the EL intensity plot shows a very distinct intensity variation even though the spectrum is similar. That is the 2 Å/s device favors efficient radiative recombination. Both of the devices have EL spectrum, which broadens on longer wavelengths and narrows with voltage. With a high enough bias, it may give a clean enough emission spectra like 0.1 Å/s. This broadening in the emission indicates the presence of excimer emission, which again is getting suppressed with the increase in voltage. The packing in the 2 Å/s film seems to provide more radiative recombination centers. 2 Å/s film probably is having more trap assisted recombination due to its relative loose packing, compared to 5 Å/s film. This combined with the improved carrier mobility due to better connectivity may provide more charge carrier imbalance for the 5 Å/s device.

3.3.1.2.b Effect of variation of C545T thickness

Device with EML deposited at 2 Å/s was found to be the most efficient, and now the next part of the study is to find out the effect of different thickness on the emission. The EML thickness is varied to be 10 nm, 20 nm, 30 nm, 60 nm, and 70 nm. The device structure remains the same. As the hole blocking on the ETL side is negligible, a lesser EML thickness can cause

the exciton recombination zone to be shifted towards ETL. Device characteristics with the increase in thickness are shown in Fig 3.7. The current density is decreasing initially, as is expected. But, the 70 nm device showing an unexpectedly high current density. However, this enhancement in current density is not getting proportionally translated to luminescence. Therefore, this increase in current density is contributing towards non-radiative recombination current. The luminescence in general is also decreasing with increase in thickness, the exception being the 30 nm device. This can be associated with a weak microcavity effect in this configuration. This is evidenced by the EL spectra of the same in Fig 3.7b.

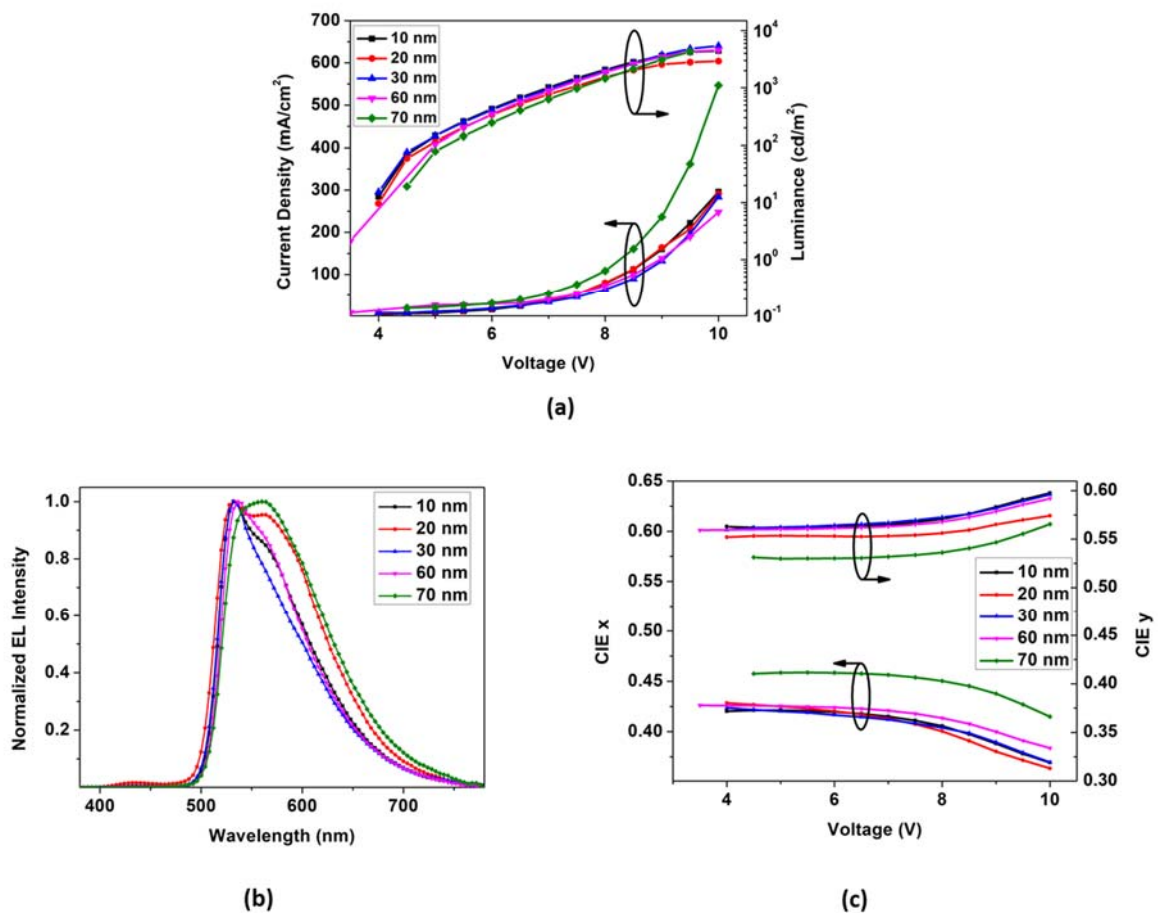


Figure 3.7 a) Current Density-Voltage-Luminance Characteristics of the C545T single emitter OLED with varying EML thickness, b) Normalized electroluminescence spectrum for different EML thickness, and c) Variation of CIE x and y coordinates with voltage for different EML thickness

In the normalized EL spectrum recorded at 8 V, the devices with EML thickness 10 nm and 20 nm have the peak wavelength of 532 nm with a ~565 nm shoulder. This 565 nm shoulder peak is higher for the 20 nm device. The 30 nm device has a comparatively narrower spectrum with a peak wavelength of 532 nm. It also has the highest spectral intensity. This may be due to the weak microcavity effect at this 30 nm optimized EML thickness. For the 60 nm device, the EL peak is slightly shifted to 536 nm with a strong shoulder at 562 nm. This trend is followed by the 70 nm device, whose total broadening of the spectra and the strengthening of the shoulder result in a 560 nm peak.

The effect of this EL spectra shift and widening effect is distinct in the CIE chart in Fig 3.7c. With the increase in EML thickness, the CIE (x y) coordinates are moving towards the yellow region with the 70 nm device tending towards yellow-red colour. The latter exhibits a pure yellow hue and the weakest luminance for a given current density (Fig 3.7a). The 30 nm device has the maximum luminescence intensity with all others falling in between. It is obvious that as the EML thickness increases, the C545T pure excitation decreases and excimer excitation increases as evidenced by the change in the relative intensity between initial 532 nm and 565 nm peaks, the peak shift and broadening.

| EML thickness | EL Intensity ratio between the 532 nm and 564 nm |
|---------------|--|
| 10 nm | 1.18 |
| 20 nm | 1.04 |
| 30 nm | 1.32 |
| 60 nm | 1.11 |
| 70 nm | 0.87 |

Table 3.2 Electroluminescent intensity ratio between pure exciton and excimer emission for different EML thicknesses for C545T single emitter device

Table 3.2 shows the relative intensity ratio between the two peak wavelengths. Along with the molecular structure and doping concentration, excimer emission depends on charge carrier

transport as well¹⁷. This can influence the excimer recombination. So, the charge carrier mobility and the local carrier density can help to improve the excimer emission by reducing C545T emission²⁵. This is in congruence with the observation in the previous section.

10 nm device shows C545T exciton and excimer peaks. When thickness increases, the C545T exciton and excimer emission become comparable at 20 nm. However, for 30 nm device, both of the emission intensities increase, but the exciton peak is visibly dominated. This may be due to a weak microcavity effect as discussed previously. Nevertheless, 60 nm device shows a reduced emission and the 70 nm has both the peaks with equal intensity. As the thickness increases, C545T molecules are grown on previously deposited C545T layer, removing the defects and reducing the traps.

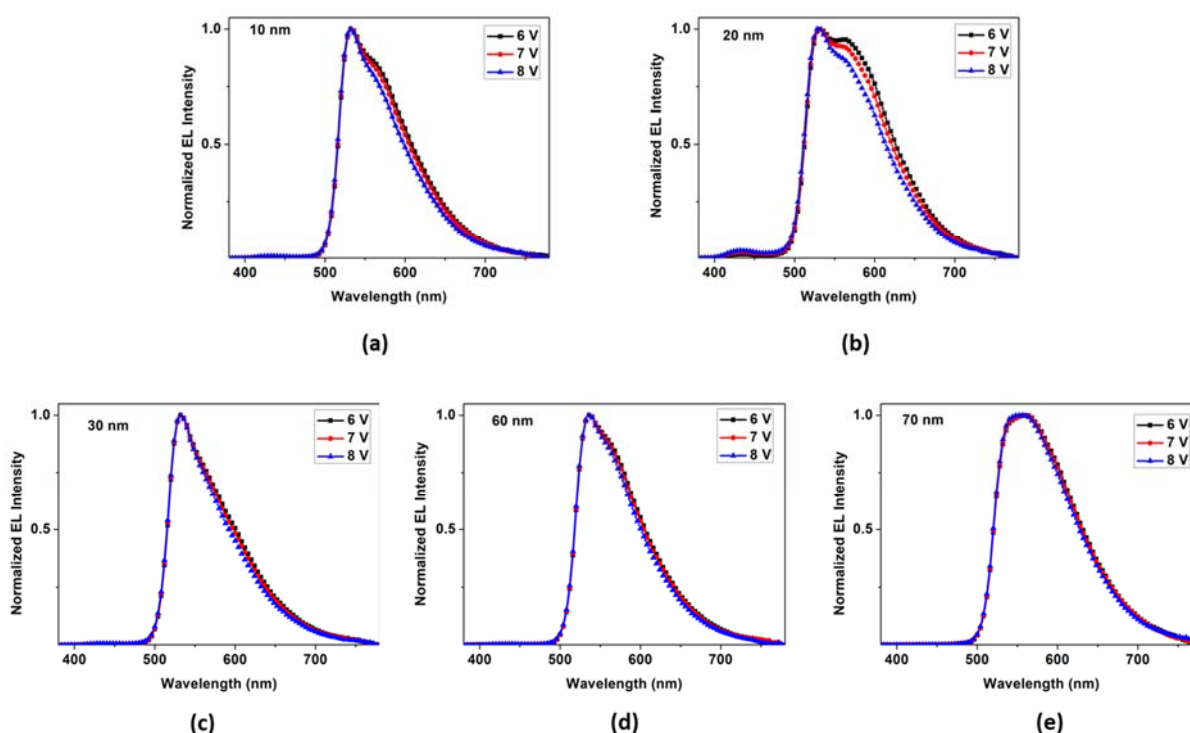


Figure 3.8 Normalized electroluminescence spectra of the OLEDs for different EML thickness and operating voltage: (a) 10 nm, (b) 20 nm, (c) 30 nm, (d) 60 nm, and (e) 70 nm

Normalized EL intensities for the OLEDs with different EML thickness and the driving voltage of 6 V, 7 V, and 8 V are given in Fig 3.8. The peaks corresponding to 10 nm, 20 nm, and 30 nm are 532 nm, and for 60 nm, it is 536 nm. For the 10 nm and 20 nm devices, the 564 nm shoulder in the peak can be found to be decreasing with applied voltage. This can be associated with the effect of applied electric field on the recombination. However, as it is absent in the thick EML device, it may also due to the change in exciton formation route: from Forster energy transfer to direct charge trapping. For the devices with EML thickness of 30 nm and above, the normalized EL spectra are unchanged when the applied voltage is changed from 6 V to 8 V. Therefore, the exciton formation route remains the same even at high applied voltage, which could only be the direct charge trapping by C545T molecule.

The initial increase in EL with thickness is due to both C545T exciton and excimer emission, which is reduced with a further increase in thickness. Here, the optimum thickness for radiative exciton recombination is obtained at 30 nm. Above 30 nm, the current density is shown to be decreased which may due to the film thickness dependent resistance. However, the 70 nm device has reported the highest current density. Nevertheless, the luminance is not likewise improved. Hence, either the excitons non-radiatively dissociate leading to increased current density or the improved hole conductivity in thicker films decreases the charge balance, leading to reduced luminance.

3.3.2 Section B: Dual Emissive layer white OLED

In the previous section, we have studied device performance with varying Alq₃: C545T doping concentration. The device with 50% doping concentration has recorded the most yellowish emission compared to the 3% optimized device. We have also explored the C545T single emitter devices with different deposition rate and EML thickness and optimized the devices for the highest yellow emission. In section B, we will insert a blue emitting layer on

one side of the yellow layer, both Alq₃: 50 wt.% C545T and C545T alone, to explore the possibilities of white emission. Here we will use 4,4'-bis(2,2'-diphenylvinyl)-1,1'-diphenyl (DPVBi) single emitter or DPVBi: 4,4'-Bis(9-ethyl-3-carbazovinyleno)-1;4,4'-Bis(9-ethyl-3-carbazovinyleno)-1,1'-biphenyl (BCzVBi) doped emitter as the blue emitting layer. In the first part of the study, the blue emitter will be inserted between yellow emitter and the cathode and in the second part; it is inserted close to the anode before the yellow emitter. The effectiveness of the energy transfer and/or carrier transfer between the two are studied in detail.

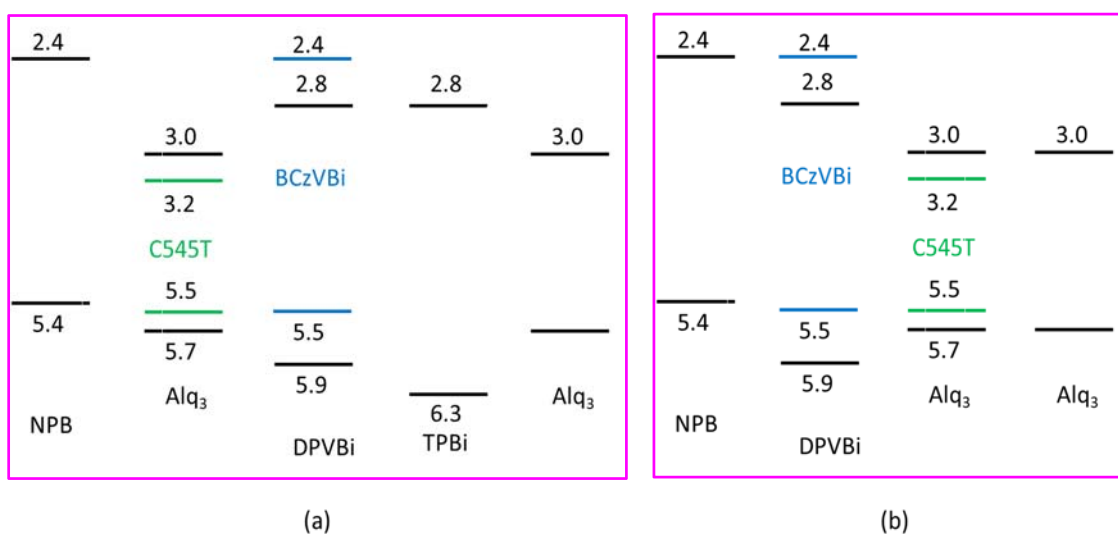


Figure 3.9 Energy level diagram of devices a) A-D, b) E-F

Here, we study the shift in emission spectra on combining the C545T emitter deposited at 2 Å/s of 30 nm with a blue emitter. We are inserting a blue emitting fluorescent host material DPVBi or a host-guest matrix of DPVBi: BCzVBi along either the C545T single emitter or a 50% doped Alq₃:C545T host-guest system. The energy level diagram is shown in Fig 3.9. Two batches of devices are fabricated with the first batch having the blue emitter deposited on top of C545T, closer to the cathode and in the second batch; C545T is deposited on top of the blue emitter. The DPVBi or DPVBi: BCzVBi layer is deposited for a thickness of 20 nm with the latter with a 5% doping concentration of BCzVBi. In the case of the blue emitter on top, 2,2',2''-

(1,3,5-Benzinetriyl)-tris(1-phenyl-1-H-benzimidazole) (TPBi) is deposited as the ETL, and for the other case, a 10 nm thick Alq₃ layer is inserted between EML and ETL. Devices A-D feature a blue on top of yellow emitter design with four different configurations as listed in table 3.3. Devices E-F has different yellow on top of blue emitter configurations.

| | | | | | | |
|---|-------------|---------------------------------|---------------------------------|--------------------------|--------------------------|----------|
| A | NPB (40 nm) | C545T (30 nm) | DPVBi (20 nm) | TPBi (30 nm) | Alq ₃ (10 nm) | LiF / Al |
| B | NPB (40 nm) | Alq ₃ :C545T (30 nm) | DPVBi (20 nm) | TPBi (30 nm) | Alq ₃ (10 nm) | LiF / Al |
| C | NPB (40 nm) | Alq ₃ :C545T (30 nm) | DPVBi:BCzVBi (20 nm) | TPBi (30 nm) | Alq ₃ (10 nm) | LiF / Al |
| D | NPB (40 nm) | C545T (30 nm) | DPVBi:BCzVBi (20 nm) | TPBi (30 nm) | Alq ₃ (10 nm) | LiF / Al |
| E | NPB (40 nm) | DPVBi (20 nm) | C545T (30 nm) | Alq ₃ (40 nm) | | LiF / Al |
| F | NPB (40 nm) | DPVBi (20 nm) | Alq ₃ :C545T (30 nm) | Alq ₃ (40 nm) | | LiF / Al |
| G | NPB (40 nm) | DPVBi:BCzVBi (20 nm) | Alq ₃ :C545T (30 nm) | Alq ₃ (40 nm) | | LiF / Al |

Table 3.3. Device structures for the blue and yellow emitter combinations to yield white emission

3.3.2.1 Yellow: Blue Emitter Unit

Among the four different blue on top of yellow device structures, the combination of C545T-DPVBi: BCzVBi (Device D) gives the highest light emission and current density. All three remaining devices give more or less similar luminance even though the current density values vary largely, with device B (Alq₃: C545T-DPVBi) having the smallest. This gives device B the maximum efficiency as shown in Fig 3.10b, while having the lowest current density and luminance among the batch. Device D is expected to have comparatively higher light and current from the energy level diagram. For device D, C545T single layer is next to the NPB layer on the hole side. There is a very high LUMO gap which can effectively block electrons while having virtually no hole barrier. This is also same for device D. However, on the other side, D has a BCzVbi doped DPVBi layer close to ETL, and A has an undoped DPVBi. The current density and luminance of device A-D follow the order $L_D > L_A > L_C > L_B$ and $J_D > J_A > J_C > J_B$.

Since, the luminance and current density follow the same trend; we do not expect any different contribution to the total current in the form of non-recombination current in the device.

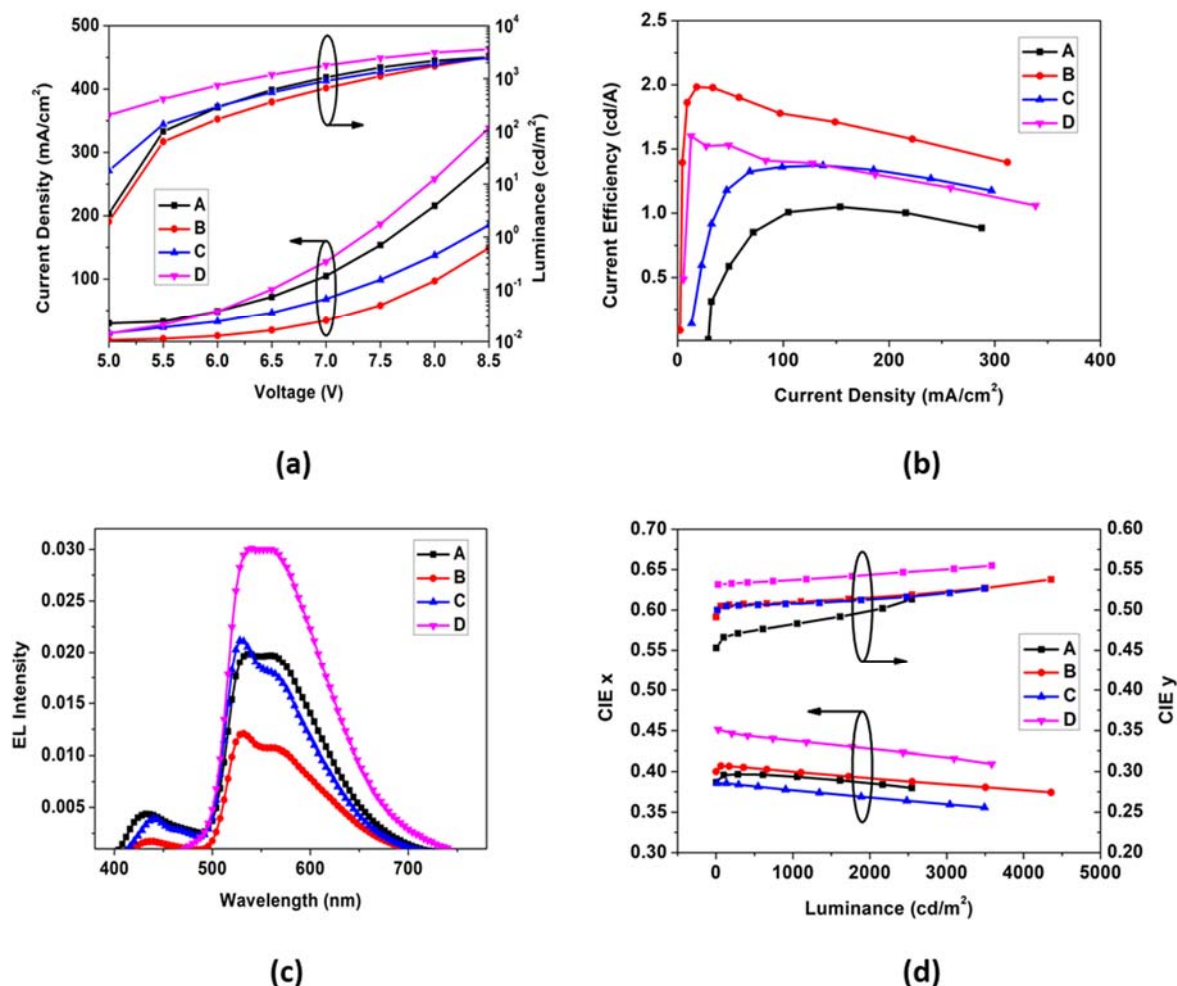


Figure 3.10 Electro-optical characteristics of Yellow: Blue emitter OLEDs a) Luminance-Current Density Characteristics, b) Current Efficiency- Current Density Characteristics, c) Electroluminescence spectrum d) CIE (x y) coordinates.

From the EL spectra in Fig 3.10c, it is clear that the single C545T emission is prominent in both the cases with the wide peak ranging from around 530 nm to 564 nm. Nevertheless, the blue peak corresponding to the device is absent for device D whereas A has a peak at 434 nm. Therefore, there is no exciton recombination leading to radiation happening in the doped DPVBi layer; rather it facilitates increased charge transport as evident from the high current

density of D. This is also evident from the high luminance value matching to the yellow emission.

With DPVBi alone layer for device A, there is a small amount of radiative recombination happening. The relative difference in the intensity between yellow and blue can be attributed to the hole injection barrier between C545T and DPVBi. CIE coordinates of device D are also corresponding to yellow at each voltage with relatively little change, whereas Y_{CIE} of A changes quickly with voltage. Therefore, as the voltage increases, the charge trapping effect of C545T also increases. Thereby it reduces the blue content from the emitted light. Change in the X_{CIE} of device D with voltage is due to the excimer effect, and the polarization effects mentioned in the previous sessions.

Devices B and C show luminance similar to device A, but a reduced current density, which brought about the relatively high-efficiency values in Fig 3.10b. These devices have a 50% C545T doped Alq₃ layer instead of undoped C545T. The lowest current density recorded for B is due to the reduced barrier at DPVBi: TPBi interface as evident from the energy level diagram in Fig 3.9. For, device C, Alq₃: BCzVBi act as a better interface, giving rise to an intense blue peak than B. The slight shift in the peak is due to the increased emission from BCzVBi rather from DPVBi. B shows a blue peak similar to A as both have an undoped DPVBi in the device structure. CIE values of B and C do not show any drastic change over the driving voltage.

Blue emission is strongest in device A, which means holes are reaching the DPVBi layer through C545T layer. The blue emission cannot be due to exciton migration from C545T to DPVBi, because the latter is a higher energy exciton. Device C has the next strongest blue contribution. We do not think Alq₃ can support appreciable hole transport. However, C545T layer can provide improved hole transport. This causes effective formation of excitons within DPVBi, which can in turn cause electroluminescence from BCzVBi due to Förster transfer. Device B has an even weaker blue emission even though the same hole current as that of the

device C may reach the blue layer in device B. However, as the quantum efficiency of DPVBi layer is less than DPVBi: BCzVBi host-dopant system, the blue emission is still weaker. The fact that device D does not have a blue emission is unexpected. However, as the C545T excimer has even lower bandgap, exciton transfer from blue layer gets easier than in the case of Alq₃:C545T system. It may be noted that the current density of the device is high as the luminescence. DPVBi: BCzVBi seems to provide transport sites for the carriers; this increases the current density, which will cause reduction in luminescence. Also since C545T is a better hole conductor, additional holes are injected to the blue EML. Having low carrier mobility in DPVBi layer improves recombination whereas DPVBi: BCzVBi layer supports non-radiative transport.

The yellow emission is caused by the excimer emission of C545T. It follows $Y_D > Y_A > Y_B > Y_C$. As expected, layer with C545T layer alone will lead to excimer formation and hence the yellow emission from A and D are equal. B and C will have reduced excimer formation and hence reduced yellow emission. Similarly, green emission will be stronger when Alq₃:C545T is used. The colour coordinates are drifting towards green at higher biases. This is expected from the findings in section A. as excimer emission is weakened at high biases. Hence, we expect this change to be visible in device A and D. However, it is not very appreciable in device D, because of the reasonably strong excimer emission.

3.3.2.2 Blue: Yellow Emitter Unit

In the device combination with yellow on top of blue, the devices F and G show similar luminance, but device F has the lowest current density as shown in Fig 3.11a. This gives device F, the highest efficiency value. The difference between device F and G is that F has an undoped DPVBi layer whereas device G has a BCzVBi doped DPVBi layer. This doped layer increases the carrier mobility and thereby the current density in the device, none of which is contributing towards radiative recombination. The undoped DPVBi resulted in the slightly less luminance

value of device F than G. However, considerable reduction in current density favored device F for a high-efficiency value. Both devices F and G show a very stable efficiency value with increase in current density.

Compared to devices F and G, device E gives the least light as the energy barrier from DPVBi to C545T is high. Here, energy transfer from DPVBi to C545T is responsible for the mobility throughout the emitter. This reduces the driving voltage. At low voltage, the electron trapping by C545T shifts the CIE coordinates drastically. When driving voltage is increased, trapping within C545T is decreased, and the carrier concentration in DPVBi increases, which shift the CIE coordinates towards blue. When C545T single layer is used instead of Alq₃:C545T, the number of electron trapping sites increases and therefore the variation in CIE coordinates with voltage also increases.

In the devices E, F and G, the blue emitting layer is closer to the anode compared to the green/yellow emitter. Current density is lowest for the device F and highest for the device G. however light emission does not follow this pattern. Luminance is lowest for device E and highest for device G. Current density is lowest for device F because compared to device E, hole transport through the green//yellow layer is diminished. However the hole transport probably is enhanced in DPVBi: BCzVBi system compared to other two and hence device G has the highest current density. Device G also exhibits the highest luminance value which means the enhanced hole transport not only reduced the hole transport in Alq₃:C545T system, but also caused more radiative recombination in the blue layer. Similarly, though the current density is lower in device F compared to device E, it shows higher luminance because of the increased quantum efficiency of the Alq₃:C545T system. Interestingly, the reduction in current density makes the device F the best performing one in terms of current efficiency.

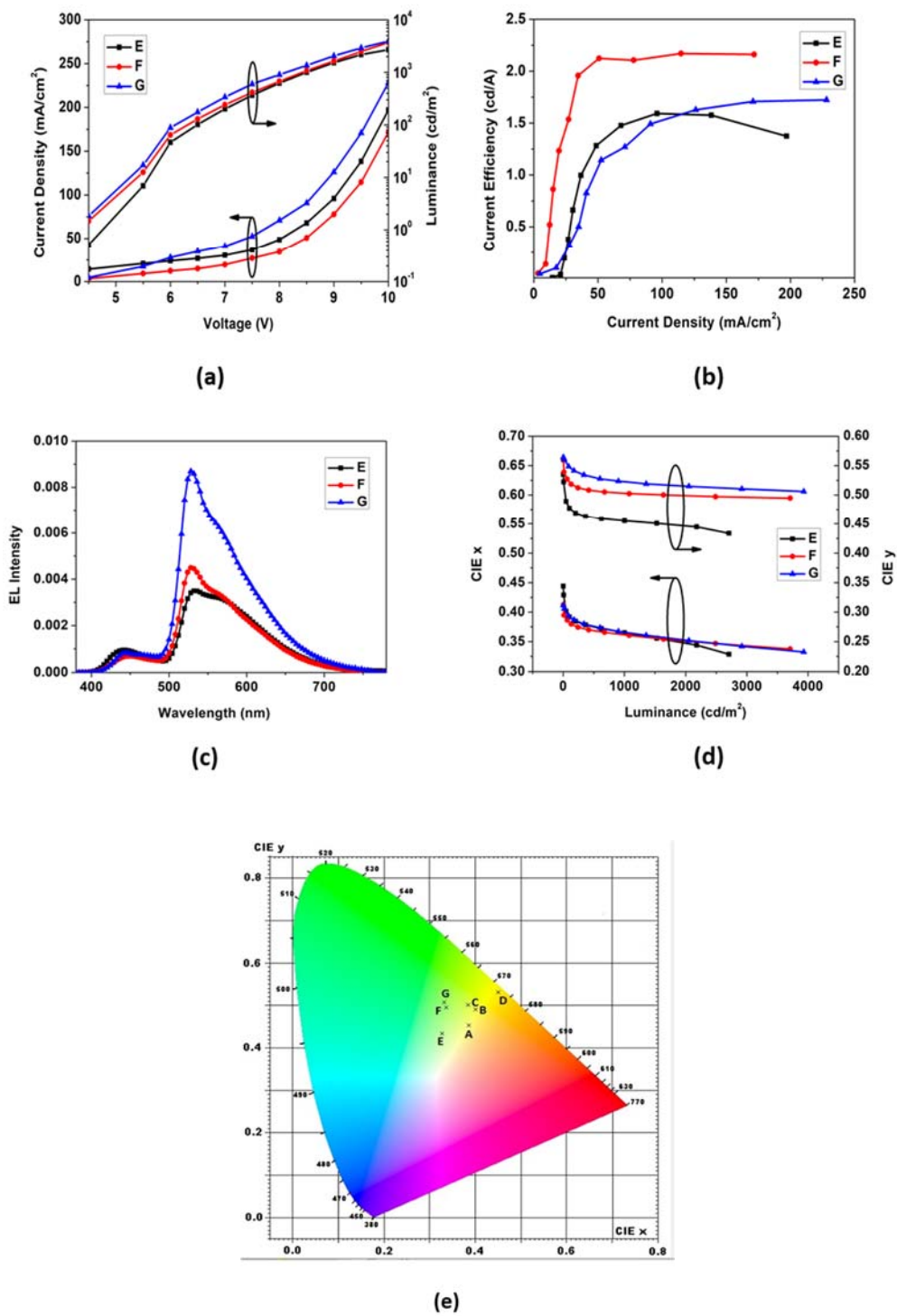


Figure 3.11 Electro-optical characteristics of Blue: Yellow emitter OLEDs a) Luminance-Current Density Characteristics, b) Current Efficiency- Current Density Characteristics, c) Electroluminescence spectrum d) CIE x and y coordinates, e) CIE 1931 Colour Chart.

In Fig 3.11d, although the three devices show similar X_{CIE} values, device E has the maximum Y_{CIE} variation compared to the other two. Here, the DPVBi single layer devices, E

and F, show the higher blue peak leading to CIE coordinates more shifted towards the blue region, which is apparent from the EL spectra in Fig 3.11c. The device combination with CIE closest to white from each batch is shown in Fig 3.11e. Device A, with blue on top of yellow configuration has a recorded CIE coordinate of (0.39, 0.45) which are more yellowish and E with yellow on top of blue has (0.33, 0.43) which is more bluish. Device A-D which have yellow emitter on hole side and blue emitter on electron side, CIE coordinates move towards yellow in the colour chart with an increase in voltage.

For the devices E-F which have blue emitter on the hole side and yellow on the electron side, the CIE coordinates tend towards blue with an increase in voltage. Device E has the strongest blue emission. Even though the quantum yield of DPVBi alone should be less than a DPVBi: BCzVBi system, the DPVBi alone system exhibits the maximum blue luminance. This could be because the energy transfer / exciton migration from the blue emitter to green/yellow emitter is probably not as strong in the case of DPVBi: BCzVBi system. Accordingly, device G has the highest luminance because of the possible energy transfer and better hole transport. The colour coordinates indicate a very feeble blue emission only as can be inferred from the emission spectra. Device E is the closest to white while device G is closest to green. Stronger blue emission is required to bring the coordinates closer to the white point.

3.4 Conclusions

Due to the dipole-dipole interaction, at high doping concentration, self-quenching occurs broadening the recombination zone. The reduced energy barrier between guest and host can reduce charge trapping. By changing the dopant concentration, EML packing, and thickness, exciton formation can be shifted from Forster energy transfer to charge trapping. In this study, by controlling deposition conditions, OLED emission could be tuned between yellow and green. The relative difference in the intensity between yellow and blue can be attributed to the

presence or absence of hole injection barriers. As the voltage increases, the charge trapping effect of C545T also increases, reducing the blue content from the emitted light for devices A-D and the CIE coordinates drift towards green. Carrier concentration in DPVBi increases with voltage, which shift the CIE coordinates towards blue for the devices E-G. The exhibited colour tunability can be used to optimize a white emission with colour coordinates (0.33, 0.33), with less production cost.

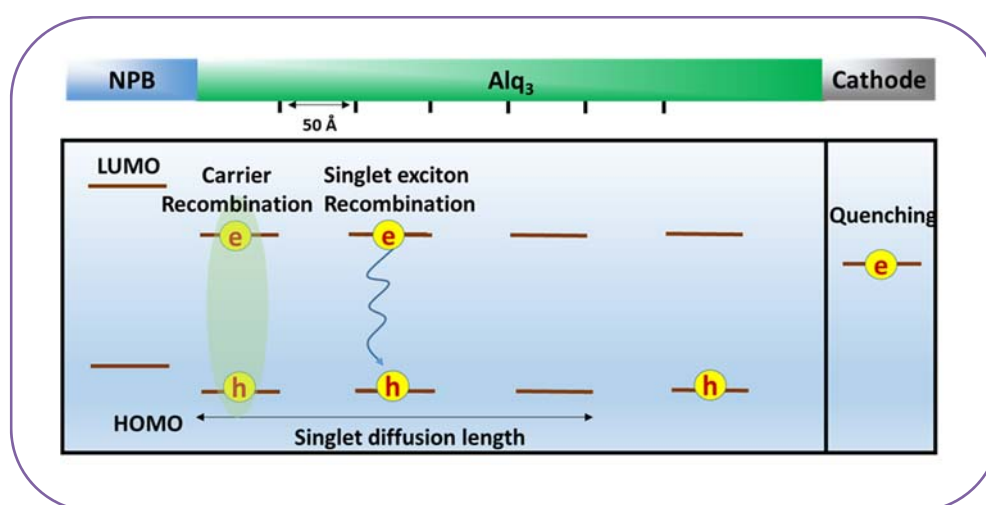
3.5 References

- 1 Tang, C. W., VanSlyke, S. A. & Chen, C. H. Electroluminescence of doped organic thin films. *Journal of Applied Physics* **65**, 3610-3616, doi:10.1063/1.343409 (1989).
- 2 Shoustikov, A. A., You, Y. J. & Thompson, M. E. Electroluminescence colour tuning by dye doping in organic light-emitting diodes. *IEEE Journal of Selected Topics in Quantum Electronics* **4**, 3-13, doi:Doi 10.1109/2944.669454 (1998).
- 3 P, S. Organic Lasers. *Scientific American* **220**, 30-41 (1969).
- 4 Reynolds, G. A. & Drexhage, K. H. New Coumarin Dyes with Rigidized Structure for Flashlamp-Pumped Dye Lasers. *Optics Communications* **13**, 222-225, doi:Doi 10.1016/0030-4018(75)90085-1 (1975).
- 5 Chen, C. H. & Tang, C. W. Efficient green organic light-emitting diodes with sterically hindered coumarin dopants. *Applied Physics Letters* **79**, 3711-3713, doi:10.1063/1.1420583 (2001).
- 6 Fletcher, A. N., Bliss, D. E. & Kauffman, J. M. Lasing and fluorescent characteristics of nine, new, flashlamp-pumpable, coumarin dyes in ethanol and ethanol: Water. *Optics Communications* **47**, 57-61, doi:10.1016/0030-4018(83)90336-x (1983).
- 7 Wakimoto, T. & Yonemot, Y. (1994).
- 8 Fox, J. L. & Chen, C. H. Benzopyrano[6,7,8-i,j]quinolizine-11-one lasing dyes and intermediates for their preparation USA patent (1988).
- 9 Inoe, T. & Nakatani, K. Japan patent (1994).

- 10 Ito, J. USA patent (1995).
- 11 Lee, J.-H. *et al.* Direct observations of energy transfer and quenching dynamics between Alq₃ and C545T in thin films with different doping concentrations. *Proceedings of SPIE 5632, Light-Emitting Diode Materials and Devices*, 66, doi:10.1117/12.569002 (2005).
- 12 E.W. Forsyth, D. C. M., Q.T. Lea, L. Yan, F. Nüesch, C.W. Tang, and Yongli Gao. in *Optoelectronics '99 - Integrated Optoelectronic Devices*. (SPIE).
- 13 Martin Pope, C. E. S. *Electronic Processes in Organic Crystals*. (Oxford University Press, 1982).
- 14 Kido, J. & Iizumi, Y. Fabrication of highly efficient organic electroluminescent devices. *Applied Physics Letters* **73**, 2721-2723, doi:10.1063/1.122570 (1998).
- 15 Ganzorig, C. & Fujihira, M. A possible mechanism for enhanced electrofluorescence emission through triplet-triplet annihilation in organic electroluminescent devices. *Applied Physics Letters* **81**, 3137-3139, doi:10.1063/1.1515129 (2002).
- 16 Luo, Y. & Aziz, H. Correlation Between Triplet-Triplet Annihilation and Electroluminescence Efficiency in Doped Fluorescent Organic Light-Emitting Devices. *Advanced Functional Materials* **20**, 1285-1293, doi:10.1002/adfm.200902329 (2010).
- 17 Rhee, S. H. *et al.* Heavily Doped, Charge-Balanced Fluorescent Organic Light-Emitting Diodes from Direct Charge Trapping of Dopants in Emission Layer. *ACS applied materials & interfaces* **7**, 16750-16759, doi:10.1021/acsami.5b04519 (2015).
- 18 Bulović, V. *et al.* Bright, saturated, red-to-yellow organic light-emitting devices based on polarization-induced spectral shifts. *Chemical Physics Letters* **287**, 455-460, doi:10.1016/s0009-2614(98)00168-7 (1998).
- 19 Bulović, V., Deshpande, R., Thompson, M. E. & Forrest, S. R. Tuning the colour emission of thin film molecular organic light emitting devices by the solid state solvation effect. *Chemical Physics Letters* **308**, 317-322, doi:10.1016/s0009-2614(99)00580-1 (1999).

- 20 Feng, S.-W., Shih, M.-C., Huang, C. J. & Chung, C.-T. *Thin Solid Films* **517**, 2719-2723, doi:10.1016/j.tsf.2008.10.049 (2009).
- 21 Liu, Z., Helander, M. G., Wang, Z. & Lu, Z. Efficient Single-Layer Organic Light-Emitting Diodes Based on C545T-Alq3 System. *The Journal of Physical Chemistry C* **114**, 11931-11935, doi:10.1021/jp101269r (2010).
- 22 Lutz, D. R., Nelson, K. A., Gochanour, C. R. & Fayer, M. D. Electronic excited state energy transfer, trapping by dimers and fluorescence quenching in concentrated dye solutions: Picosecond transient grating exp. *Chemical Physics* **58**, 325-334, doi:10.1016/0301-0104(81)80068-7 (1981).
- 23 Wortmann, R., Rösch, U., Redi-Abshiro, M. & Würthner, F. Large Electric-Field Effects on the Dipolar Aggregation of Merocyanine Dyes. *Angewandte Chemie International Edition* **42**, 2080-2083, doi:doi:10.1002/anie.200250782 (2003).
- 24 Luo, Y., Aziz, H., Popovic, Z. D. & Xu, G. Electric-field-induced fluorescence quenching in dye-doped tris(8-hydroxyquinoline) aluminum layers. *Applied Physics Letters* **89**, 103505, doi:10.1063/1.2337269 (2006).
- 25 Williams, E. L., Haavisto, K., Li, J., Jabbour, G.E. Excimer-Based White Phosphorescent Organic Light-Emitting Diodes with Nearly 100 % Internal Quantum Efficiency. *Advanced Materials* **19**, 197-202, doi:10.1002/adma.200602174 (2007).

Singlet and triplet exciton migration: Optimized emission zone in electron transporting host Alq₃



4.1. Abstract

The mapping of exciton diffusion and emission profile was characterized in an undoped fluorescent organic light emitting diode (OLED) by the spatial deployment of luminescent probes and studying the electroluminescence (EL) spectrum. This was done with an aim to optimize the emission layer (EML) thickness for maximum exciton harvesting without sacrificing carriers towards non-recombination current, by the spatial deployment of luminescent probes and studying the EL spectra. As the region outside the emission zone in an emitter acts as a transport layer only, affecting the current density and carrier balance, the device efficiency can be influenced in turn. The singlet, as well as triplet emission zone in Alq₃, was mapped by inserting a fluorescent probe layer of 4-(Dicyanomethylene)-2-tert-butyl-6-

(1,1,7,7-tetramethyljulolidin-4-yl-vinyl)-4H-pyran (DCJTb) and a phosphorescent probe layer of platinum octaethylporphyrin (PtOEP), respectively each having thickness of 30 Å.

4.2 Introduction

Identifying and addressing the key factors affecting electroluminescent device stability is of greater importance now more than ever as organic light emitting diode (OLED) technology is gaining significant market share in lighting and display applications. Device architecture, chemical purity of the emitters, physical and electrochemical properties of transport materials, interfaces and traps, recombination region, etc., are important factors affecting the stability of the devices. Hence, understanding the many processes involved in the operation of OLED such as charge injection, transport, exciton diffusion, recombination, etc., become crucial, as it has been observed that the emission zone is marked by the exciton diffusion.

In a host-guest doped emitter organic light emitting diode (OLED), when the absorption spectrum of the guest overlaps with the emission spectrum of the host, efficient energy transfer from the host to the dye can occur via Förster energy transfer. Hence, for a fluorescent emitter, the maximum external quantum efficiency, Φ_{el} , i.e. the number of photons extracted in the forward direction per injected electron, is:

$$\Phi_{el} \propto \gamma \Phi_{pl} \eta_s \eta_{out} \quad (1)$$

γ is the charge balance factor, Φ_{pl} is the photoluminescent efficiency of the dye, η_s is the fraction of luminescent excitons, which from spin statistics is presumed to be $\sim 1/4$, and η_{out} is the light out-coupling efficiency¹. As both the charge balance factor and fluorescent efficiency can approach unity for an optimized device, the efficiency of the OLED is primarily limited by extraction losses and a singlet exciton restriction especially for a fluorescent OLED. In addition, the singlets have exciton diffusion length of a few hundred angstroms compared to the longer triplet diffusion length ~ 1400 Å.

The location of the charge carrier recombination zone (exciton formation zone) in the device depends on the electron and hole mobilities and the relative injection efficiencies into the emitter³. This can push the recombination zone towards either of the interfaces of the emitter with the electron transport layer (ETL) or hole transport layer (HTL). Depending on the exciton diffusion lengths, the emission zone may be different from the recombination zone, where the former acts as the upper limit for the latter. Theoretically, the exciton diffusion coefficient of materials might be changed by the addition of impurities, which can trap excitons, or by modifying the disorder in the thin film⁴. As the recombination zone is fixed for an electroluminescent device, it follows that the emission zone will be, as well. Even though we do not have any direct means of locating the charge carrier recombination zone, locating the emission zone can provide insight into the carrier recombination region. Emission zone can be studied by using a thin dopant layer placed at fixed intervals as a sensing layer in the emitter.

Tang et al.³ studied the recombination zone in host-guest OLED by separating the emitter layer into doped and undoped regions with diamine as the hole transport layer (HTL) and 8-hydroxyquinoline aluminum (Alq₃) host and Coumarin 540, and 4-(Dicyanomethylene)-2-methyl-6-julolidyl-9-enyl-4H-pyran (DCM2) dopants. The ratio of the thickness between the two was varied, keeping the total thickness a constant. The emission zone, as well as the recombination zone for a doped device was found to be located within 50 Å from HTL – emission layer (EML) interface. Here, the electrons injected to the EML have to come close to the HTL interface for recombination. The emission zone in the undoped device was studied by using a 40 Å sensing layer between HTL and cathode, and the extent of emission zone is found to be up to 400 Å. As Alq₃ has a reasonable electron transport property and negligible hole transport ability, the electron-hole recombination is presumed to occur at the HTL-EML interface. Thus, generated excitons diffuse towards the cathode. Therefore, the emission zone

of the device is established by the combined exciton diffusion coefficient, D and exciton lifetime, τ . The exciton diffusion length, L is given by³:

$$L = \sqrt{D\tau} \quad (2)$$

The exciton density distribution $\rho(x)$ is given by:

$$\rho(x) = \rho(0) \exp(-x/L), \quad (3)$$

where x is the distance measured from the HTL interface and $\rho(0)$ is the exciton density at the interface. For a device with the sensing layer placed at a distance q from HTL interface, the total emission at a given wavelength, $I_{EL}(\lambda)$ can be given by³:

$$I_{EL}(\lambda) \propto \Phi_{HOST}(\lambda)(1 - e^{-q/L}) + \Phi_{HOST-DYE}(\lambda)(1 - e^{-q/L}), \quad (4)$$

where Φ_{HOST} and $\Phi_{HOST-DYE}$ are the relative EL quantum efficiencies of the undoped and the doped host. Using these equations, EL spectra, and the lifetime of 16 ns for Alq₃ film, the values are calculated to be $L = 200 \text{ \AA}$ and $D = 7.6 \times 10^{-4} \text{ cm}^2 \text{ s}^{-1}$. If the electron-hole recombination zone is not a narrow one but rather extended, these results can only be explained by short exciton diffusion length limited by the hole carrier as the dopants act as efficient hole traps³.

In a multilayer device with poly(methylphenylsilane) (PMPS) as HTL and Alq₃ as ETL, and 3-(2'-Benzothiazolyl)-7- (diethylamino)coumarin (Coumarin 6) doped polystyrene as EML, the EL emission is described with the support of the band diagram, by a wide electron-hole capture zone model⁵. Here, both the carrier recombination and emission are found to occur in EML as well as in ETL with the emission zone having $>300 \text{ \AA}$ width. Two possible mechanisms can generate emission from both these layers. One is that the exciton generated in one layer migrating to another layer. This can be discarded based on the fluorescence spectra. The other most probable mechanism is that the charge carrier recombination occurs in both of

the layers. The holes are assumed to be injected to both of the layers. Injected electrons are blocked by the PMPS layer, which explains the wide electron-hole capture zone across ETL and EML. Therefore, while the device current density depends on the holes, the EL emission depends on the electron injection.

Emission zones in a single layer (EML) alone, double layer (HTL-EML and EML-ETL), and triple layer (HTL-EML-ETL) OLEDs were studied⁶ with a thin sensing layer located in the EML at different distances where HTL, EML and ETL were 4,48-bis[(3-methylphenyl)phenylamino]biphenyl (TPD), 9,10-bis[(4-~diphenylamino)stryryl]anthracene (BSA-2), and 1,3-bis[(4tert-butylphenyl)-1,3,4-oxadiazolyl]phenylene (OXD-7), respectively and a squarilium dye, 2,4-bis[4-(diethylamino)-2-hydroxyphenyl]cycrobutenediylum-1,3-dioxide (Sq) as a dopant for BSA-2. For the single layer, the emission zone was extended throughout the device and for the HTL-EML device, the emission zone is found to be close to HTL-EML interface. However, for the EML- ETL and triple layer device, the emission zone was located in a 10 nm narrow stripe close to EML-ETL interface. The latter devices recorded relatively high efficiencies as well.

Inserting a hole blocking layer is found to affect the chromaticity of OLEDs⁷. Inserting a thin BCP (Bathocuproine) layer between Alq₃ and DCM2 doped α -NPD has resulted in a reduction in α -NPD emission, increase in Alq₃ emission, and a decrease in α -NPD to DCM2 relative emission ratio, by promoting Förster transfer from α -NPD to Alq₃. When BCP was inserted between the cathode and DCJTb doped Alq₃, in which 4,4'-bis[N-(1-naphthyl)-N-phenylamino]biphenyl (NPB) acts as the HTL, luminescence has shown a 100% improvement compared to the device with no BCP⁸. This was attributed with the narrowing of recombination zone with the addition of hole blocking layer (HBL), BCP. In an undoped OLED, inserting an ultrathin layer of 5,6,11,12-tetraphenylnaphthacene (Rubrene) within 4,4'-bis(2,2'-

diphenylvinyl)-1,1'-biphenyl (DPVBi) emitter and controlling its thickness and location could vary the CIE coordinates of the device from (0.17, 0.15) to (0.51, 0.48) through (0.33, 0.32)⁹.

When a DCJTB probe layer has been inserted into an EML consisting of a blend of NPB and Alq₃, irrespective of the location, the green emission increased with voltage¹⁰. This point towards a wide recombination zone for mixed EML device. In a hybrid OLED with blue fluorescent component and red phosphorescent component separated by a spacer to reduce Förster transfer, the emission spectra suggested that the dominant electron-hole recombination occurs in the blue EML situated close to HTL. The red emission was sensitized by the triplet migration from blue to red.¹¹

Red fluorescent dyes like DCM are excellent dopants for Alq₃. However, at high concentrations, dye-dye interactions cause concentration quenching and excimer generation resulting in efficiency reduction and spectral shift. To reduce concentration quenching, a sterically modified 4-(Dicyanomethylene)-2-methyl-6-(1,1,7,7-tetramethyljulolidyl-9-enyl)-4H-pyran (DCJT) molecule has been developed¹² which has improved chromaticity but required difficult purification steps. This molecule was further modified to produce DCJTB which can easily be synthesized in pure form without the contamination of the non-fluorescent bis-condensation by-product which is unavoidable in the DCJT preparation¹³. DCJTB shows slight enhancement in the reduction of concentration quenching and better device efficiency with superior operational stability. DCJTB has a peak emission wavelength of 615 nm and a wide absorption peak across ~480-550 nm, which makes it suitable to dope Alq₃. In this work, DCJTB is used as the fluorescent probe layer.

Under low excitation density, intersystem crossing from singlets controls the triplet generation and decay dynamics of Alq₃. This changes to triplet-triplet annihilation (TTA) and singlet fission at high excitation density¹⁴. Triplet exciton yield in Alq₃ is seen to be increasing with exciton concentration unlike the case of singlets. Using the delayed fluorescence method,

a wide TTA zone for Alq₃ has been mapped¹⁵. This corresponds to the measured triplet diffusion length of 60 nm compared to the singlet's 20 nm. If a phosphorescent sensing layer is used, the triplet properties of the host can be studied as well. Red emitting PtOEP (2,3,7,8,12,13,17,18-octaethyl-21H,23H-porphine platinum(II)) dye is well known for its high room temperature phosphorescence and weak fluorescence efficiency¹. PtOEP shows strong absorption at 530 nm, corresponding to the peak emission of Alq₃. This makes PtOEP a suitable dopant for Alq₃-based OLEDs¹⁶. PtOEP also has a narrow EL spectrum around 650 nm and is almost colour saturated without any tail in infrared¹⁷. On having a PtOEP doped Alq₃ layer next to the DCJTb doped Alq₃ layer, both being separated by a thin Alq₃ layer, no significant increase in emission intensity was found, which was associated with the high fluorescence efficiency of DCJTb¹⁸.

At low electric fields, recombination zone contracts with field and at high fields, the width of the recombination zone is found to be proportional to the ratio between carrier recombination time, τ_{rec} and charge carrier transit time τ_t ¹⁹. This combined with the carrier accumulation at the interfaces with the energy barrier reduces the recombination time. This leads to a decrease in the recombination zone width, resulting in increased EL efficiency²⁰. The ratio of carrier recombination time to transfer time can also be expressed as the ratio between recombination zone width, w and EML thickness, d ²¹. The probability of recombination, P_R in this case is given by:

$$P_R = (1 + w/d)^{-1} \quad (5)$$

For Alq₃ based EML, w can be defined as the average distance the electrons traverse during recombination time and is characterized by the electron mobility, μ_e . So, recombination zone width with an electric field, F can be expressed as:

$$w \cong \mu_e F \tau_{rec} \quad (6)$$

where $\tau_{rec} = (\gamma n_h)^{-1}$.²¹ Here, $\gamma = e(\mu_h + \mu_e)/\epsilon_0\epsilon$ is the coefficient of recombination, μ_h is the hole mobility and n_h , the hole concentration. With our concerned structure having Alq₃ as ETL as well, d becomes $d_{EML} + d_{ETL}$. If the Alq₃ in the EML is doped, the dopant molecules act as hole traps and act as recombination centres, thereby reducing the probability of finding excitons in ETL region. These models however do not distinguish between exciton generation and diffusion²². Several other methods have also been employed to find exciton diffusion length in organic materials such as photo-response of Schottky diode²³, thickness dependent PL quenching²⁴, spectrally resolved PL quenching²⁵, etc. Using different methods, exciton diffusion length in various organic materials such as N,N'-di-1-naphthalenyl-N,N'-diphenyl-[1,1':4',1'':4'',1''':4''',1''''-quaterphenyl]-4,4''-diamine (4P-NPD)^{26,27}, C₆₀²⁸, N,N'-dicarbazolyl-3,5-benzene (mCP)²⁹, bis[2-(4-tertbutylphenyl)benzothiazolato-N,C2']iridium(acetylacetonate) [(tbt)2Ir(acac)] doped NPB³⁰, etc., were studied later on.

In the present work, the emission zone of an OLED is studied to develop a better understanding of the exciton diffusion process by inserting a thin fluorescent “probe” layer at a fixed distance away from the hole transport layer interface in the emission layer. This sensing layer is located at regular intervals between the two interfaces viz. HTL-EML interface and EML-ETL interface. The corresponding EL spectra at each location are recorded. This is similar to the study done on exciton migration in photoluminescence by Simpson on naphthalene coated anthracene³¹ and later adapted to the case of electroluminescence³. We have studied the effect of the applied field on the exciton diffusion observed by changing the potential drop across the emission layer via selectively doping the hole and electron transport layers.

Here, we aim to harvest maximum singlets as well as triplets generated in Alq₃ simultaneously by studying the exciton diffusion and emission profile. We use a thin fluorescent sensing layer of DCJTb doped in Alq₃ to record the singlet exciton recombination

profile and a phosphorescent sensing layer of PtOEP doped in Alq₃ to record the triplet exciton recombination profile. The change in the emission profile with transport doping of ETL and HTL is also studied. Therefore, the resultant structure is in effect a simple bilayer PIN OLED. A simple NPB: Alq₃ bilayer device is used as a control device. Combining the fluorescent and phosphorescent probes together the Alq₃ emission is suppressed.

4.3 Results and discussion*

The reference diodes fabricated have a bilayer structure with NPB as HTL (70 nm) and Alq₃ as EML and ETL (70 nm) (device A1) as shown in Fig 4.1a. HTL and ETL are interface doped with thin layers of 2,3,5,6-Tetrafluoro-7,7,8,8-tetracyanoquinodimethane (F4-TCNQ) and Lithium Fluoride (LiF) respectively in devices A2 and A3. In A4, both these doping are combined. Fig 4.1b shows J-V-L characteristics of these four devices. Devices A1 and A2 show similar current density and luminance even with the additional insertion of F4-TCNQ in A2. However, both of these devices have an absence of LiF layer in common. As is well known, n-doping of Alq₃ with LiF in the presence of Al can cause Fermi level shift in Alq₃³² and the Al work function can get modified to 3.2 eV³³. So, in the absence of LiF, there is a high energy barrier between Alq₃ and Al which prevents efficient electron injection. p-doping organic materials with F4TCNQ is reported to shift the material's Fermi level towards its HOMO level³⁴. This also causes reduction in the width of space charge layer in the doped region leading to efficient injection due to tunnelling^{35,36}. F4TCNQ is also reported to enhance the electron-blocking ability in doped poly(3-hexylthiophene) (P3HT) due to increased polaronic property³⁷. J-V characteristics of A3 and A4 are in accordance with this as both exhibit a higher current density. Here, even though A4 with an additional F4-TCNQ shows lower current

* A detailed discussion on the device fabrication process and the materials used are given in annexure A

density, it has recorded a higher luminance. The improvement in luminance is related to the increased charge balance in both n and p-doped devices.

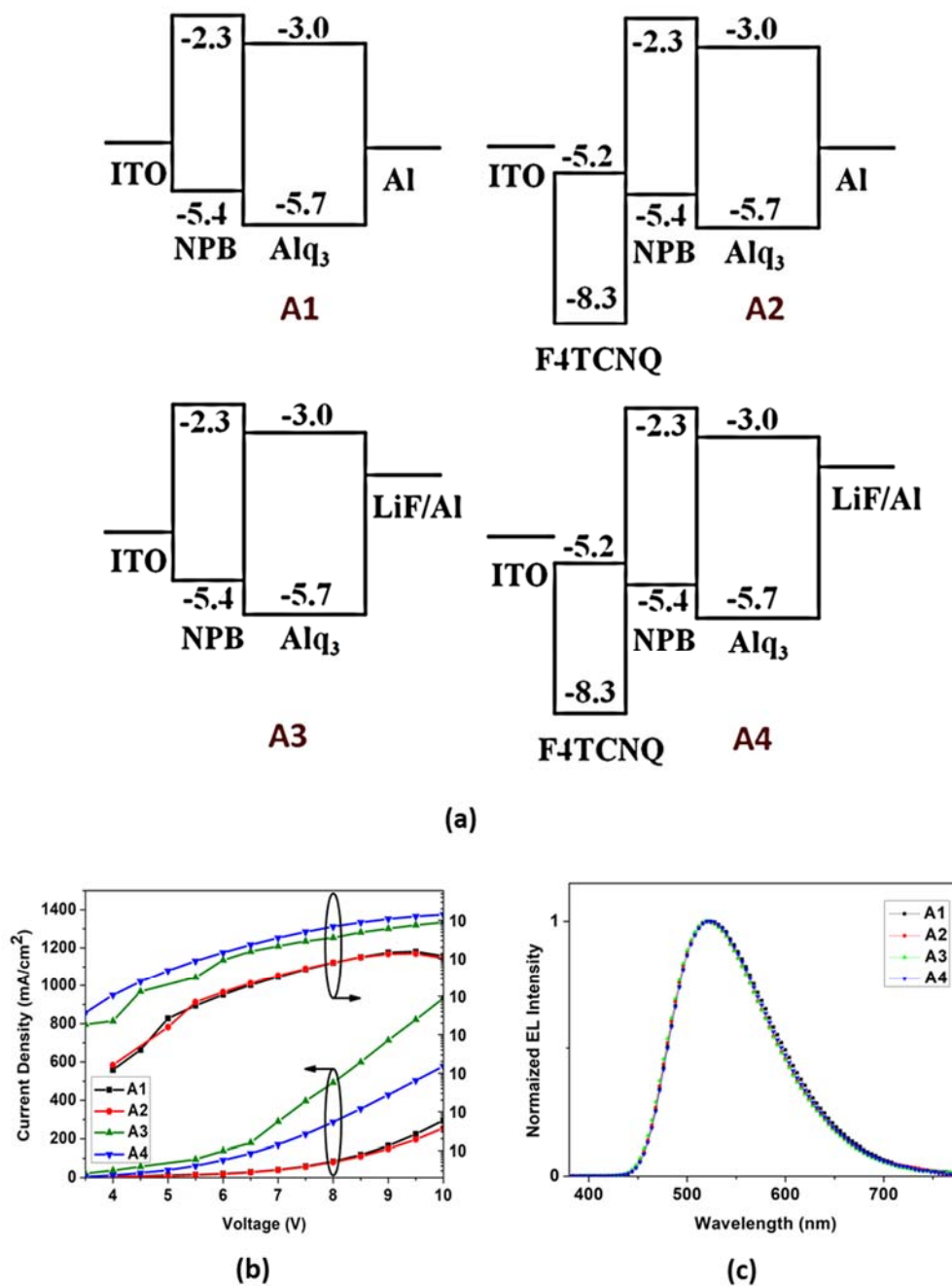


Figure 4.1 a) Energy level diagram, b) Current density-Voltage-Luminance characteristics, and c) Normalized EL spectra for devices A1, A2, A3 and A4. The HOMO-LUMO values are given in eV.

Doping increases the carrier injection to and carrier transport through the transport layers. Both of these materials doped at the interface penetrate a small distance into the ETL and HTL.

This interface doping reduces the energy barrier at the interface which facilitates increased carrier injection to EML and thereby enhances carrier concentration and balance. They screen the electric field available to the EML. In this case, the potential drop across the EML increases. Nevertheless, there is no effect on the chromaticity of the devices as is evident from Fig 4.1c. All the devices show a similar spectrum irrespective of the applied voltage. The maximum intensity is at a wavelength of 520 nm with Commission Internationale de L'Eclairage (CIE) coordinates around ($x=0.33$, $y=0.52$).

Now, to study the emission zone in detail, a fluorescent and phosphorescent material separately are doped into a thin layer of the host at different distances away from HTL-EML interface. As shown in Fig 4.2a, these probe layers are inserted to the device combinations A1 and A4, which is marked by the presence of transport layer interface doping. Here, DCJTb and PtOEP are selected as the fluorescent and phosphorescent dopants respectively due to their distinct emission spectrum from that of the Alq₃ emission. Using these fluorescent and phosphorescent probes, we can also infer the best way to efficiently harvest maximum excitons, both singlets and triplets, from the host simultaneously.

4.3.1 Singlet exciton sensing in Alq₃

To investigate the singlet exciton migration and emission zone in OLED, we inserted a sensor layer of DCJTb doped Alq₃ with a thickness of 3 nm and a concentration of 3 wt % at a location in Alq₃ as EML defined at a distance 'x' ($x=0, 2.5, 5, 10, 15, 20$ and 25 nm) from NPB: Alq₃ interface in the device A1 and A4 (Fig 4.2a). Fig 4.2b1 and 4.2b2 show the J-V-L characteristics of the devices with sensor layer at a different location in the modified control devices A1 and A4 respectively. A1 has undoped transport layers where A4 has transport layers with interface doping. From here on, these will be mentioned as undoped and doped devices respectively.

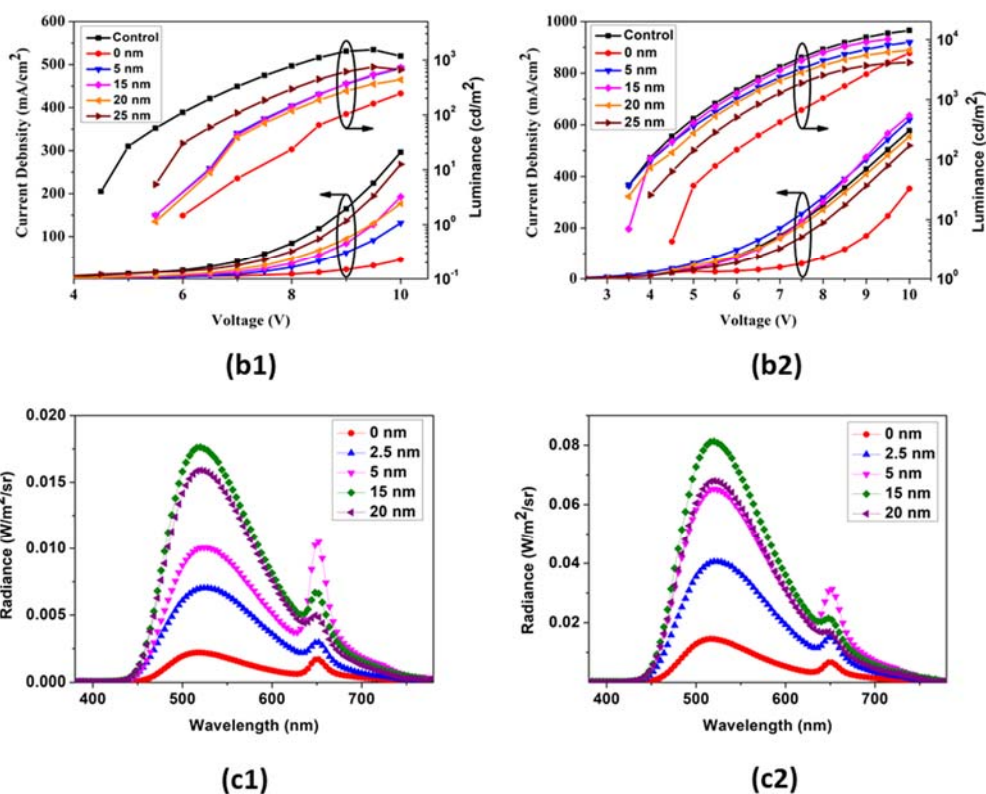
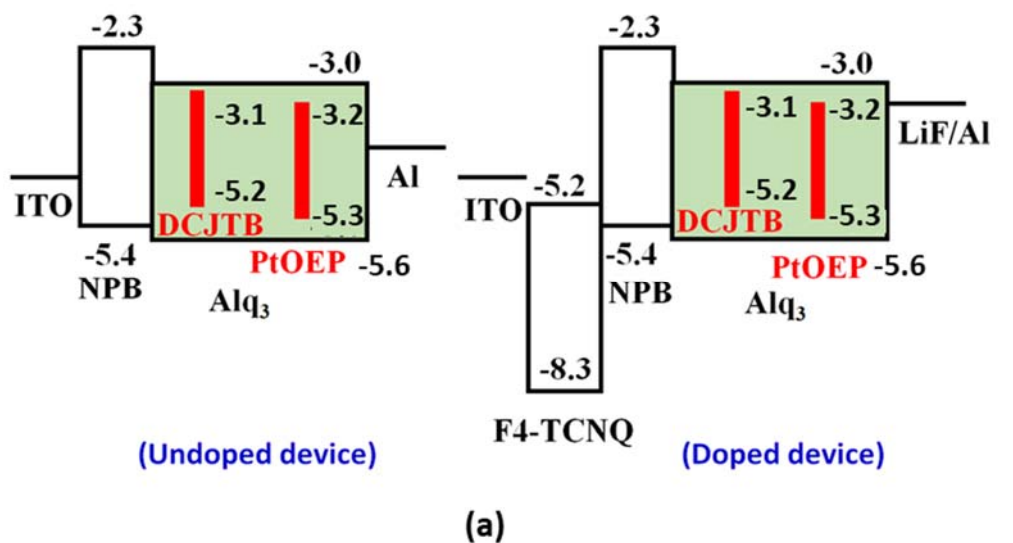


Figure 4.2 a) Energy level diagram of the devices with the probe layer inserted in devices, undoped and doped, b1) J-V-L characteristics for the undoped device with DCJTB sensing layer, b2) J-V-L characteristics for the doped HTL and ETL device with DCJTB sensing layer, and EL spectra at 8V for the c1) undoped device, c2) doped device; legends show the distance of the probe location in nm from HTL-EML interface with respect to the control devices A1 or A4. The HOMO-LUMO values are given in eV.

When the DCJTB layer was placed at the interface itself (0 position), in both the doped and undoped cases, we have the lowest current density and hence the lowest luminance. In the undoped case, the current density is increasing with the distance x . This trend is closely followed in the luminance measurement as well. Here even if the recombination is assumed to happen at the interface, we have to infer that the recombination zone is wide at least up to 5 nm range. It is clear from Figs 4.2c1 and 4.2c2 that the highest intensity red emission is measured for the 5 nm device, at ~650 nm, for both the undoped and doped devices. The same device also records lowest relative green contribution of peak ~520 nm. This means the maximum singlet excitons are captured by the 5 nm device, whether they could be relaxed radiatively or not. The fraction of excitons received by the Alq₃ must have been exceedingly reduced causing a diminished green peak. We can observe a steady increase in green contribution and decrease in red for the 15 and 20 nm device, which again continue as the distance increases.

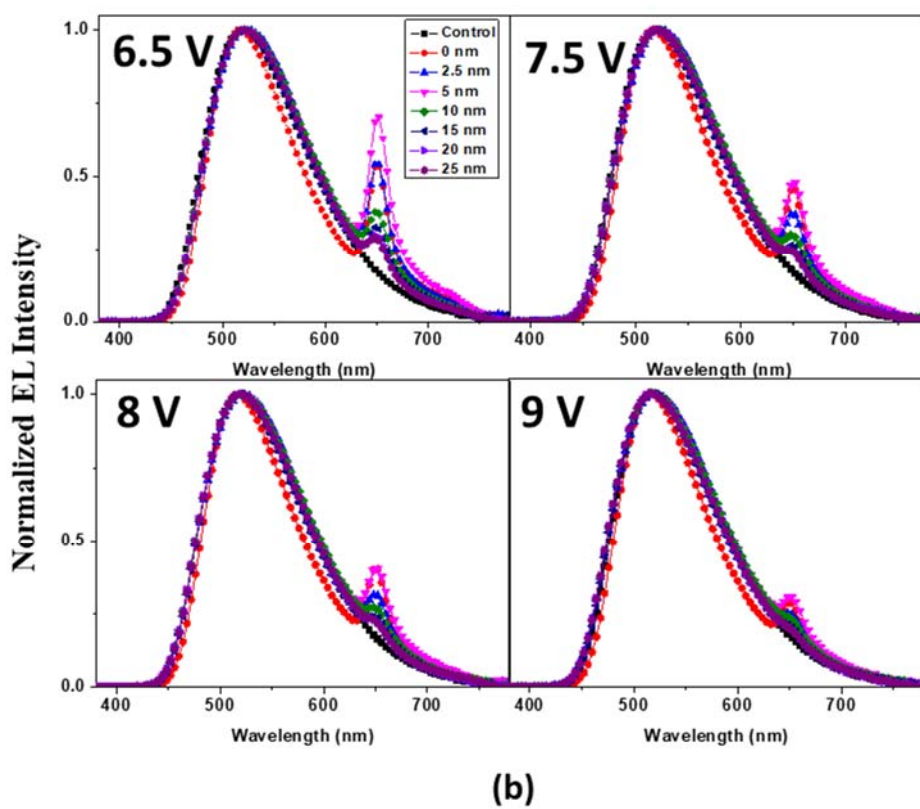
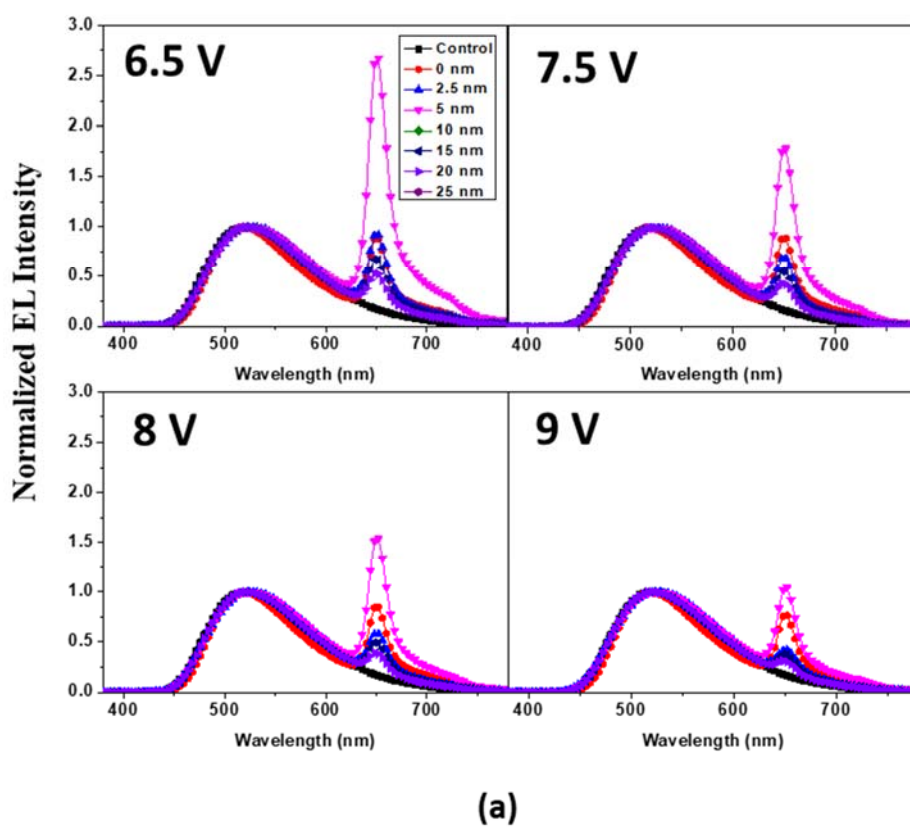
The over all emission of 0 nm device and 2.5nm device are affected due to the presence of the probe layer within the recombination zone. This may be because the generated excitons tend to migrate out of this region. The energy levels of DCJTB confine them and they are in turn non-radiatively relaxed. The generated exciton in this small range may then be diffused away and further captured by the 5 nm device. This may be the reason for the higher intensity ratio between red and green for the same as shown in Fig 4.3c. All other devices are showing a lower intensity ratio between red and green. Therefore, within 5 nm distance, the DCJTB probe layer seems to inhibit radiative recombination due to the longer exciton diffusion distance.

When the devices are doped, the 5 and 15 nm devices have recorded a current density even higher than the control device, which enabled them to have an increased luminescence as well. With doping, the availability of injected charge carriers increases as well as carrier balance, as

seen by an almost ten times increase in luminance compared to the undoped device and more than two times increase in current density. Whereas carrier balance is the reason for the former, carrier availability is responsible for the latter. This also causes a decrease in red/green relative peak intensity. What happens is that the Alq₃ alone utilizes the enhancement in exciton generation when the DCJTB's contribution is not increased proportionally. Indeed at least a measurable increase in the red emission is expected and is recorded. That means the increase in red emission is overshadowed by the increase in green emission.

Figs 4.3a and 4.3b show normalized EL spectra with an increase in voltage for the undoped and doped devices respectively. As the driving voltage increases, the intensity of the red peak is reduced. At low voltages, undoped devices show approximately three times increase in red peak intensity. The ratio is reduced to almost one as the driving voltage is increased. The increase in voltage results in an increased green emission with only a small enhancement in red emission. , the 5 nm device seems to give the relatively highest red peak. The red/green peak intensity ratio for all the devices is plotted in Fig 4.3c. More than 100% reduction in the relative intensity is visible when the devices are doped.

However, even this explosive increase in red emission at lower fields cannot be maintained at high fields. For the doped devices, the red peak tends to become negligibly small with an increase in voltage and remains almost constant at high voltages. The probe layer's contribution in the EL emission is diminished, as the distance x becomes larger than 25 nm. This approximates the singlet emission zone in the undoped Alq₃ layer. So, doping this host for a thickness more than 25 nm becomes unnecessary, as the singlet emission zone seems to be concentrated in this region. Further doping may have contributed towards enhanced carrier transport in the EML depending on the transport or trapping properties of the dopant.



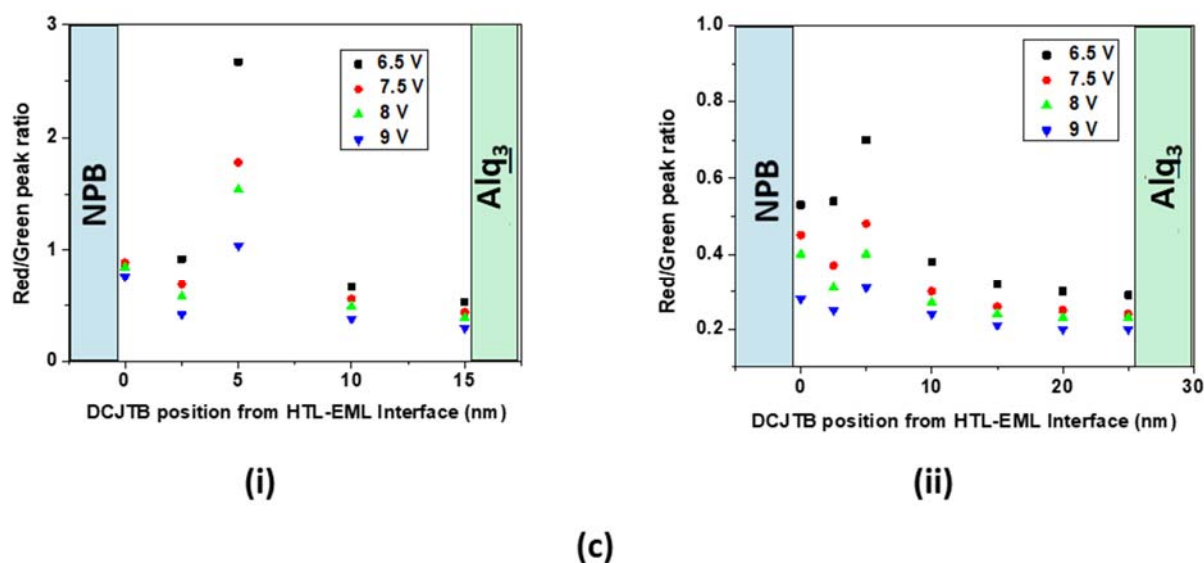


Figure 4.3 a) EL spectra for the undoped device having DCJTB sensing layer at different voltages, b) EL spectra for the doped device having DCJTB sensing layer at different voltages; legends show the distance in nm from HTL-EML interface with respect to the control devices A1 or A4, and c) Ratio of EL intensity peak between red and green with respect to the sensor layer position for i) undoped device, and ii) doped device.

However, this enhancement in carrier density would be added towards non-radiative relaxation of the exciton. That is, an increase in current density might be observed but it could not translate to an increased emission. Following the electron-hole recombination at the NPB-Alq₃ interface, the generated excitons are diffused towards ETL. That means exciton migration is also a dominant process along with exciton generation in defining the emission zone of the devices which is controlled by exciton diffusion coefficient and exciton lifetime.

4.3.2 Triplet exciton sensing in Alq₃

The triplet exciton zone in the Alq₃ are mapped, and the exciton migration is studied by inserting a phosphorescent PtOEP doped into Alq₃ of the thickness of 3 nm and concentration of 8 wt. %, at ‘y’ distance from NPB: Alq₃ interface in the A1 and A4 devices (Fig 4.2a). Here, we are not going to map the emission zone in the 0-10 nm range from the interface as this area can effectively harvest singlets and we aim to harvest both triplets beyond 10 nm from the

interface. So, for the triplet exciton sensing, the area of interest focused on will be $y = 10\text{-}25$ nm. A relatively higher doping concentration compared to the DCJTb probe layer is required here as both the triplets and singlets are required to be part of energy transfer.

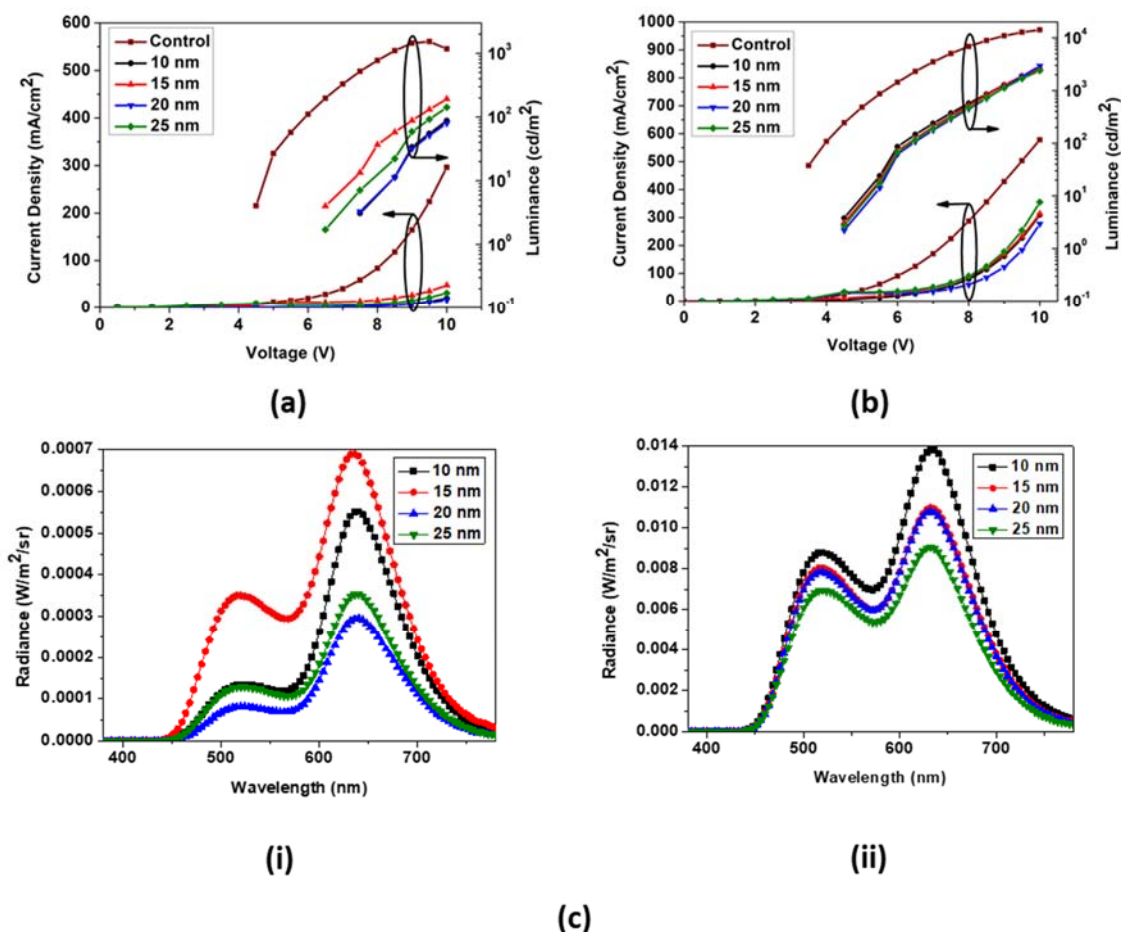


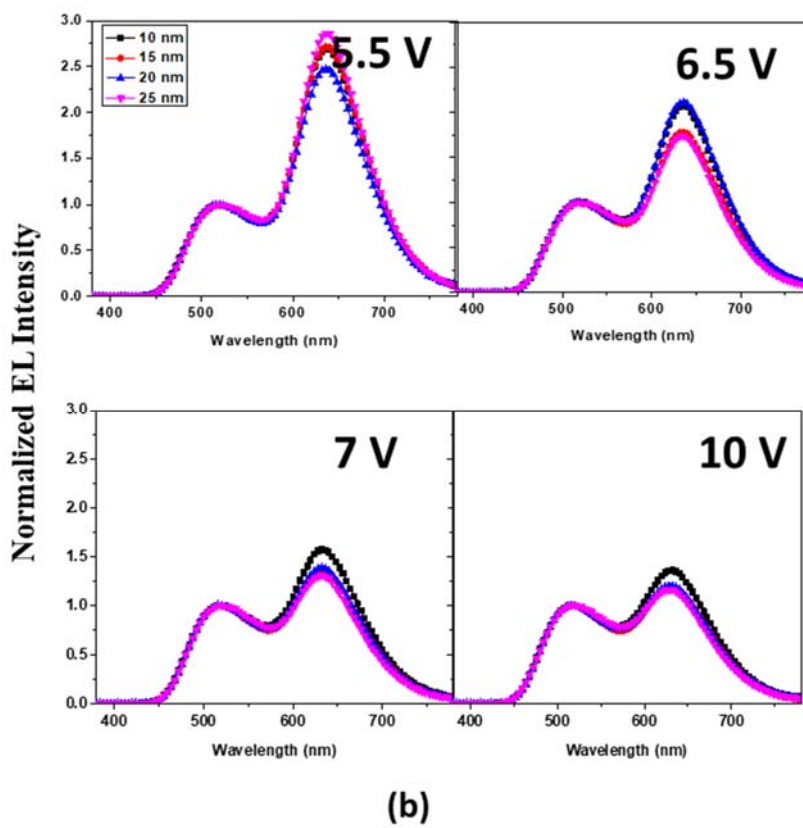
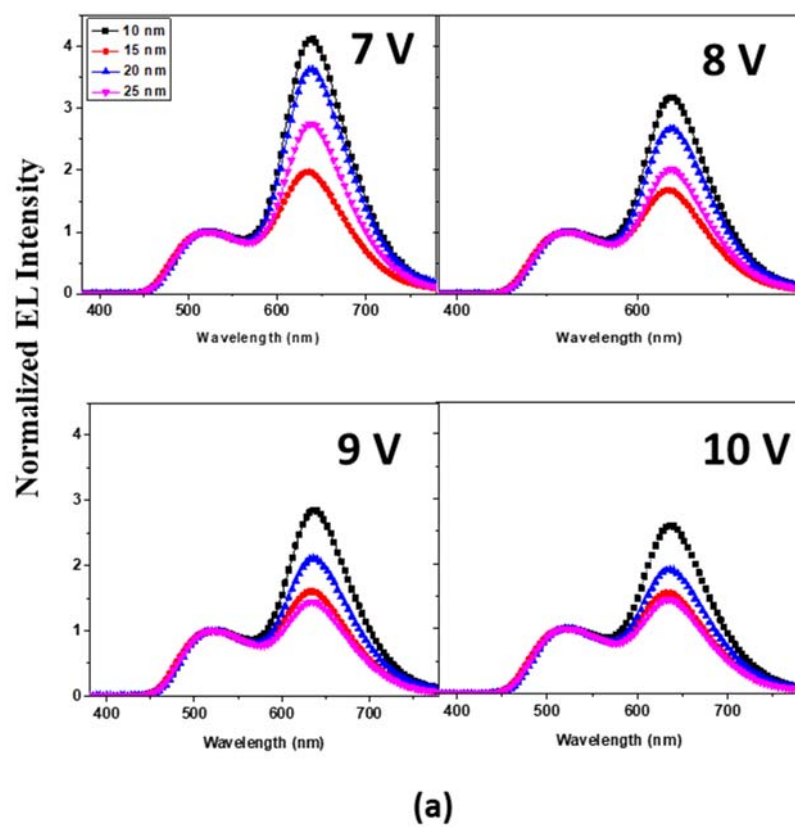
Figure 4.4 a) J-V-L characteristics for the undoped device with PtOEP sensing layer, b) J-V-L characteristics for the doped device with PtOEP sensing layer, c) EL spectra of the i) undoped device, ii) doped device; legends show the distance of the probe location in nm from HTL-EML interface with respect to the control devices A1 or A4.

Fig 4.4a and b show the J-V-L characteristics of the devices with sensor layer at a different location in the control devices A1 and A4 respectively. Here, the 15 nm device is exhibiting the relatively higher current density and luminance among the undoped devices. The 25 nm device is a close runner up. 10 and 20 nm devices show similar current density as well as luminance. Comparing with the control and the fluorescent probe devices, it is clear that the

current devices are recording lower values on both counts. Nevertheless, on doping these devices, the current density and the luminance values are surging up. With doping, there is a pronounced decrease in the turn-on voltage as well. As mentioned in the previous section increase in the applied field along with enhanced carrier balance can increase the exciton generation and the probability of radiative recombination. With the doping, the current density and luminance become independent of the sensor layer position, at higher voltages. As can be observed, devices with sensor layers positioned at various locations have shown matching device performance which gets more overlapped with an increase in voltage.

Fig 4.4c is the EL spectra of the doped and undoped devices with PtOEP probe, recorded at a voltage of 7V. In this, the emission intensities are distinctive with the spectrum of 15 nm and 10 nm devices slightly above all others for the undoped and doped devices respectively. Here, we have to assume a wider recombination zone for the triplet excitons, closely embedded in the 15 nm range. This slightly contracts when the transport layers are doped, so that maximum number of excitons is available to the sensor layer anchored closely. As the voltage increases, the field-dependent mobility of the carriers increases as well thereby reducing the probability of carrier trapping. In addition, the possibility of the field-induced fluorescent quenching increases as well for the doped devices as the potential drop across EML increases with doping. There is no singlet state emission of PtOEP, which could be identified at the expected 580 nm wavelength³⁸. However, strong emission is observed at 632 nm, with phosphorescent origins.

More singlet excitons are harvested by PtOEP from Alq₃ as is evident from the decrease in Alq₃ contribution at 520 nm, which otherwise is acting as a trap. As the driving voltage increases, increased available carriers saturate PtOEP emission due to the long triplet lifetime and short range of Dexter transfer. This saturation effect can be seen from the EL spectra shown in Fig 4.5b for the doped device compared to the undoped device spectra of 4.5a.



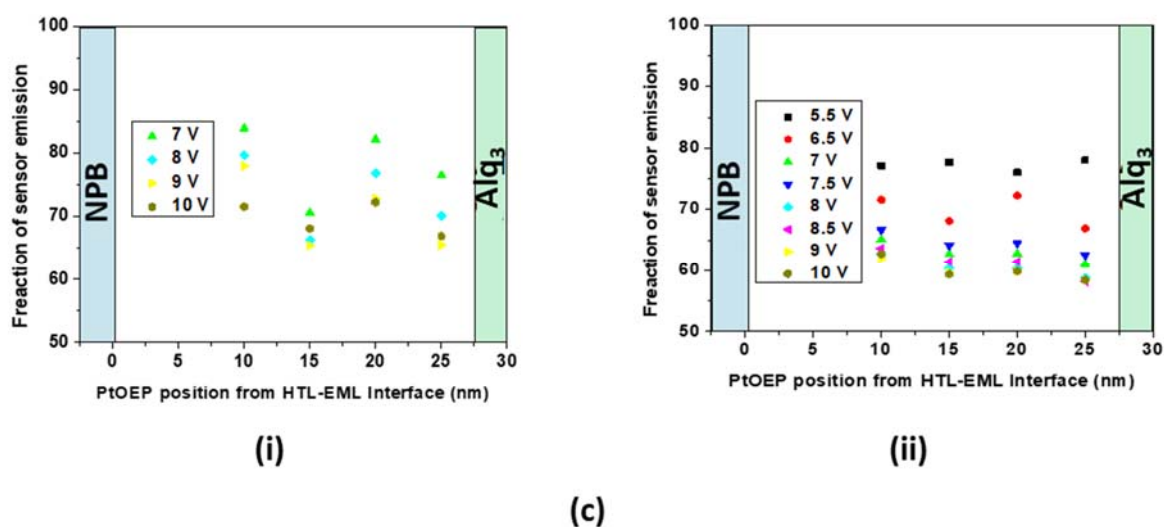


Figure 4.5 a) EL spectra for the undoped device having PtOEP sensing layer at different voltages, b) EL spectra for the doped device having PtOEP sensing layer at different voltages; legends show the distance of the probe location in nm from HTL-EML interface with respect to the control devices A1 or A4, and c) percentage of red sensor contribution to the total emission with respect to the sensor layer position for i) undoped device and ii) doped device.

At higher voltages, the spectra try to band together irrespective of the sensor layer location. With an increase in voltage also, the intensity change is minimal as compared to the fluorescent probe devices. Even for the undoped devices, the relative intensities can be observed to stay constant at high voltages.

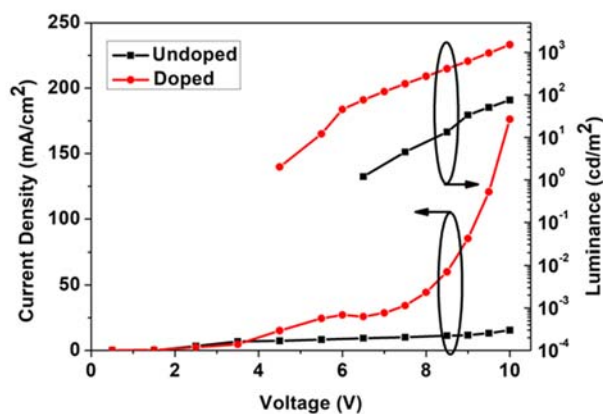
For the doped devices, at low field, the 25 nm devices have relatively higher red to green ratio. However, as voltage increases, it is unable to maintain this. The 10 nm device is the most successful in retaining the ratio and becomes the one with the highest fraction of the red contribution. With the increased field, the exciton diffusion length is extended and more excitons are migrated away towards cathode. The absence of a hole-blocking layer increases this leakage. That is without a proper confinement, more carriers are being quenched, as they get further away from the carrier recombination zone.

Bimolecular interactions like triplet-triplet annihilation (TTA) also cause exciton quenching at high voltage, thereby reducing emission. This causes the increase in the fraction of available

carriers to Alq₃ thereby decreasing the relative contribution from the PtOEP emission as shown in Fig 4.5c. Even though this sensor contribution decreases with voltage, it remains constant regardless of its location in the EML. This indicates that in a device with good carrier balance, the emission zone and therefore recombination zone remain evenly distributed. We can see the trend up to 28 nm range. As the triplet diffusion length is generally in the range of 100 nm, this necessitates the insertion of a good hole blocking layer between EML and ETL. As we have used Alq₃ as EML and ETL here, the majority of the triplet excitons are expected to be migrated away towards the cathode. This emission zone map also acts as the indicator of good carrier balance in the device as well as the possible ambipolar nature of the mixed EML³⁹. As Alq₃ is a complete electron transporter, we have to assume PtOEP be taking up the part of hole transport.

4.3.3 Combined fluorescent and phosphorescent emitters in host Alq₃

In this section, we are combining both the DCJTb as well as the PtOEP emission in a single Alq₃ layer to extract both singlets and triplets. Here 30 nm of DCJTb and 20 nm PtOEP doped Alq₃ layers separated by a 20 nm Alq₃ undoped layer act as EML. DCJTb should be able to remove the maximum number of singlet excitons. The triplet states are expected to be diffused through the middle Alq₃ layer to reach the PtOEP doped Alq₃ layer.



(a)

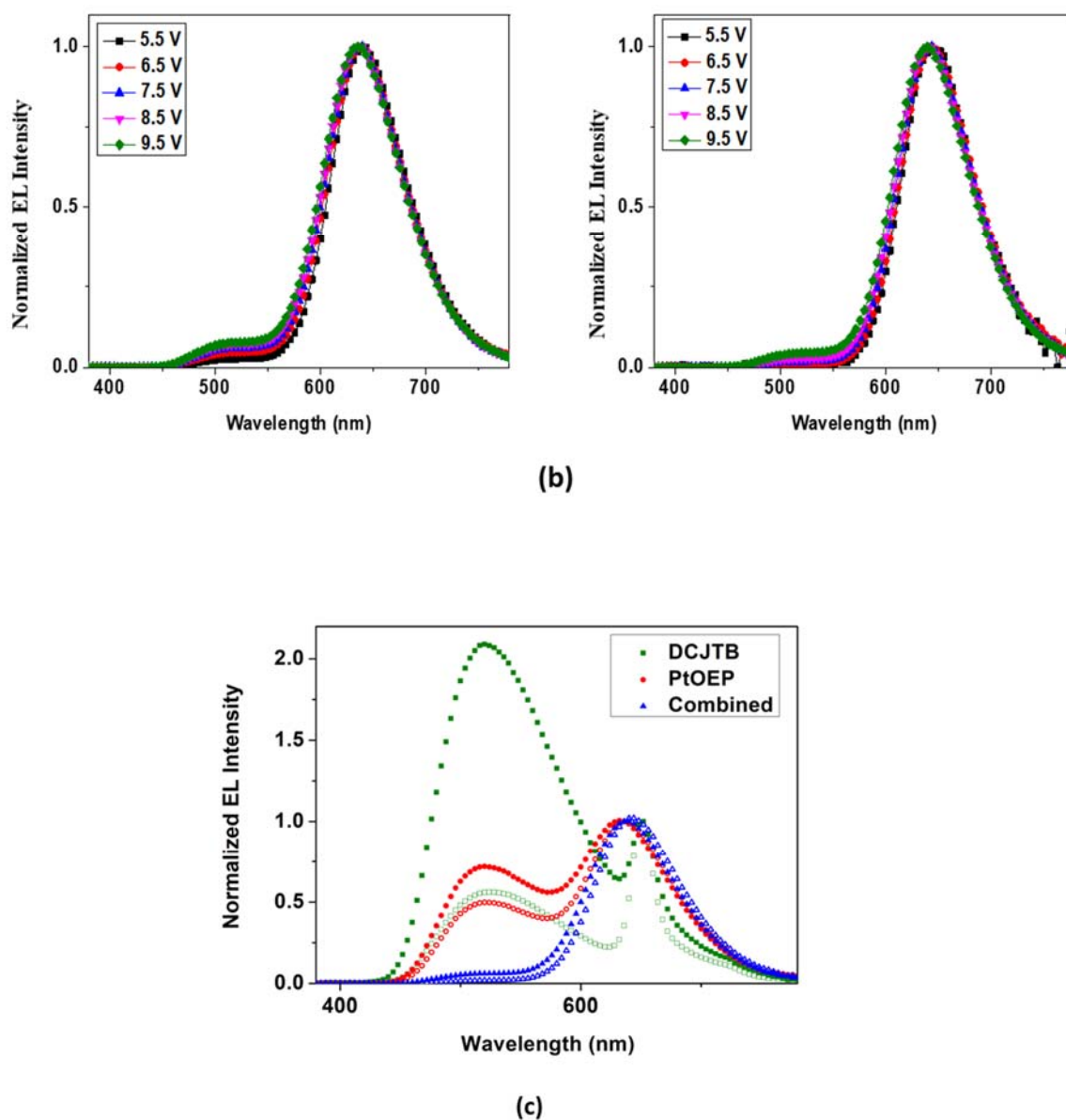


Figure 4.6 a) J-V-L characteristics for the undoped and doped devices with both DCJTB and PtOEP, b) Normalized EL spectra of the i) undoped device, ii) doped device with change in voltage, and (c) Comparison of EL spectra of devices with either DCJTB or PtOEP alone and the combined device; open: undoped devices, closed: doped devices.

The J-V-L characteristics of the doped and undoped devices are showing marked differences in Fig 4.6a with an explosive enhancement in device performance. This is completely the contribution of the dopants as there is virtually no Alq₃ emission around 520 nm other than a small bump as shown in Fig 4.6b. This is because the undoped Alq₃ layer has been inserted

outside the singlet diffusion range. As triplets have longer diffusion length as shown in the previous section, PtOEP emission can be expected. The only downside is the absence of a blocking layer, which can lead to carrier leakage.

The EL profiles of both the doped and undoped devices remain almost completely unchanged with a change in the applied voltage. The slight increase in the green emission at higher voltages can be attributed to the TTA happening and the resultant singlets diffusing towards Alq₃ undoped layers. This is in no way contributing significantly towards the total emission, but can adversely affect the hue of the emission. Fig 4.6c shows a comparison between normalized EL spectra of devices with DCJTB or PtOEP probe layer alone and the combined device, at 8 V. The peaks of both the doped and undoped are recorded to be widened slightly at the longer side around 650 nm to accommodate the DCJTB part. However the total emission is significantly weakened. This could be due to the fact that we doped the device only in a very narrow region, unlike a functional OLED. The PtOEP probe seems to have harvested the triplet states filtered out from DCJTB and the undoped Alq₃ layer.

4.4 Conclusions

Exploring the emission profile and thereby estimating the recombination profile in an OLED can help design improved device structures. Exciton migration and emission in Alq₃ device are studied by way of fluorescent and phosphorescent sensing layers. By positioning the probe layers within the EML at different intervals, the recombination preference could be studied. It was found that excitons tend to recombine near minority carrier interfaces. In the case of devices probed by the phosphorescent layer, the emission was found to be unaffected by the location of the sensor due to the long triplet exciton diffusion length. The studies also shed light on the effect of applied electric field on the device as well as the probabilities of carrier leakage. While the phosphorescent probe has shown an emission profile extending

almost throughout the EML, the fluorescent probe has shown the limited extent of the singlet emission zone.

4.5 References

- 1 Baldo, M. A. *et al.* Highly efficient phosphorescent emission from organic electroluminescent devices. *Nature* **395**, 151-154, doi:10.1038/25954 (1998).
- 2 Baldo, M. A., O'Brien, D. F., Thompson, M. E. & Forrest, S. R. Excitonic singlet-triplet ratio in a semiconducting organic thin film. *Physical Review. B* **60**, 14422-14428, doi:10.1103/PhysRevB.60.14422 (1999).
- 3 Tang, C. W., Vanslyke, S. A. & Chen, C. H. Electroluminescence of Doped Organic Thin-Films. *Journal of Applied Physics* **65**, 3610-3616, doi:Doi 10.1063/1.343409 (1989).
- 4 Burin, A. L. & Ratner, M. A. Exciton migration and cathode quenching in organic light emitting diodes. *The Journal of Physical Chemistry A* **104**, 4704-4710, doi:10.1021/Jp994162x (2000).
- 5 Suzuki, H., Meyer, H., Hoshino, S. & Haarer, D. Electroluminescence from multilayer organic light-emitting diodes using poly(methylphenylsilane) as hole transporting material. *Journal of Applied Physics* **78**, 2684-2690, doi:10.1063/1.360063 (1995).
- 6 Aminaka, E., Tsutsui, T. & Saito, S. Effect of layered structures on the location of emissive regions in organic electroluminescent devices. *Journal of Applied Physics* **79**, 8808-8815, doi:10.1063/1.362475 (1996).
- 7 Deshpande, R. S., Bulovic, V. & Forrest, S. R. White-light-emitting organic electroluminescent devices based on interlayer sequential energy transfer. *Applied Physics Letters* **75**, 888-890, doi:10.1063/1.124250 (1999).
- 8 Xie, Z. Y., Hung, L. S. & Lee, S. T. High-efficiency red electroluminescence from a narrow recombination zone confined by an organic double heterostructure. *Applied Physics Letters* **79**, 1048-1050, doi:10.1063/1.1390479 (2001).

- 9 Choukri, H. *et al.* White organic light-emitting diodes with fine chromaticity tuning via ultrathin layer position shifting. *Applied Physics Letters* **89**, doi:10.1063/1.2382730 (2006).
- 10 Hsiao, C. H., Lee, J. H. & Tseng, C. A. Probing recombination-rate distribution in organic light-emitting devices with mixed-emitter structure. *Chemical Physics Letters* **427**, 305-309, doi:10.1016/j.cplett.2006.06.073 (2006).
- 11 Deaton, J. C., Kondakova, M. E., Kondakov, D. Y., Pawlik, T. D. & Giesen, D. J. P-174: Triplet Exciton Diffusion in Hybrid Fluorescent/Phosphorescent OLEDs. *SID Symposium Digest of Technical Papers* **38**, 849-851, doi:10.1889/1.2785441 (2007).
- 12 Chen, C. H. & Tang, C. W. in *Proceedings of the 2nd International Symposium on Chemical Functional Dyes*. 536.
- 13 Chen, C. H., Tang, C. W., Shi, J. & Klubek, K. P. Improved red dopants for organic electroluminescent devices. *Macromol Symp* **125**, 49-58, doi:10.1002/masy.19981250103 (1998).
- 14 Watanabe, S., Furube, A. & Katoh, R. Generation and decay dynamics of triplet excitons in Alq3 thin films under high-density excitation conditions. *The Journal of Physical Chemistry A* **110**, 10173-10178, doi:10.1021/jp0618227 (2006).
- 15 Luo, Y. C. & Aziz, H. Probing triplet-triplet annihilation zone and determining triplet exciton diffusion length by using delayed electroluminescence. *Journal of Applied Physics* **107**, doi:10.1063/1.3410678 (2010).
- 16 Liu, H. Y., Switalski, S. C., Coltrain, B. K. & Merkel, P. B. Oxygen Permeability of Sol-Gel Coatings. *Applied Spectroscopy* **46**, 1266-1272, doi:10.1366/0003702924123881 (1992).
- 17 O'Brien, D. F., Baldo, M. A., Thompson, M. E. & Forrest, S. R. Improved energy transfer in electrophosphorescent devices. *Applied Physics Letters* **74**, 442-444, doi:10.1063/1.123055 (1999).
- 18 Oh, H. Y. *et al.* Organic light emitting diode fabricated using DC JTB and Pt OEP. *Journal of the Korean Physical Society* **39**, 49-51 (2001).

- 19 Kalinowski, J. Electroluminescence in organics. *Journal of Physics D: Applied Physics* **32**, R179-R250, doi:10.1088/0022-3727/32/24/201 (1999).
- 20 Kalinowski, J., Palilis, L. C., Kim, W. H. & Kafafi, Z. H. Determination of the width of the carrier recombination zone in organic light-emitting diodes. *Journal of Applied Physics* **94**, 7764, doi:10.1063/1.1624477 (2003).
- 21 Kalinowski, J., Di Marco, P., Fattori, V., Giulietti, L. & Cocchi, M. Voltage-induced evolution of emission spectra in organic light-emitting diodes. *Journal of Applied Physics* **83**, 4242-4248, doi:10.1063/1.367181 (1998).
- 22 Zhou, Y. C., Ma, L. L., Zhou, J., Ding, X. M. & Hou, X. Y. Effect of a sensing layer on triplet exciton diffusion in organic films. *Physical Review. B* **75**, doi:10.1103/Physrevb.75.132202 (2007).
- 23 Ghosh, A. K. & Feng, T. Merocyanine organic solar cells. *Journal of Applied Physics* **49**, 5982-5989, doi:10.1063/1.324566 (1978).
- 24 Powell, R. C. & Soos, Z. G. Singlet exciton energy transfer in organic solids. *Journal of Luminescence* **11**, 1-45, doi:10.1016/0022-2313(75)90077-0 (1975).
- 25 Lunt, R. R., Giebink, N. C., Belak, A. A., Benziger, J. B. & Forrest, S. R. Exciton diffusion lengths of organic semiconductor thin films measured by spectrally resolved photoluminescence quenching. *Journal of Applied Physics* **105**, 053711, doi:10.1063/1.3079797 (2009).
- 26 Wunsche, J., Reineke, S., Lussem, B. & Leo, K. Measurement of triplet exciton diffusion in organic light-emitting diodes. *Physical Review. B* **81**, doi:10.1103/Physrevb.81.245201 (2010).
- 27 Hofmann, S., Rosenow, T. C., Gather, M. C., Lussem, B. & Leo, K. Singlet exciton diffusion length in organic light-emitting diodes. *Physical Review. B* **85**, doi:10.1103/Physrevb.85.245209 (2012).
- 28 Dashan Qin, Gu, P., Dhar, R. S., Razavipour, S. G. & Ban, D. Measuring the exciton diffusion length of C₆₀ in organic planar heterojunction solar cells. *Physica Status Solidi A* **8**, 1967-1971, doi:10.1002/pssa.201026724 (2011).

- 29 Zhang, W., Yu, J. S., Wen, W. & Jiang, Y. D. Study on triplet exciton diffusion length of mCP in phosphorescent organic light-emitting devices using electroluminescent spectra. *Journal of Luminescence* **131**, 1260-1263, doi:10.1016/j.jlumin.2011.03.005 (2011).
- 30 Zhao, J., Yu, J. S., Ma, Z., Li, L. & Jiang, Y. D. Optimization of yellow phosphorescent organic light-emitting devices based on triplet exciton diffusion length. *Synthetic Metals* **161**, 2417-2421, doi:10.1016/j.synthmet.2011.09.018 (2011).
- 31 Simpson, O. & Mott, N. F. Electronic properties of aromatic hydrocarbons. III. Diffusion of excitons. *Proceedings of the Royal Society of London. Series A. Mathematical and Physical Sciences* **238**, 402-411, doi:doi:10.1098/rspa.1957.0008 (1957).
- 32 Parthasarathy, G., Shen, C., Kahn, A. & Forrest, S. R. Lithium doping of semiconducting organic charge transport materials. *Journal of Applied Physics* **89**, 4986-4992, doi:10.1063/1.1359161 (2001).
- 33 D'Andrade, B. W., Forrest, S. R. & Chwang, A. B. Operational stability of electrophosphorescent devices containing p and n doped transport layers. *Applied Physics Letters* **83**, 3858-3860, doi:10.1063/1.1624473 (2003).
- 34 Blochwitz, J. *et al.* Interface electronic structure of organic semiconductors with controlled doping levels. *Organic Electronics* **2**, 97-104, doi:https://doi.org/10.1016/S1566-1199(01)00016-7 (2001).
- 35 Zhou, X. *et al.* Enhanced Hole Injection into Amorphous Hole-Transport Layers of Organic Light-Emitting Diodes Using Controlled p-Type Doping. *Advanced Functional Materials* **11**, 310-314, doi:doi:10.1002/1616-3028(200108)11:4<310::AID-ADFM310>3.0.CO;2-D (2001).
- 36 Blochwitz, J., Pfeiffer, M., Fritz, T. & Leo, K. Low voltage organic light emitting diodes featuring doped phthalocyanine as hole transport material. *Applied Physics Letters* **73**, 729-731, doi:10.1063/1.121982 (1998).
- 37 Arafat Mahmud, M. *et al.* Enhanced stability of low temperature processed perovskite solar cells via augmented polaronic intensity of hole transporting layer. *physica status*

-
- solidi (RRL) – Rapid Research Letters* **10**, 882-889, doi:doi:10.1002/pssr.201600315 (2016).
- 38 Ponterini, G., Serpone, N., Bergkamp, M. A. & Netzel, T. L. Comparison of radiationless decay processes in osmium and platinum porphyrins. *Journal of the American Chemical Society* **105**, 4639-4645, doi:10.1021/ja00352a020 (1983).
- 39 Kuttipillai, P. S. *et al.* Mapping recombination profiles in single-, dual-, and mixed-host phosphorescent organic light emitting diodes. *Organic Electronics* **57**, 28-33, doi:10.1016/j.orgel.2018.02.025 (2018).

OLED performance metrics and fabrication details

A.1 OLED: Characterization details

Parameters required to assess the performance of a working OLED device are listed below.

i. Current density

The current measured at a typical luminescence and/or voltage for the unit device area usually expressed as mA/cm² or A/m² unit.

ii. Luminance

Luminance is the luminous intensity, which is the power emitted per the unit solid angle, per unit device area. Unit is cd/m² (candela/sq.meter).

iii. Current efficiency

Current efficiency is the ratio of luminous intensity to injected current density. It is calculated by dividing luminance by current density. SI unit of current efficiency is cd/A.

iv. Power efficiency/Luminous efficacy

Efficacy is the ratio between total visible light emitted to input power expressed in lm/W (lumen/Watt). It is a measure of how well the electrical energy can be converted into visible part of electromagnetic radiation.

$$\text{Power efficiency} = \frac{\text{Current efficiency} \times \pi}{V}$$

as $1 \text{ lumen} = \pi \times cd$ for a Lambertian surface (a surface which reflects all the incident light and appears to be have the same apparent brightness from all the angles).

v. Internal quantum efficiency

The internal quantum efficiency of OLED is the number of photons generated per injected electrons.

$$\eta_{\text{int}} = \gamma \eta_{\text{singlet}} \eta_f$$

where γ is the charge balance factor, η_{singlet} is the fraction of spin-allowed excitons, and η_f is the photoluminescent quantum yield.

vi. External quantum efficiency

External quantum efficiency is the fraction of the total number of photons emitted outside the device in the forward direction to the total number of electrons injected.

$$\eta_{\text{ext}} = \eta_{\text{int}} \eta_c$$

where η_c is the out-coupling efficiency, which measures the device ability to extract the light generated inside without losses.

vii. CIE color coordinates

CIE color coordinates are device independent representation of color, connecting the wavelength weighed emission spectra to the color as perceived by the human eye. Every color in the visible range can be adapted to the CIE XYZ tristimulus values, which act as a standard reference against all the defined color spaces. CIE 1931 XYZ color space, which was created by the International Commission on Illumination (CIE), is widely used to compare the color of OLED

emission. The chromaticity diagram converts all combination of tristimulus values into (x, y) coordinates. Tristimulus values for a color with radiance $\varphi(\lambda)$ is given by,

$$X = \int_{\lambda} \varphi(\lambda) x(\lambda) d\lambda$$

$$Y = \int_{\lambda} \varphi(\lambda) y(\lambda) d\lambda$$

$$Z = \int_{\lambda} \varphi(\lambda) z(\lambda) d\lambda$$

where λ is the wavelength and $x(\lambda)$, $y(\lambda)$, and $z(\lambda)$ are the CIE standard observer color matching functions for red, green, and blue (RGB). Then the CIE color coordinates x and y are,

$$x = \frac{X}{X + Y + Z}$$

$$y = \frac{Y}{X + Y + Z}$$

viii. Threshold voltage

The threshold voltage of an OLED is normally defined as the voltage at which luminance reaches 10 cd/m^2 . For the best performing device, this should be as low as possible.

ix. Lifetime ($T_{1/2}$)

It is the time required for the luminance of the device to become half of its initial value, when driven at a constant current density. Lifetime is closely related to the operating brightness of the device and follows a power law,

$$T_{1/2} = J^{-\beta}$$

where $1.5 < \beta < 3$ is called acceleration coefficient.

x. Efficiency roll-off

Critical current density J_0 or the luminance L_0 , which represents the current density or luminance respectively at which the EQE drops to half of its maximum value represents the efficiency roll-off. Major factors responsible for efficiency roll-off are charge carrier imbalance, non-radiative bimolecular processes, field-induced quenching, Joule heating, and degradation. Roll-off mostly affects phosphorescent devices.

xi. Color rendering index (CRI)

CRI is the measure of the accuracy of the light source to render the color of the objects compared to the natural light sources, on a scale of 1 to 100. Higher the CRI better will be the color rendering. Sources with CRI of above 90 can be used for task lighting applications.

xii. Correlated color temperature (CCT)

CCT indicates the apparent color of a light source in Kelvin (K). It is defined by the proximity of the chromaticity coordinates to the Planckian locus (locus of the wavelengths emitted by a black body with temperature in a particular chromaticity space), as the temperature of the blackbody radiator closely resembling the emission wavelength. It represents the color appearance of a white source by a single number rather than the two chromaticity coordinates. White light emission having lower CCT values, ~2700 K to 3000 K, are called warm white and those with high CCT values, ~4000 K to 6500 K, are called cool white.

A.2 OLED: Fabrication details

Pre-patterned indium tin oxide (ITO) coated glass substrates (Kintec Company, Hong Kong) were brushed with liquid detergent solution (Alkanox), and then sonicated in deionized water and 2-propanol for 10 minutes. The hot air dried substrates were UV-ozone treated (Novascan) and loaded into the thermal evaporation chamber (Angstrom Inc.) maintained under $\sim 10^{-8}$ Torr vacuum, integrated to the glovebox (Purelab), shown in fig A.1. Organic layers were deposited sequentially at a rate of 1-2Å/s except for the dopant materials, whose deposition rate varied with EML composition. Lithium fluoride (LiF) was deposited at the rate of 0.1Å/s and Aluminum at 2Å/s. Evaporation process was automatically controlled by Inficon software. Each of the film thickness and the tooling factors for the deposition were optimized using Dektak XT stylus profilometer.



Figure A.1 Glovebox integrated evaporation system; inset shows the internal view of the evaporation chamber

The final device was encapsulated under nitrogen environment in the glove box (oxygen and moisture~ 0.1 ppm) using a UV curable epoxy (Epoxy Technology Inc.). Then the encapsulated devices were taken outside. A Keithley 2400 source meter combined with Spectrascan PR655 Spectro- radiometer (Photo Research Inc.) interfaced with a PC was used to characterize all the devices as shown in fig A.2.

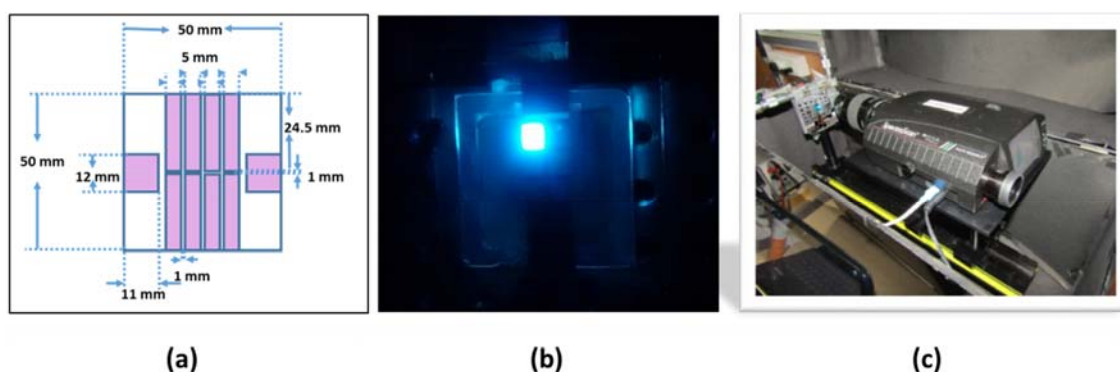


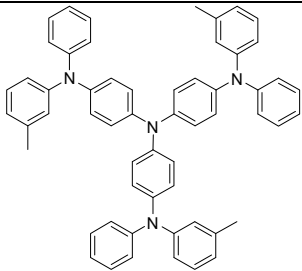
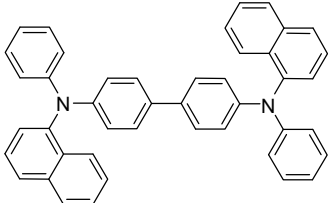
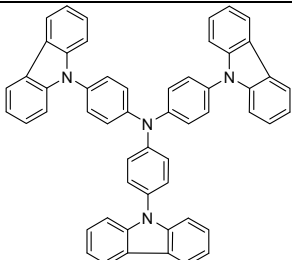
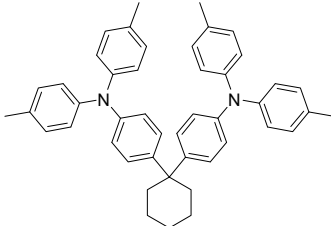
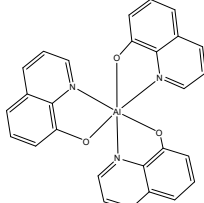
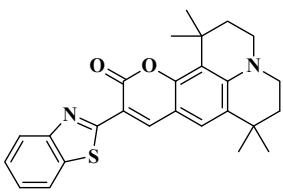
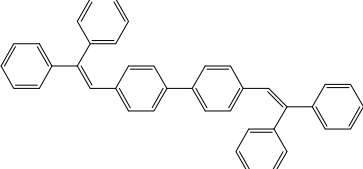
Figure A.2 a) A typical substrate design, b) OLED device, and c) PR655 Spectro-radiometer

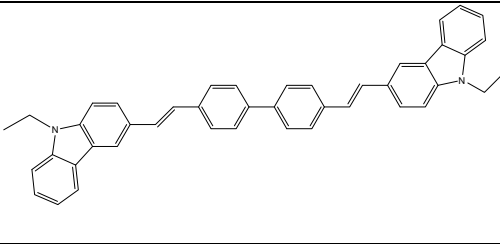
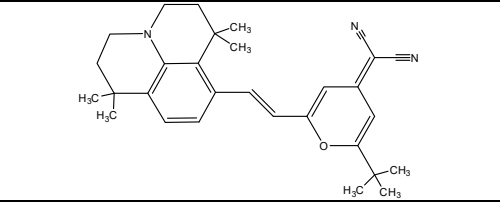
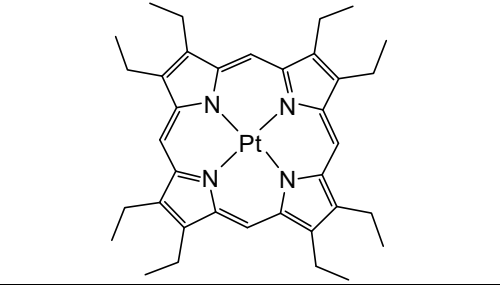
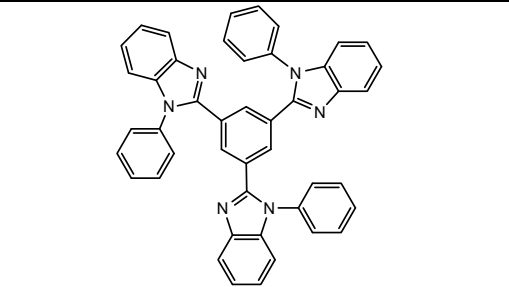
Thus, we have 8 pixels on a substrate and the typical performance from one of these is taken for all comparative studies, since the reproducibility and the repeatability are excellent.

A.3 Materials used in the thesis

All the materials used as part of the thesis are purchased from Luminescence Technology Corp., Taiwan and is listed below.

| Role | Material | Name | Structure |
|----------------------|--|---------|-----------|
| Hole injection layer | 2,3,5,6-Tetrafluoro-7,7,8,8-tetracyanoquinodimethane | F4-TCNQ | |

| | | | |
|--|--|------------------|---|
| Hole injection layer | 4,4',4''-Tris[phenyl(mtolyl)amino] triphenyl amine | m-MTDATA |  |
| Hole transport layer/ electron blocking layer | N,N'-Bis(naphthalen-1-yl)-N,N'-bis(phenyl)-benzidine | NPB |  |
| Electron blocking layer | Tris (4-carbazoyl-9-ylphenyl)amine | TCTA |  |
| Electron blocking layer | Di-[4-(N,N-di-p-tolyl-amino)-phenyl]cyclohexane | TAPC |  |
| Emitter/ electron transport layer | Tris-(8-hydroxyquinoline) aluminium | Alq ₃ |  |
| Green emitter | 2,3,6,7-Tetrahydro-1,1,7,7,- tetramethyl-1H, 5H,11H-10-(2-benzothiazolyl)quinolizino-[9,9a, 1n gh]Coumarin | C545T |  |
| Blue emitter (host) | 4,4 -bis(2,2 -diphenylvinyl)-1,1 -diphenyl | DPVBi |  |

| | | | |
|--------------------------|---|--------|---|
| Blue emitter (dopant) | 4,4'-Bis(9-ethyl-3-carbazovinyleno)-1;4,4'-Bis(9-ethyl-3-carbazovinyleno)-1,1'-biphenyl | BCzVBi |  |
| Red emitter (dopant) | 4-(Dicyanomethylene)-2-tert-butyl-6-(1,1,7,7-tetramethyljulolidin-4-yl-vinyl)-4H-pyran | DCJTb |  |
| Red emitter (dopant) | Platinum(II) 2,3,7,8,12,13,17,18-octaethyl-21H,23H-porphyrin | PtOEP |  |
| Electron transport layer | 1,3,5-Tris(1-phenyl-1Hbenzimidazol-2-yl)benzene | TPBi |  |

LIST OF PUBLICATIONS

1. **Anjaly Soman** and K. N. Narayanan Unni, Enhancement in electron transport and exciton confinement in OLEDs: role of n-type doping and electron blocking layers, *Eur. Phys. J. Appl. Phys.*, 190020, **2019**.
2. **Anjaly Soman**, Manuraj M. and K. N. Narayanan Unni, Addressing the efficiency roll-off in a fluorescent OLED by facile electron transport layer doping and carrier confinement, *Optical Materials*, 79, 413-419, May, **2018**.
3. Shameel Thurakkal, **Anjaly Soman**, K. N. Narayanan Unni, Joshy Joseph and D. Ramaiah, Simple solution processable carbazole-oxadiazole hybrids for undoped deep-blue OLEDs, *Journal of Photochemistry and Photobiology A: Chemistry*, 358, 192-200, May, **2018**.
4. Shameel Thurakkal, K. S. Sanju, **Anjaly Soman**, K. N. Narayanan Unni, Joshy Joseph and D. Ramaiah, Design and synthesis of solution processable green fluorescent D- π -A dyads for OLED applications, *New Journal of Chemistry*, 42, 7, 5456-5464, Feb, **2018**.
5. Naoki Okamura, Takeshi Maeda, Hideki Fujiwara, **Anjaly Soman**, K. N. Narayanan Unni, Ayyappanpillai Ajayaghosh and Shigeyuki Yagi, Photokinetic study on remarkable excimer phosphorescence from heteroleptic cyclometalated platinum(ii) complexes bearing a benzoylated 2-phenylpyridinate ligand, *Physical Chemistry Chemical Physics*, 20, 1, 542-552, Month, **2017**.

PAPERS/POSTERS PRESENTED IN CONFERENCE PROCEEDINGS

1. "Aggregation-induced Tuning of Electroluminescence in an Organic Light Emitting Diode", **Anjaly Soman**, Ansu Varghese, Rajeev V R, K N Narayanan Unni, *National Conference on Materials Science and Technology- 2015 (NCMST-15)* in IIST, Thiruvananthapuram during July 6-8, 2015.
2. "Improved performance of a green organic light emitting diode by doped transport layer and carrier confinement", **Anjaly Soman**, K N Narayanan Unni, *12th JNC conference on Chemistry of Materials* at Vivanta by Taj at Kovalam, Trivandrum from September 23-25, 2016.
3. "The effect of electric field on the exciton diffusion process in OLEDs", **Anjaly Soman**, K N Narayanan Unni, *National Conference on Luminescence and Applications [NCLA-17]* at CSIR- Indian Institute of Chemical Technology [IICT], Hyderabad, 9-11th January, 2017.
4. "Exciton Confinement and Carrier Transport: Role of Electron Blocking Layers", **Anjaly Soman**, K N Narayanan Unni, *8th East Asia Symposium on Functional Dyes and Advanced Materials*, at CSIR-NIIST, Thiruvananthapuram, Kerala, India on 20-22 September 2017.